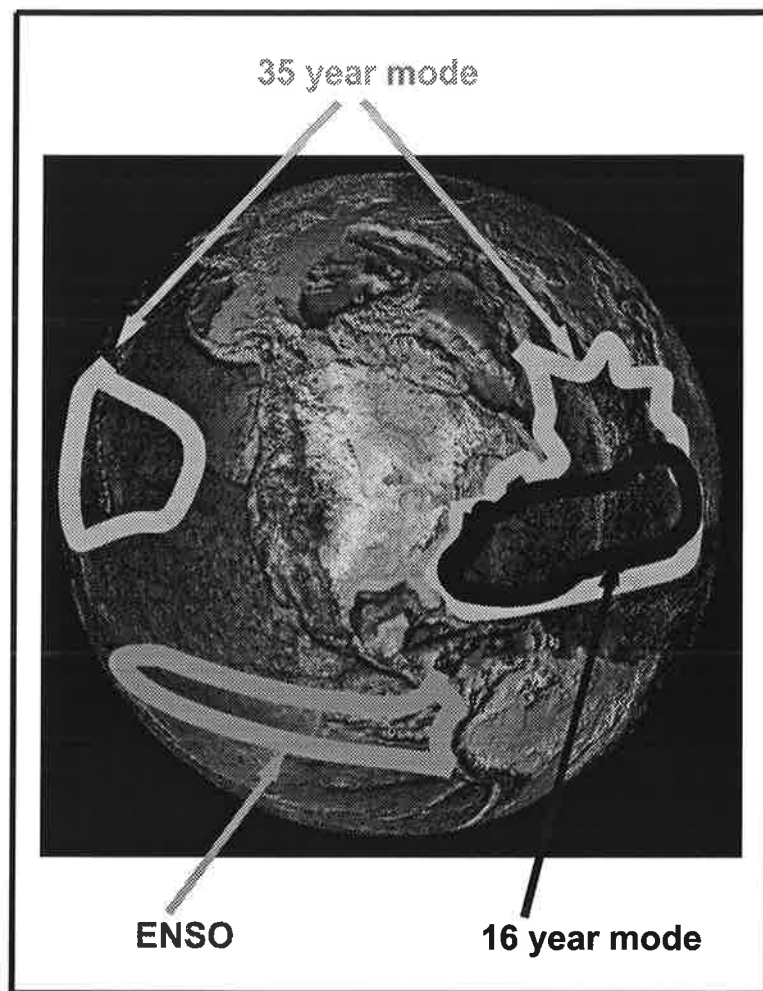




# Max-Planck-Institut für Meteorologie

## EXAMENSARBEIT Nr. 64



MODES OF VARIABILITY AS SIMULATED BY  
A GLOBAL CLIMATE MODEL

VON

Axel Timmermann

HAMBURG, März 1999

Dissertation zur Erlangung des Doktorgrades

Autor:

Axel Timmermann

Max-Planck-Institut  
für Meteorologie

KNMI  
Postbus 201  
3730 AE De Bilt  
the Netherlands

MAX-PLANCK-INSTITUT  
FÜR METEOROLOGIE  
BUNDESSTRASSE 55  
D - 20146 HAMBURG  
GERMANY

Tel.: +49-(0)40-4 11 73-0  
Telefax: +49-(0)40-4 11 73-298  
E-Mail: <name> @ dkrz.de



# **Modes of Variability as Simulated by a Global Climate Model**

Dissertation  
zur Erlangung des Doktorgrades  
der Naturwissenschaften im Fachbereich  
Geowissenschaften  
der  
Universität Hamburg

vorgelegt  
von  
**Axel Timmermann**  
aus Dortmund

Hamburg

8. September 1998

**ISSN 0938-5177**

Als Dissertation angenommen vom Fachbereich Geowissenschaften der  
Universität Hamburg

auf Grund der Gutachten von Prof. Dr. Klaus Hasselmann  
und Dr. habil. Mojib Latif

Hamburg, den 22. Januar 1999

Prof. Dr. G. Miehlich  
Dekan  
des Fachbereichs Geowissenschaften

# Contents

<b>1</b>	<b>Introduction</b>	<b>1</b>
1.1	Internal Climate Variability – Null hypothesis: Red Noise . . . . .	1
1.2	Internally generated climate modes and why we are interested in them . . .	3
1.3	Concept of this thesis . . . . .	5
1.4	References . . . . .	6
<b>2</b>	<b>The Coupled General Circulation Model ECHAM3/LSG</b>	<b>8</b>
2.1	Model description . . . . .	8
2.2	Simulated Climate . . . . .	10
2.3	References . . . . .	12
<b>3</b>	<b>ENSO-like climate variability and its low-frequency modulation</b>	<b>15</b>
3.1	Abstract . . . . .	15
3.2	Introduction . . . . .	15
3.3	ENSO physics in a coarse resolution CGCM . . . . .	17
3.4	Phase Locking to the Annual Cycle . . . . .	21
3.5	ENSO modulation . . . . .	22
3.6	ENSO response to greenhouse warming . . . . .	27
3.7	Summary . . . . .	27
3.8	References . . . . .	29
<b>4</b>	<b>Decadal Climate Variability in the North Atlantic</b>	<b>33</b>
4.1	Abstract . . . . .	33
4.2	Introduction . . . . .	33
4.3	Identification of the decadal climate mode . . . . .	35
4.4	Decadal ocean dynamics . . . . .	39
4.5	Decadal sea ice variability . . . . .	45
4.6	Discussion and Summary . . . . .	46
4.7	References . . . . .	47

---

<b>5</b>	<b>Interdecadal Climate Variability in the Northern Hemisphere</b>	<b>50</b>
5.1	Abstract . . . . .	50
5.2	Introduction . . . . .	51
5.3	Interdecadal time scales . . . . .	53
5.4	Physics of the North Atlantic interdecadal mode . . . . .	59
5.4.1	Atlantic air-sea interactions . . . . .	60
5.4.2	The dynamics of the THC . . . . .	66
5.5	Northern Hemispheric interactions . . . . .	70
5.6	Interdecadal variability and greenhouse warming . . . . .	74
5.7	Summary and Discussion . . . . .	77
5.8	References . . . . .	79
<b>6</b>	<b>Outlook and Summary</b>	<b>84</b>
6.1	Climate predictability . . . . .	84
6.2	External forcing and long-term climate variability . . . . .	86
6.3	Future plans . . . . .	88
6.4	Summary . . . . .	89
6.5	References . . . . .	91

# List of Figures

1.1	Schematic spectrum of surface temperatures . . . . .	2
2.1	Mean temperature and salinity in the North Atlantic . . . . .	9
2.2	Barotropic streamfunction . . . . .	9
2.3	Potential energy loss by convection . . . . .	10
2.4	Zonally integrated stream function (Sv) in the Atlantic . . . . .	11
2.5	Standard deviation of observed and simulated SST anomalies . . . . .	12
3.1	Niño 3 SSTA index . . . . .	18
3.2	Lag regression patterns of the Niño 3 SSTA index on the heat content field of the upper 575m . . . . .	19
3.3	Lag regression patterns of the Niño 3 SSTA index upon the subsurface temperature anomaly field along 2.8°S . . . . .	20
3.4	Teleconnection patterns of ENSO . . . . .	21
3.5	Phase locking of ENSO . . . . .	22
3.6	Wavelet analysis of Niño 3 SSTA . . . . .	23
3.7	Interannual Wavelet energy of Niño 3 SSTA index . . . . .	24
3.8	Discrete power spectrum of Fig.3.7 . . . . .	24
3.9	ENSO variance modulations and associated subsurface temperature dynamics	25
3.10	Thermocline structure associated with interdecadal ENSO modulations . .	26
3.11	ENSO response to greenhouse Warming in the ECHAM3/LSG model . . .	28
4.1	POP patterns of North Atlantic heat content . . . . .	36
4.2	POP coefficients of the decadal heat content POP . . . . .	37
4.3	Cross spectral analysis of POP coefficients . . . . .	38
4.4	CCA of SLP and SST anomalies . . . . .	39
4.5	CCA/POP relationship . . . . .	40
4.6	Associated imaginary and real patterns of SST, SLP, $\nabla \times \tau/\beta$ . . . . .	41
4.7	Mean zonal crossing time of virtual tracer particles . . . . .	42
4.8	Associated imaginary and real patterns of the upper ocean currents . . . . .	43

4.9	Cross correlation between SSTA index and net heatflux, upper ocean current and upper ocean vertical velocity anomalies . . . . .	44
4.10	NAO and ice thickness in the Labrador Sea . . . . .	45
4.11	Schematic diagram of the feedback loop for the decadal North Atlantic mode	47
5.1	Detrended time series of the maximum of the Atlantic meridional overturning	54
5.2	Power spectrum of the meridional overturning index . . . . .	55
5.3	Power spectrum of North Atlantic and North Pacific SST anomalies . . . .	56
5.4	Spectral analysis of the 500hPa EOF . . . . .	57
5.5	Cross spectrum of North Pacific and North Atlantic SSTA . . . . .	58
5.6	Table of different hypotheses that can explain interdecadal variability . . .	59
5.7	Lag regressions of SLP, SST, freshwater flux, SSS, surface currents and potential energy loss by convection with THC index . . . . .	60
5.8	Same as Fig.5.7, but for lag -5 a. . . . .	61
5.9	Same as Fig.5.7, but for lag 0 a. . . . .	62
5.10	Same as Fig.5.7, but for lag +5 a. . . . .	65
5.11	Origin of SSS anomalies in the sinking region . . . . .	66
5.12	Zonally averaged salinity anomalies in the North Atlantic . . . . .	67
5.13	Total density contribution in the North Atlantic . . . . .	68
5.14	Meridional streamfunction . . . . .	69
5.15	Schematic diagram of the interactions that lead to the interdecadal cycle .	70
5.16	Lag regression patterns between the bandpass filtered THC index anomaly and the oceanic heat content anomalies . . . . .	71
5.17	Atmospheric response to SST anomalies in mid-latitudes . . . . .	72
5.18	Interdecadal and greenhouse warming 2m temperature EOF . . . . .	75
5.19	Projection of the observed 2m temperatures on Fig.5.18 . . . . .	76
5.20	SLP in Stykkisholmur (Iceland), mid-latitudinal SSTA . . . . .	79
6.1	Predictability of the THC . . . . .	86
6.2	Solar influence on NAO . . . . .	87
6.3	Schematic diagram of the simulated climate modes . . . . .	90

# 1 Introduction

*In dieser Welt hat nur die Unbeständigkeit Bestand. (Jonathan Swift)*

Climate variability is generated by a complex interplay of different components: the atmosphere, the hydrosphere, the cryosphere, the biosphere, the lithosphere and additionally by astronomical forcing. Each of the constituents is characterized by its own relevant physical processes and its individual range of time and space scales. Fig.1.1 illustrates schematically the variance spectrum of global surface temperatures as a function of period. It shows that climate variability on short time scales is dominated by atmospheric processes. Towards longer periods, the ocean, the cryosphere and the geosphere become more and more important. Apart from an overall red background the spectrum also exhibits pronounced variability peaks at different periods. **External** astronomical processes govern e.g the diurnal cycle, the annual cycle and the quaternary ice volume cycles. On the other hand there are **internal** resonances of the climate system, such as the Quasi-Biennial Oscillation or the El Niño-Southern Oscillation phenomenon. The focus of this thesis will be the investigation of internal climate oscillations, which are distinct from the background and which result primarily from atmosphere-ocean interactions.

This thesis investigates climate variability on interannual to interdecadal time scales. On these time scales there is no significant feedback from the atmosphere-ocean system back to the much slower climate components. Thus, within the context of this thesis variations on centennial and longer time scales are treated as external forcing.

## 1.1 Internal Climate Variability – Null hypothesis: Red Noise

In his pioneering work Hasselmann (1976) demonstrated with a conceptual model that the dominant part of climate variability (e.g the variability of sea surface temperatures) in the time scale-range between a few months up to decades or even up to much longer time scales (1000 ka) can be explained by a stochastic ansatz. The basic idea is the existence of a time scale separation of fast atmospheric and slow oceanic or cryospheric processes.

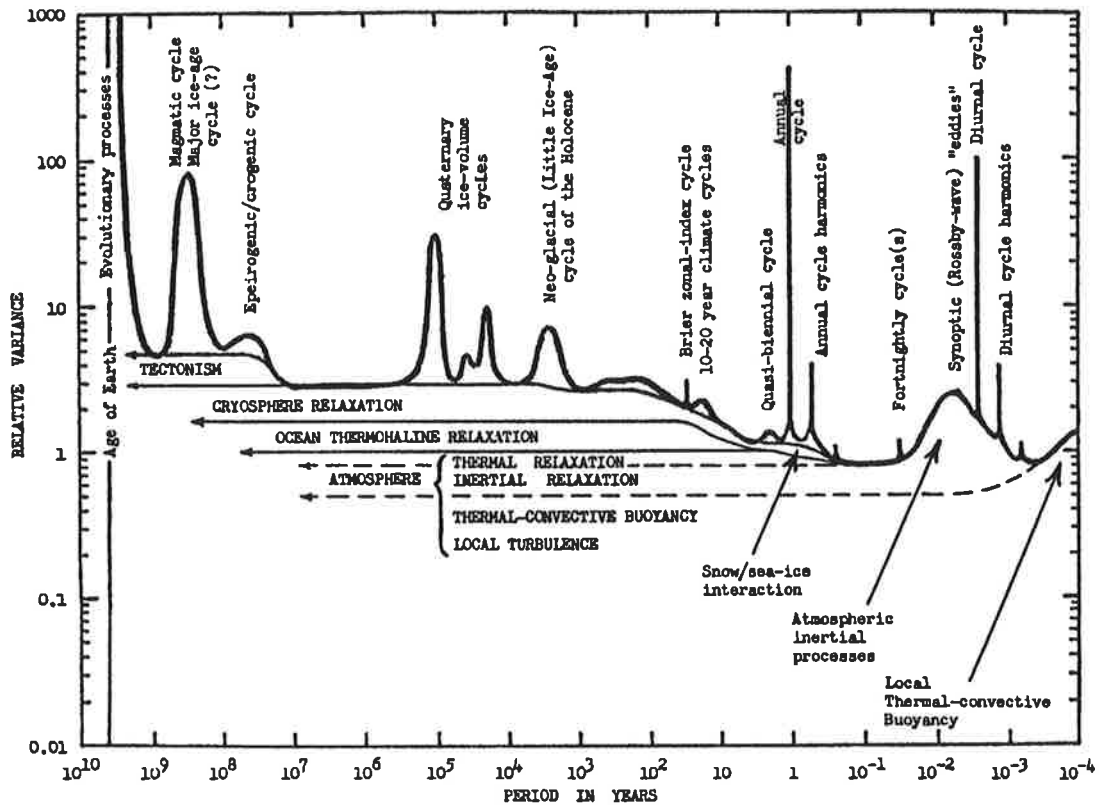


Figure 1.1: Schematic spectrum of surface temperatures as a function of period [years]. Figure from Mitchell (1968)

In analogy to Brownian motion describing the slow movement of a macroscopic particle in a fast randomly fluctuating medium of microscopic particles, the small deviation  $y(t)$  around the mean (climate) state can be described by a Langevin equation. Hasselmann's (1976) approach is based on a multivariate and nonlinear stochastic differential equation. To keep things simple we restrict ourselves to the univariate linear case as discussed thoroughly by Frankignoul and Hasselmann (1977)

$$\dot{y}(t) = -\lambda(t)y(t) + \xi(t). \quad (1.1)$$

This stochastic climate model parameterizes the atmospheric fluctuations  $\xi(t)$  as a Gaussian white noise process, with  $\langle \xi(t)\xi(t') \rangle = \sigma(t)\delta(t-t')$ .  $y(t)$  denotes the temporal evolution of a climate variable (such as e.g. the deviation of SST from a long-term mean), whereas  $\lambda(t)$  represents the damping factor associated with the system's inertia against changes of the forcing term  $\xi(t)$ . In the paper of Hasselmann (1976)  $\sigma$  and  $\lambda$  are regarded as constants in time. In our simple notation the climate variance spectrum  $G(\omega)$  is given

in analogy to the Ornstein-Uhlenbeck process by

$$G(\omega) = \frac{F(0)}{\omega^2 + \lambda^2}. \quad (1.2)$$

The shape of this spectrum is characterized by high variances at low frequencies and low variance at high frequencies. Such spectra are often referred to as red noise spectra. Many observations e.g from sea surface temperature anomalies in high latitudes (Frankignoul and Hasselmann 1977) and ice-coverage anomalies (Lemke et al. 1980) are consistent with the red noise behaviour.

Substantial deviations from this null-hypothesis of climate variability may be found in those regions where ocean dynamics play an important role in generating anomalies. Furthermore, the seasonal modulations of  $\sigma(t)$  and  $\lambda(t)$  (Ruiz de Elvira and Lemke 1982) as well as the presence of complicated feedbacks and resonances (Mikolajewicz and Maier-Reimer 1990) or the existence of multiple equilibria (Benzi 1982, Nicholis 1982) may lead to deviations from the linearized version of the stochastic climate model. One major goal of climate research consists in detecting and understanding such deviations. Apart from the analysis of observations, climate models of varying complexity can be adopted for this purpose.

## 1.2 Internally generated climate modes and why we are interested in them

Distinct modes of climate variability which cannot be explained by the red noise hypothesis can arise, for instance, from instabilities within the ocean or the atmosphere. Here we shall restrict ourselves to the coupled ocean-atmosphere system. Ice dynamics is neglected. There are basically four paradigms which can explain deviations from red-noise climate variability.

- 1.) the coupled air-sea mode concept
- 2.) the (noise driven) ocean mode concept
- 3.) the atmosphere-only mode concept
- 4.) complex stochastic processes such as e.g. multiplicative noise or stochastic resonance.

The coupled air-sea mode concept is based on the idea that the atmosphere-ocean system supports coupled oscillations. The oceanic memory and the strength of the atmosphere-ocean interactions determine the period. The most famous example for a coupled air-sea mode is the El Niño-Southern Oscillation (ENSO) phenomenon.

The concept of a noise driven ocean oscillator can be regarded as a generalization of the linearized univariate stochastic climate model. The first order equation (1.1) is generalized to a second (or higher) order equation in time, allowing for oscillations.

The atmosphere-only concept was suggested by James and James (1989). Through non-linear interactions atmospheric motions can transfer energy directly to longer time scales, thereby reddening the spectrum of atmospheric variability. Whether such processes can produce distinct atmospheric time scales is an open question. However, there are examples of atmospheric variability modes which are not fully understood yet such as the Madden-Julian Oscillation with a time scale of 30-60 days and the stratospheric Quasi-Biennial Oscillation with a period of about 28 months. These oscillations might be regarded at least as candidates for atmosphere-only modes.

The knowledge of climate oscillations and the resulting potential to predict future climate conditions is old and can be illustrated with the following historical citation:

*Seven years of great abundance are coming throughout the land of Egypt, but seven years of famine will follow them. Then all the abundance in Egypt will be forgotten, and the famine will ravage the land. The abundance in the land will not be remembered, because the famine that follows it will be so severe. ... They should collect all the food of these good years that are coming and store up the grain under the authority of Pharaoh, to be kept in the cities for food. This food should be held in reserve for the country, to be used during the seven years of famine that will come upon Egypt, so that the country may not be ruined by the famine. (1. Moses, 41, 29-30, 36).*

This citation from the bible, if taken literally, reveals that even the ancient Jewish nation was aware of the problem of climate variability. The story of Joseph is modern in many respects. The Egyptian Pharaoh had a dream, which none of his priests could interpret. The prisoner Joseph was called to interpret the symbols of the dream. It turned out that the dream symbols described a 14 year climate oscillation facing Egypt with 7 anomalously wet and 7 anomalously dry years. Moreover, the dream could be regarded as a kind of climate prediction. The bible also describes how the predicted severe famines could be avoided: saving corn from the rich years to bridge over the poor period. The story of Joseph shows elements not only of modern psychoanalytical methods, but also of climate prediction and modern disaster management.

It has always been a challenge to mankind to make predictions of the future climate. The knowledge of the most probable climate trajectory for the next years might help to optimize e.g. crops or to determine optimal fishing quotas. We are in the position nowadays to investigate this problem scientifically by means of modern climate models. Climate predictions, however, have to compete against the simplest statistical model, the damped persistence forecast of a first order autoregressive process (AR(1)). The identification and understanding of climate modes is therefore of particular importance to the predictability problem.

Another motivation for a rigorous analysis of climate variability arises from the fact that natural long-term climate variability on time scales up to centuries is an important

factor in masking the anthropogenic greenhouse warming signal in the present climate record. Detection studies such as the work by Hegerl et al. (1996) estimate the level of natural climate variability both from observations and from coupled climate model integrations. Physical processes which are not well represented in coupled climate models could lead to a misrepresentation of the natural climate variability. Hence it is crucial not only to monitor the statistics of long-term climate variability but also to consider the responsible physical mechanisms.

### 1.3 Concept of this thesis

**The aim of this thesis is to determine those physical processes which lead to the generation of climate variability on interannual to interdecadal time scales.**

The basis of the analysis is a 700 year integration performed with the coupled general circulation model (CGCM) ECHAM3/LSG. The model and the simulation of the climate mean are briefly summarized in Chapter 2. In Chapter 3 the simulated El Niño-Southern Oscillation phenomenon is described with a focus on the interdecadal ENSO amplitude modulations. Although the CGCM is not able to resolve the upwelling of the tropical Pacific Ocean, it is reasonably successful in simulating ENSO-like climate variations. The simulated ENSO dynamics are consistent with the widely accepted ENSO paradigm, the delayed action oscillator. Chapter 4 is devoted to the analysis of a decadal climate mode in the North Atlantic, which originates from an interaction of the atmospheric circulation and the subtropical and subpolar ocean gyres. In Chapter 5 the physics of an interdecadal climate mode are explored. This chapter is published in *Journal of Climate* (Timmermann et al. 1998). The interdecadal mode described here can also be understood in terms of the coupled air-sea mode concept. The long-term memory is provided here by the slow thermohaline circulation in the North Atlantic. Each of these chapters is concluded with an individual discussion and a summary. In Chapter 6 an outlook and a summary of this thesis are given. A recent publication by Grötzner, Latif, Timmermann and Voss (1998) (submitted to *Journal of Climate*) on the climate predictability issue is briefly reviewed and a general predictability approach is formulated in terms of information theory. This framework might help to determine physical processes which constrain climate predictions. Furthermore using a solar variability simulation conducted with the same CGCM the impact of solar variability on longterm climate variability is analyzed.

A major focus of this thesis is to reveal which parts of the climate system are responsible for the generation of climate modes on interannual, decadal and interdecadal time scales. Do these modes result from coupled atmosphere-ocean dynamics, or can they be explained in terms of stochastically forced oceanic oscillators or internal nonlinear atmospheric processes? These are the questions which will accompany us during the analysis

presented here.

## 1.4 References

Benzi, R., A. Sutera, A. Vulpiani, 1982: Stochastic resonance in climatic change. *Tellus*, **34**, 10-16.

Frankignoul, C., and K. Hasselmann, 1977: Stochastic climate models, II, Application to sea-surface temperature variability and thermocline variability. *Tellus*, **29**, 284-305.

Grötzner, A., M. Latif, A. Timmermann and R. Voss, 1998: Interannual to Decadal Predictability in a Coupled Ocean-Atmosphere General Circulation Model. *J. Climate* submitted.

Hasselmann, K., 1976: Stochastic climate models, Part I: Theory. *Tellus*, **28**, 473-485.

Hegerl, G.C., H.v. Storch, K. Hasselmann, B.D. Santer, U. Cubasch, P.D. Jones, 1996: Detecting Greenhouse Gas induced Climate Change with an Optimal Fingerprint method. *J. Climate*, **9**, 2281.

James, I.N, P.M. James, 1989: Ultra-low-frequency variability in a simple atmospheric circulation model. *Nature*, **342**, 53-55.

Lemke, P., E.W. Trinkl and K. Hasselmann, 1980: Stochastic dynamic analysis of polar sea-ice variability. *J. Phys. Oceanogr.*, **10**, 21000-2120.

Mikolajewicz, U., E. Maier-Reimer, 1990: Internal secular variability in an ocean general circulation model. *Climate Dyn.*, **4**, 145-156.

Mitchell, J.M. (ed.) 1968: Causes of Climatic Change. *Met. Mono.*, **8**, Am. Meteorol. Soc., Boston, Mass.

Nicolis, C. 1982: Stochastic aspects of climatic transitions – response to a period forcing. *Tellus*, **34**, 1-9.

Ruiz de Elvira, A., and P. Lemke, 1982: A Langevin equation for stochastic climate models with period feedback and forcing variance. *Tellus*, **34**, 313-320.

Timmermann, A., M. Latif, R. Voss and A. Grötzner, 1998: Northern Hemispheric

interdecadal climate variability: A coupled air-sea mode. *J. Climate*, **11**, 1906-1931.

# 2 The Coupled General Circulation Model ECHAM3/LSG

The analysis presented here is based on a 700 year control integration conducted with the coupled atmosphere-ocean model ECHAM3/LSG. The model consists of the atmospheric general circulation model ECHAM3, the third Hamburg version of the European Centre operational weather forecasting model (see Roeckner et al. 1992) and the ocean general circulation model LSG ("Large Scale Geostrophic") (Maier-Reimer et al. 1993).

## 2.1 Model description

For purposes of clarification: The LSG ocean model (Maier-Reimer et al. 1993) does not use the Large Scale Geostrophic filter proposed by Hasselmann (1982). It is a primitive equation model. The ocean model is integrated with a fully implicit scheme filtering out the fast ocean wave modes, namely barotropic waves, thereby allowing for a long time step of one month. Therefore, the LSG ocean model provides an appropriate representation of slow ocean modes only. Furthermore, the model adopts the hydrostatic, the Boussinesq and incompressibility approximations. Nonlinear momentum advection and explicit vertical friction are neglected. In the version used in this study 11 vertical levels were chosen and the model is integrated on an E-grid (Arakawa and Lamb 1977) with an effective horizontal resolution of approximately  $4^{\circ} \times 4^{\circ}$ . A thermodynamic sea ice model is also included. The uppermost layer (50m) of the LSG model represents a mixed layer, which integrates the daily atmospheric fluxes. The atmospheric model ECHAM3 is a global low-order spectral model with a triangular truncation at wavenumber 21 (T21) and 19 levels in the vertical. This corresponds to a horizontal resolution of about  $5.6^{\circ} \times 5.6^{\circ}$ . As compared to earlier versions of the ECHAM model (ECHAM1,2) major improvements have been achieved in the representation of diffusion, gravity wave drag, cumulus convection, stratiform clouds, soil processes and radiation.

The LSG ocean model and the ECHAM3 atmosphere model are coupled via the heat, fresh water and momentum fluxes. Ocean SSTs are taken as boundary conditions for the atmosphere. In order to avoid climate drift in the coupled mode, the flux correction tech-

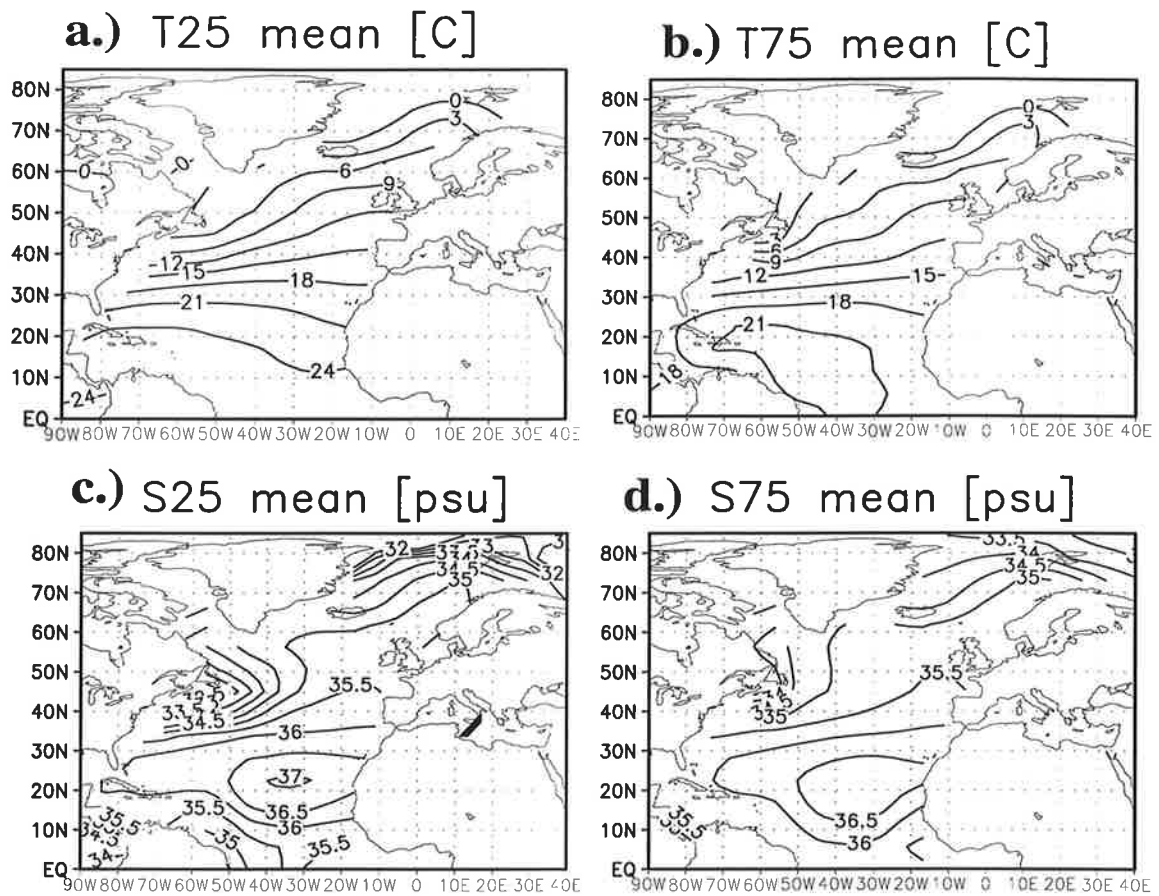


Figure 2.1: Mean fields of the temperatures at 25m and 75 m depth ( $^{\circ}\text{C}$ ) (upper panels) and salinities (psu) (lower panels) averaged over all 700 model years.

nique (Sausen et al. 1988) is applied, which is equivalent to coupling both subsystems by their individual flux-anomalies relative to their equilibrium states. Further details

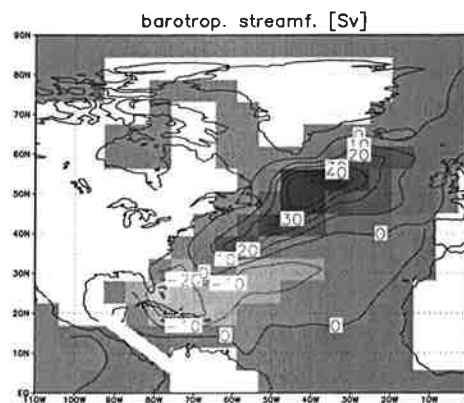


Figure 2.2: Barotropic streamfunction of the North Atlantic in Sv.

about the model and the coupling strategy can be found in Voss et al. (1998). The ECHAM3/LSG model has been used in a number of climate change and response experiments (e.g. Hasselmann et al. 1995, Cubasch et al. 1997, Schiller et al. 1997, Voss et al. 1998, Timmermann et al. 1998, Grötzner et al. 1998).

## 2.2 Simulated Climate

In order to demonstrate the overall model performance the oceanic mean fields of temperature, salinity, convection, meridional overturning and the oceanic transports are analyzed. The mean state of the coupled model might help in the following chapters to interpret results which are derived from statistical analyses of the simulated climate variability. Fig.2.1 displays the mean temperature and salinity fields averaged over all 700 years of the detrended control run at 25m and 75m depth (1st and 2nd ocean level, respectively). The mean temperature and salinity fields are simulated reasonably well at both depths, as

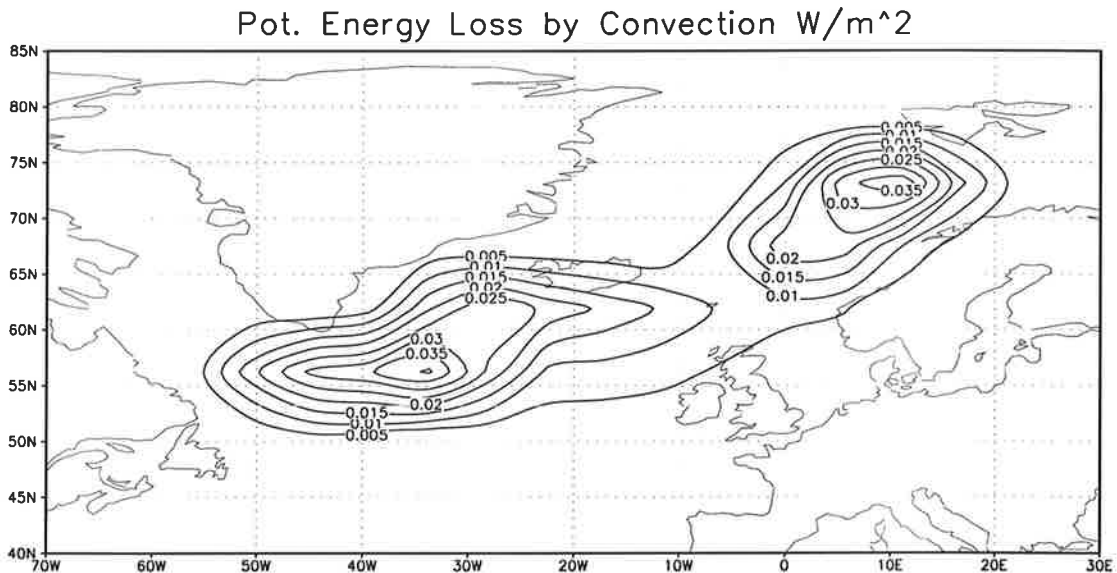


Figure 2.3: Regions of mean potential energy loss by convection ( $\text{W}/\text{m}^2$ ) in the North Atlantic averaged over all 700 model years.

expected when flux corrections (Sausen et al. 1988) are applied. However, a comparison with the Levitus (1982) climatology reveals that the temperature structure of the Gulf Stream is rather broad in the ECHAM3/LSG model. South of  $30^{\circ}\text{N}$  the isotherms are too zonal as compared to the observations. This feature is associated with an overestimation of the subpolar gyre in the model as compared to the subtropical gyre (Fig.2.2). Thus, the physics of the North Atlantic climate variability might be biased towards the dominant role of the subpolar gyre in the model.

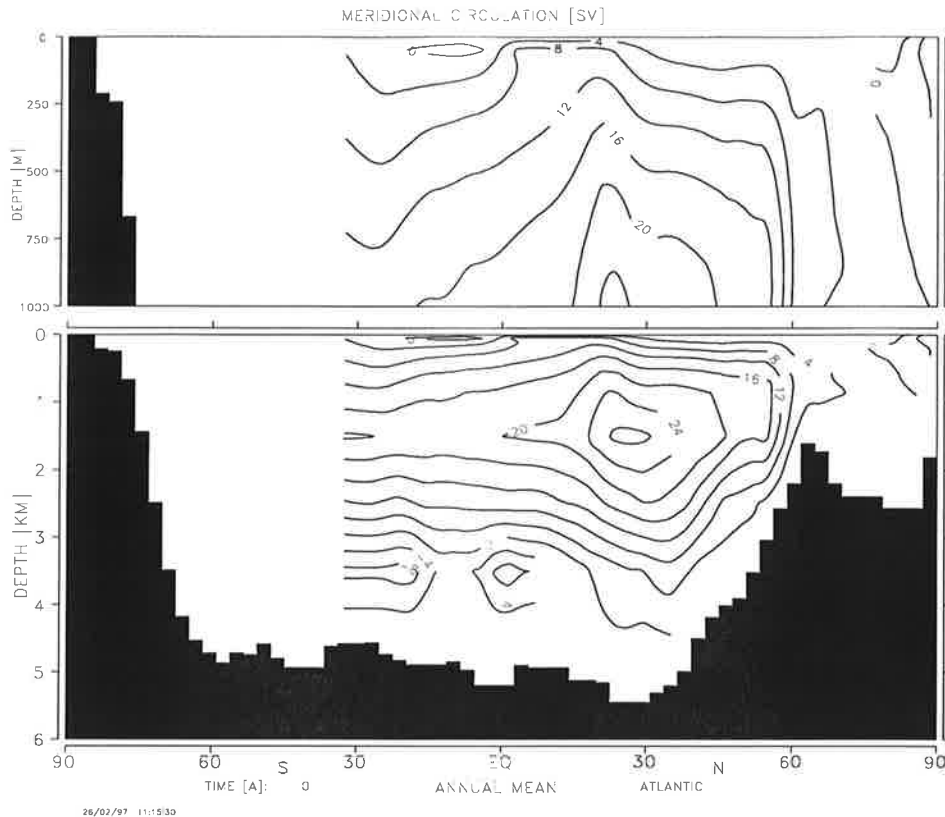


Figure 2.4: Zonally integrated stream function [Sv] in the Atlantic as a function of depth and latitude averaged over all 700 model years.

The regions of oceanic convection simulated by the CGCM are shown in Fig.2.3, which displays the mean potential energy loss by convection.

In the coupled model deep convection takes place south of Greenland and in the Greenland-Iceland Norway Sea (GIN) Sea. Among other mechanisms the convection generates pressure gradients thereby forcing the thermohaline circulation (THC) which plays a crucial role in the oceanic poleward heat transport and may therefore serve as an important component for the generation of long-term variability.

The mean of the meridional streamfunction in the Atlantic is shown in Fig.2.4, where positive values of the meridional streamfunction stand for a clockwise circulation.

The meridional overturning shows an outflow of North Atlantic Deep Water (NADW) of about 18 Sv at 30°S and an inflow of Antarctic Bottom Water (AABW) of about 6-8 Sv into the North Atlantic. Thus, the coupled model used here reproduces the principal features of the North Atlantic THC in a reasonable manner. The simulated mean atmospheric conditions are almost identical to those simulated by the uncoupled atmosphere model (Roeckner 1992). In order to show that also the variability is simulated reasonably well by the coupled model, the standard deviations of detrended North Atlantic SST

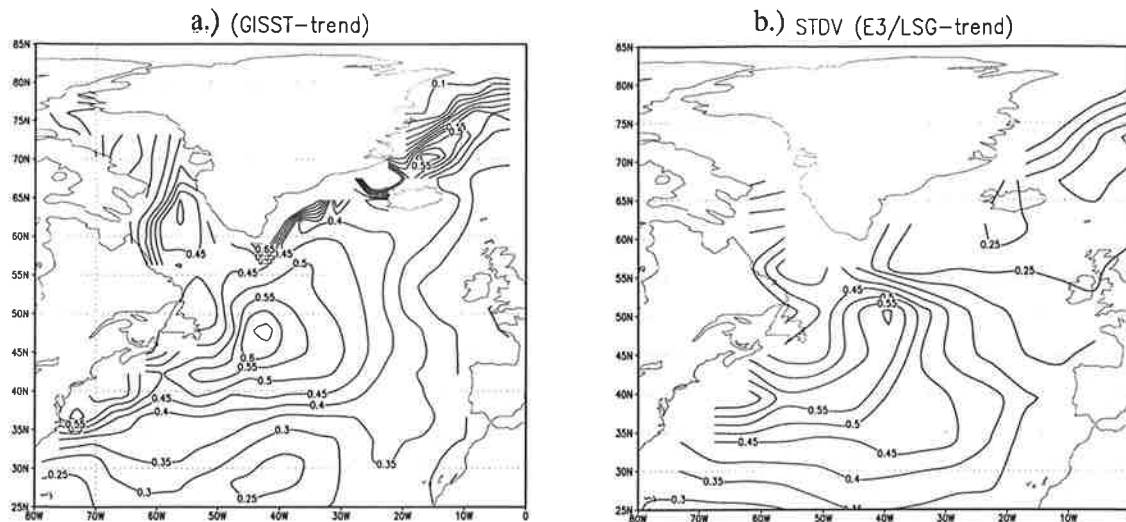


Figure 2.5: (a): Standard deviation of the observed annual SSTAs for the period 1903-1994. A least square fit was applied to remove the trend in the data. Note that the GISST data are not corrected for sea ice variability. (b): same as in (a) but for the SSTA of the 700 year model integration.

anomalies (based on annual means) as obtained from observations (a) (taken from the GISST dataset of the UKMO) and from the 700 year CGCM integration (b) are displayed in Fig.2.5 .

The two patterns correspond reasonably well to each other, which gives us confidence that the principal feedbacks in the North Atlantic region are simulated correctly.

However, one should note that the flux correction technique used in the coupled model might have an effect on the climate variability if nonlinearities in the system become important. For further information on this subject the reader is referred to a number of recent studies exploring the effect of flux corrections (Nakamura et al. 1994, Marotzke and Stone 1995, Cai et al. 1997) on climate feedbacks. However, a detailed analysis regarding the influence of the flux correction technique on the simulated climate variability in the model is beyond the scope of this study<sup>1</sup>. On the other hand, most state of the art CGCMs integrated without flux corrections still have climate drift problems.

## 2.3 References

Arakawa, A., and V.R. Lamb 1977: Computational design of the basic dynamical process of the UCLA general circulation model. *Meth. Comp. Phys.*, **16** 173-263.

<sup>1</sup>It should be mentioned that although the flux correction technique is used in the 700 year integration, there is a strong climate drift in the Antarctic Ocean. Almost all the Antarctic sea ice is melted within the first 150 years of the coupled model integration.

- Cai, W., J. Syktus, H.B. Gordon and S. O'Farrell, 1997: Response of a Global Coupled Ocean-Atmosphere-Sea Ice Climate Model to an Imposed North Atlantic High-Latitude Freshening. *J. Climate*, **10**, 929-948.
- Cubasch, U., Hegerl G.C., Voss R., Waszkewitz J. and Crowley T. J., 1997: Simulation of the influence of solar radiation variations on the global climate with an ocean-atmosphere general circulation model, *Clim. Dyn.* **13**, 757-767.
- Grötzner, A., M. Latif, A. Timmermann and R. Voss, 1998: Interannual to Decadal Predictability in a Coupled Ocean-Atmosphere General Circulation Model. *J. Climate* submitted.
- Hasselmann, K., 1982: An ocean model for climate variability studies. *Prog. Oceanogr.*, **11**, 69-92.
- Hasselmann, K., Bengtsson L., Cubasch U., Hegerl G.C., Rodhe H., Roeckner E., v. Storch H., Voss, R. and Waszkewitz J. (1995): Detection of anthropogenic Climate Change using a fingerprint method. In: *Proc. Modern Dynamical Meteorology, Symposium in Honor of Aksel Wiin-Nielsen*, (P. Ditlevsen ed.), (ECMWF press), 203-221.
- Levitus, S., 1982: Climatological Atlas of the World Ocean, National Oceanic and Atmospheric Administration, 173 pp. and 17 microfiche.
- Maier-Reimer, E., U. Mikolajewicz, K. Hasselmann, 1993: Mean Circulation of the Hamburg LSG model and its sensitivity to the thermohaline surface forcing. *J. Phys. Oceanogr.*, **23**, 731-757.
- Marotzke, J. and P. Stone, 1995: Atmospheric transports, the thermohaline circulation, and flux adjustments in a simple coupled model. *J. Phys. Oceanogr.*, **25**, 1350-1364.
- Nakamura, M., P. Stone and J. Marotzke, 1994: Destabilizing the thermohaline circulation by atmospheric eddy transports. *J. Climate*, **7**, 1870-1882.
- Roeckner, E., K.Arpe, L. Bengtsson, S. Brinkop, L. Dümenil, M. Esch, E. Kirk, F. Lunkeit, M. Ponater, B. Rockel, R. Sausen, U. Schlese, S. Schubert, M. Windelband, Simulation of the present-day climate with the ECHAM model: Impact of model physics and resolution, Report no.93, October 1992, 171 pp. Available from: Max-Planck-Institut für Meteorologie, Bundesstr.55, 20146 Hamburg, Germany.

Sausen, R., R.K. Barthels and K. Hasselmann, 1988: Coupled ocean-atmosphere models with flux correction. *Climate Dyn.*, **2**, 154-163.

Schiller, A., U. Mikolajewicz, R. Voss, 1997: The stability of the thermohaline circulation in a Coupled Ocean-Atmosphere General Circulation Model. *Climate Dyn.*, **13**, 325-347.

Timmermann, A., M. Latif, R. Voss and A. Grötzner, 1998: Northern Hemispheric interdecadal climate variability: A coupled air-sea mode. *J. Climate*, **11**, 1906-1931.

Voss, R., R. Sausen, U. Cubasch, 1998: Periodically synchronously coupled integrations with the atmosphere-ocean general circulation model ECHAM3/LSG. *Climate Dyn.*, **14**, 249-266.

# 3 ENSO-like climate variability and its low-frequency modulation

*“I am, half sick of shadow,” she said, the Lady of Shalott. (Alfred Lord Tennyson, The Lady of Shalott.)*

## 3.1 Abstract

The El Niño-Southern Oscillation is investigated in a multi-century integration conducted with the coupled general circulation model (CGCM) ECHAM3/LSG. The quasi-periodic interannual oscillations of the simulated equatorial Pacific climate system can be understood within the framework of the delayed action oscillator. Through the interplay of equatorial wave dynamics and coupled air-sea interactions an interannual eigen oscillation is excited. It has a characteristic period of 5-8 years. Due to the coarse resolution of the ocean model the ENSO amplitude is underestimated by a factor of three as compared to observations. The model ENSO is associated with rather realistic atmospheric teleconnection patterns. Using wavelet statistics two characteristic interdecadal modulations of the ENSO variance are identified. The origins of a 22 and a 35 year ENSO modulation as well as the characteristic ENSO response to greenhouse warming are discussed.

## 3.2 Introduction

The strongest natural interannual climate fluctuation is the El Niño/Southern Oscillation phenomenon. It can be regarded as an irregular coupled atmosphere-ocean oscillation originating in the tropical Pacific. The warm phase is referred to as El Niño, whereas the cold phase is called La Niña. The ENSO phenomenon represents a famous example of a deviation from the red noise null hypothesis for climate variability (Frankignoul and Hasselmann 1977).

El Niño events occur at intervals of 2-8 years and last typically 12-18 months. They are accompanied by swings in the Southern Oscillation (SO), an interannual see-saw in global

sea level pressure between the eastern and western hemispheres.

ENSO dynamics is considered to be a result of equatorial ocean wave dynamics linked to a positive atmosphere-ocean feedback. An ENSO paradigm which became very influential is the “delayed action oscillator” theory of Suarez and Schopf (1988), Schopf and Suarez (1990) and Battisti and Hirst (1989). The idea is that a weakening of the prevailing westward trade winds along the equatorial Pacific during an El Niño force on the one hand downwelling Kelvin waves. On the other hand the changes in the wind stress force also westward traveling upwelling Rossby waves, which will reflect on the western boundary and reverse the temperature tendency in the eastern Pacific after some delay. This kind of delayed negative feedback gives rise to the phase reversal and hence, to oscillations. According to this picture ENSO has to be regarded as an inherently coupled air-sea mode. The delayed action oscillator theory predicts regular ENSO oscillations. However, we know from observations that ENSO is an irregular phenomenon. The understanding of the possible sources of irregularity is crucial, in order to refine ENSO predictions. Using simple models Münnich et al. (1991) and Tziperman et al. (1994) explain the irregularity of ENSO by deterministic chaos. These results are somewhat confirmed by simulations with intermediate coupled models (e.g. Chang et al. 1994, Jin et al. 1994). On the other hand, the highly irregular nature of ENSO can also be explained by the action of white noise which has been added or multiplied to coupled models (Eckert and Latif 1997, Blanke et al. 1997). In a recent conceptual study (Stone et al. 1998) ENSO dynamics is characterized by an interaction of low dimensional chaos and additive noise. This gives rise to the typical stochastic resonance behaviour (Benzi 1982, Nicholis 1982). Apart from these approaches a series of studies (Lysne et al. 1997, Gu and Philander, 1997, Barnett et al. 1998) focussed on the physical processes that provide an oceanic or atmospheric link between the extratropics and the tropics on decadal time scales and therefore might contribute to ENSO irregularities.

The occurrence of the very strong El Niños of 1982/83, 1997/1998 and of the long lasting warm conditions during 1990-1995 raise the question whether enhanced greenhouse warming, which can be detected at a 95% confidence level (Hegerl et al. 1996), has already changed the ENSO statistics. This question is investigated in two recent studies (Trenberth and Hoar 1996, 1997) adopting simple univariate statistical methods. Basically, one ends up with the problem of estimating the probability of very rare events from short time series. Such estimates are in fact highly sensitive to the statistical model which is used (Rajagopalan et al. 1997).

Two recent studies by Timmermann et al. (1998a) and Timmermann (1998) investigate how ENSO dynamics respond to greenhouse warming. Their analysis is based on a global climate model simulation which simulates ENSO realistically. The authors find that the long-term changes in the tropical Pacific due to greenhouse warming are similar to those observed during present-day El Niños. Furthermore, changes in the mean state lead to a nonlinear response of ENSO dynamics: alterations of the tropical annual cycle, a

breakdown of ENSO phase locking to the annual cycle, abrupt regime shifts, increase of ENSO variance, bimodal splitting of the phase space trajectory and a tendency towards more La Niñas.

Multi-century integrations performed with CGCMs are an important component in understanding the nature of ENSO with respect to both its irregularity and its sensitivity to external forcing. Here we analyze a CGCM integration performed with the ECHAM3/LSG model. Although the model employs rather coarse resolution, it captures the basic physics of ENSO. The relatively low computational costs of this model enable long climate simulations, which are necessary for the understanding of ENSO irregularity.

In Section 3 the delayed action oscillator concept is identified within our multi-century CGCM simulation. The characteristic phase-locking features of ENSO are described in Section 4. The main focus of this investigation is the analysis of ENSO variance modulations which is presented in Section 5. The ENSO response to greenhouse warming is discussed in section 6. A summary of our main findings concludes this chapter.

### 3.3 ENSO physics in a coarse resolution CGCM

Although coarse resolution CGCMs (Meehl 1990, Lau et al. 1992, Meehl et al. 1993, Tett 1995) are not able to simulate ENSO variability fully, some of the principal physical mechanisms of ENSO are captured surprisingly well, as pointed out recently by Knutson et al. (1997). Our study confirms the basic findings of Knutson et al. (1997). This model has been used also to study the interdecadal variability over the Northern Hemisphere (Timmermann et al. 1998b) and to investigate the predictability of interannual and decadal variability (Grötzner et al. 1998). Fig.3.1a shows the time series of the Niño 3 SSTA index (index region:  $150^{\circ}\text{W}$ - $90^{\circ}\text{W}$ ,  $5^{\circ}\text{N}$ - $5^{\circ}\text{S}$ ) for the 700 year integration. The SST anomalies fluctuate on an interannual time scale. A high degree of irregularity is simulated as well as multi-decadal to centennial modulations of the ENSO amplitude. This will be addressed in more detail below. The standard deviation of the annual mean Niño 3 SSTA index in the ECHAM3/LSG model amounts to approximately  $0.2^{\circ}\text{C}$ , which is much too weak compared to observations, which attain values of at least  $0.6$ - $0.7^{\circ}\text{C}$ . Fig.3.1b shows a variance spectrum of the model's Niño 3 index. The spectrum is calculated using a Bartlett window with 15 degrees of freedom. The result is compared to the red noise null-hypothesis for climate variability (Hasselmann 1976, Frankignoul and Hasselmann 1977). The 95% significance level for rejecting the null-hypothesis is also depicted. The Niño 3 SSTA spectrum is characterized by a broad band of enhanced variability in the range of 4 to 8 years (with maxima at 5.5 and 8 years).

Fig.3.2 displays a collection of 6 lag regression patterns which were obtained by regressing the bandpass filtered (transparent for periods between 4-7 years) Niño 3 SSTA index on the heat content anomaly field of the upper 575m for lags of -3,-2,-1,0,1,2 years, respectively.

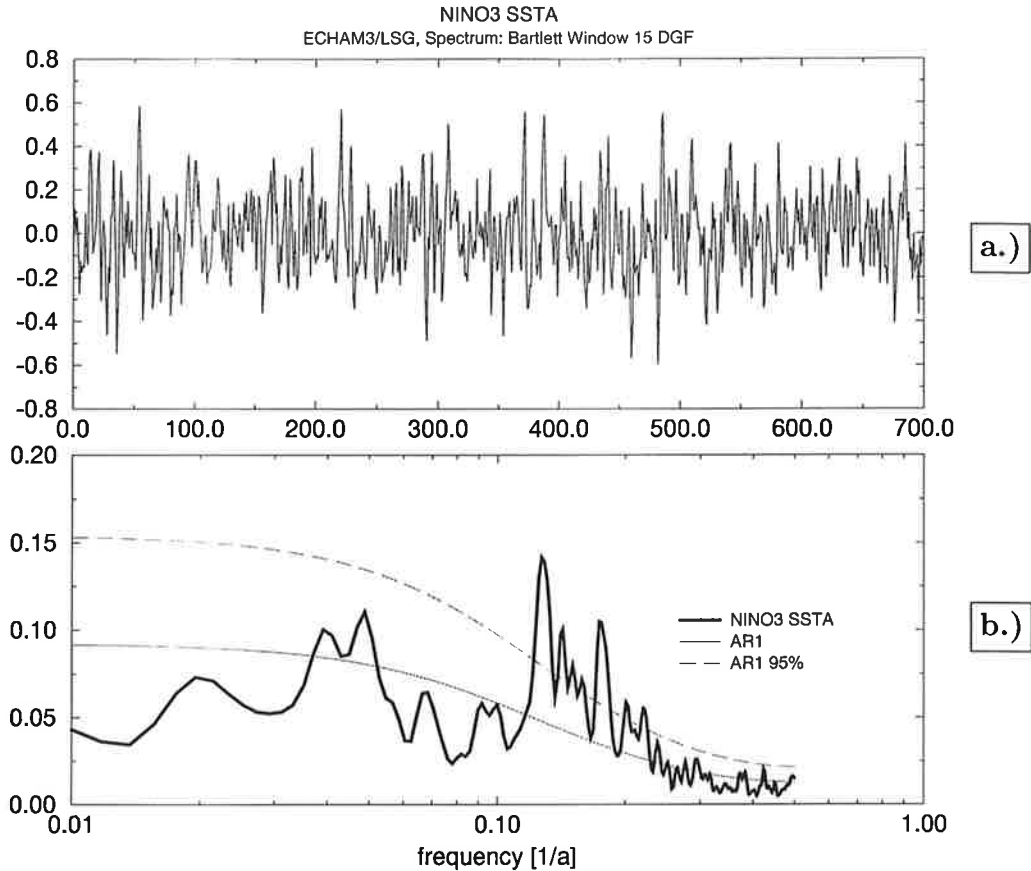


Figure 3.1: a) The Niño 3 SSTA index obtained from yearly data, b.) Power Spectrum of a.) obtained by using a Bartlett window with 15 degrees of freedom. The equivalent red noise process and its 95% confidence limit are displayed.

Negative lags indicate that the heat content is leading the SSTA index. Starting with lag -3 years the typical La Niña situation is simulated with an anomalously shallow thermocline in the eastern equatorial Pacific and off-equatorial Rossby wave-like signals in the west with opposite polarity. This warm anomaly seems to reflect into Kelvin wave-like signals at the western boundary, which carry the signal slowly eastward (lags -2 and -1). By definition the mature phase of El Niño is simulated at lag 0 with anomalous warm waters in the eastern tropical Pacific. The further evolution at lags 1 and 2 years is just the reverse of that discussed for lags -2 and -1 years. This series of patterns gives us confidence that the essential dynamics of ENSO are captured reasonably well by our coarse resolution model, although the ENSO signal is much too weak. The wave dynamics which is considered to be a crucial part within the framework of the “delayed action oscillator” obviously exist in the model. In order to study the vertical temperature evolution which is associated with the ENSO mode, lag regression patterns are calculated of the Niño 3 SSTA index upon the subsurface temperature anomaly field of the upper 500m along  $2.8^{\circ}\text{S}$  for various

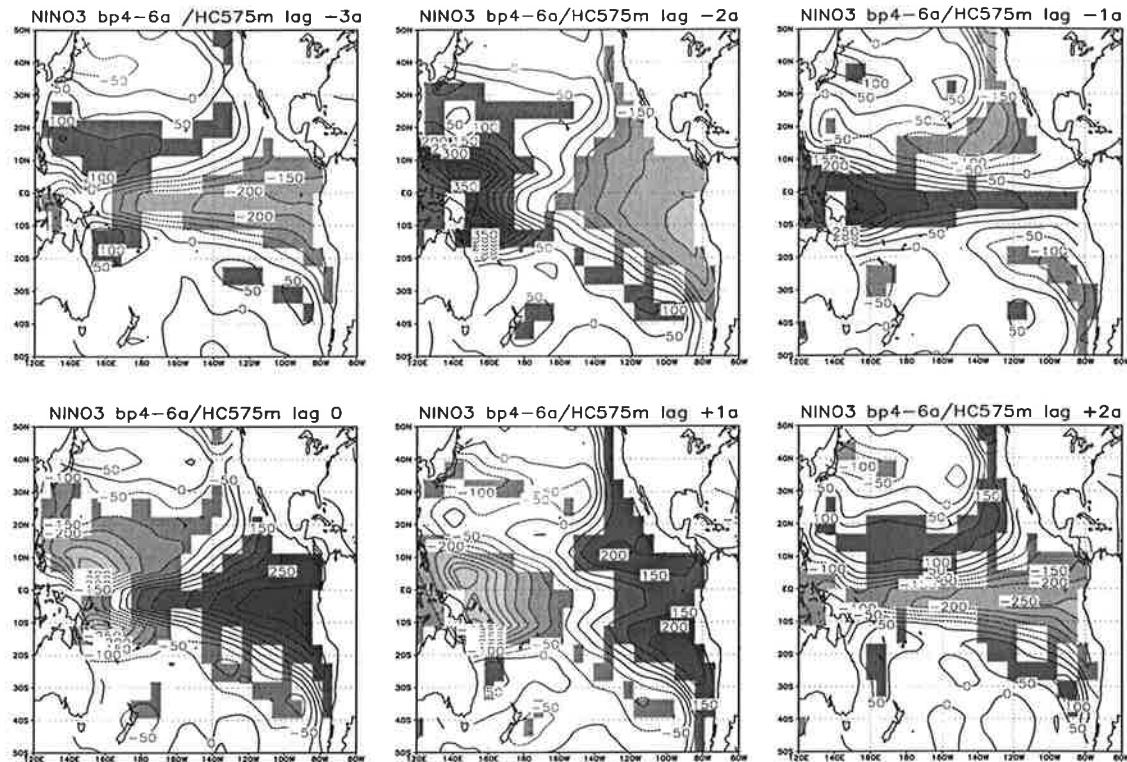


Figure 3.2: Lag regression patterns of the Niño 3 SSTA index on the heat content field of the upper 575m for lag -3,-2,-1,0,1,2 years.

lags (Fig.3.3). These regression patterns can be regarded as the 3-d extension to Fig.3.2. Starting at lag -3 typical La Niña conditions are simulated. At lags -2 and -1 an eastward propagation of positive subsurface temperature anomalies is seen, replacing the original cold anomalies. These positive anomalies originated from the reflection of the downwelling Rossby waves at the western boundary of the tropical Pacific, as can be seen from Fig.3.2. Lag 0 depicts the mature El Niño phase with maximum warming located slightly east of the dateline at around  $160^{\circ}\text{W}$ . Lags +1,+2 characterize the phase reversal back to the La Niña stage.

Another important component of ENSO is the positive atmosphere-ocean feedback. This is analyzed by regressing the atmospheric anomaly fields of SLP, precipitation and zonal wind stress onto the Niño 3 SSTA index (Fig.3.4). The teleconnection pattern for SLP (Fig.3.4a) is consistent with the Southern Oscillation (Berlage 1957), with anomalous low pressure east of  $160^{\circ}\text{W}$  and anomalously high pressure over the Indian Ocean and western Pacific. This justifies the denotation “El Niño-Southern Oscillation” for the interannual tropical Pacific climate mode simulated in the ECHAM3/LSG model. Maximum warming can be seen in the central Pacific, which is rather unrealistic (Fig.3.4b). This is due to

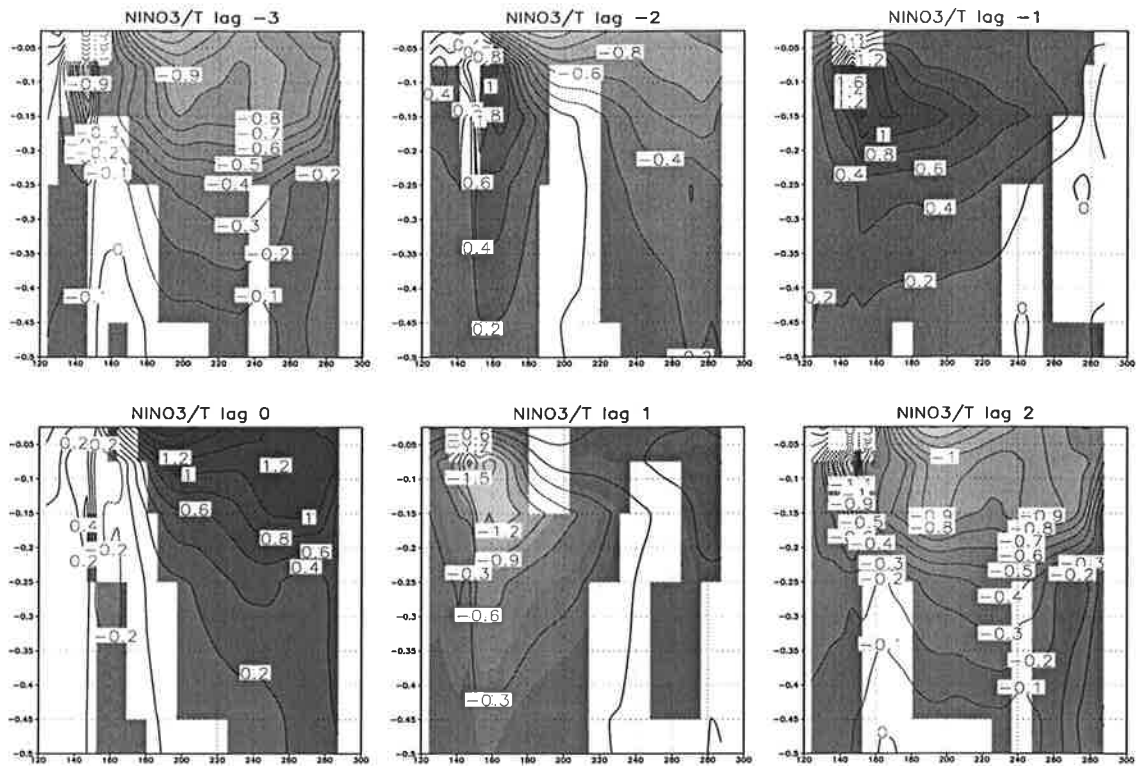


Figure 3.3: Lag regression patterns of the Niño 3 SSTA index upon the subsurface temperature anomaly field along  $2.8^{\circ}\text{S}$  for lag -3,-2,-1,0,1,2 years. The depth unit is kilometer. Significant regressions at the 95% level are shaded.

the misrepresentation of oceanic upwelling processes in our ocean model. Fig.3.4c shows the regression of the SSTA index on the precipitation anomaly field. The model simulates a large increase of precipitation between  $150^{\circ}\text{W}$ - $180^{\circ}$  and anomalously dry conditions to the west, north and south, affecting the climate of Australia and Southeast Asia. In Fig.3.4d the characteristic ENSO related anomaly in the zonal wind stress is displayed. A very important feature of this pattern is the positive anomaly in the western Pacific, which is the expression of weakened South-East trade winds. This zonal stress anomaly serves as a positive feedback in the ENSO life-cycle. A positive SSTA in the eastern tropical Pacific reduces the SST gradient and hence the position and the strength of the Walker circulation. This leads to a reduction of the trade winds at the equator, causing a deepening of the thermocline and reduced upwelling in the eastern Pacific. These processes promote a further amplification of the initial positive SSTA. Such unstable air-sea interactions are the reason why ENSO has to be regarded as a coupled air-sea mode.

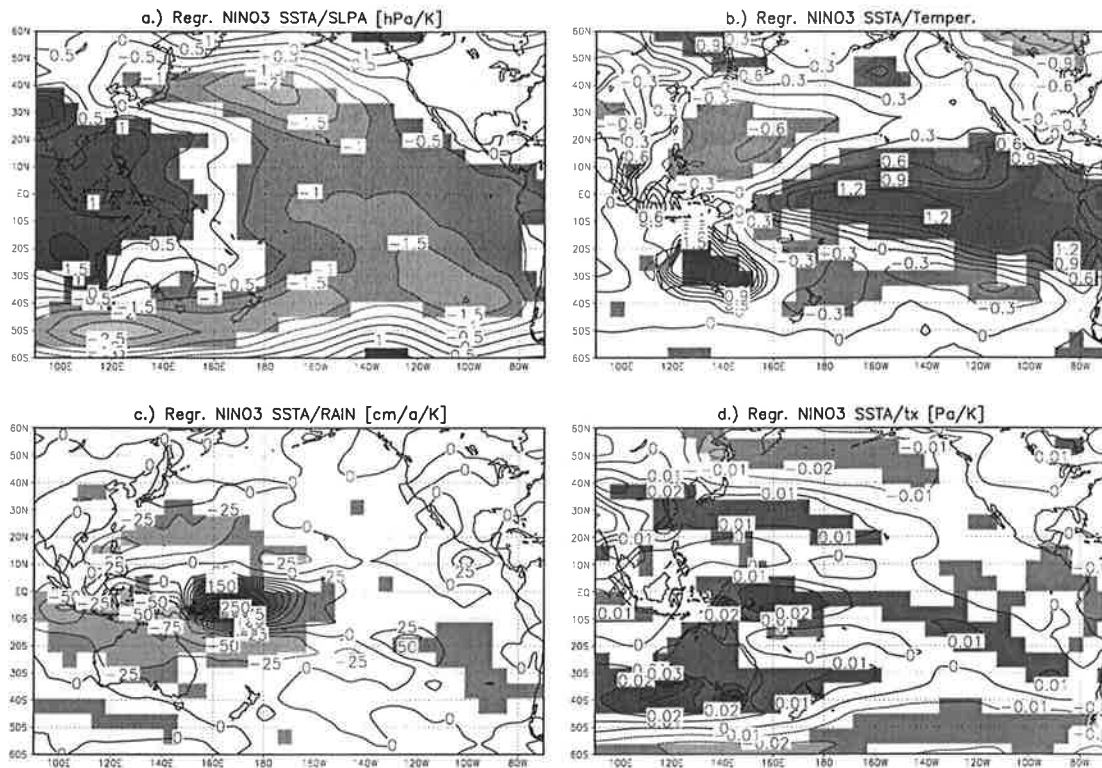


Figure 3.4: Lag 0 Regression patterns of the Niño 3 SSTA index and the anomaly patterns of SLP, precipitation, SST and the zonal component of the wind stress. The shaded regions highlight regression coefficients which are significantly different from zero at the 95% significance level.

### 3.4 Phase Locking to the Annual Cycle

A characteristic feature of ENSO is its phase locking to the annual cycle. Maximum temperature anomalies in the eastern equatorial Pacific occur in boreal winter. Many investigations are devoted to this phase locking phenomenon (Jin et al. 1994, Xie 1995, Chang et al. 1994). Phase locking features are quite often regarded as a signature of nonlinear processes governing the system's behaviour.

The phase locking of the simulated model El Niño can be visualized by calculating the standard deviation of the monthly mean Niño 3 SSTA for each month separately. A very weak phase locking is simulated with maximum SST variability occurring in November and minimum variability during June (Fig.3.5). The standard deviations are modulated by the annual cycle as about 15 %, whereas observed range is of the order of 60 %. The weakness of this phase locking behaviour in our CGCM may be explained partly by the weakness of the simulated annual cycle itself (Latif et al. 1998) and partly by the weakness of the simulated ENSO phenomenon. Furthermore, the flux corrections applied in the coupled model integration may have an impact on the simulation of the SST annual

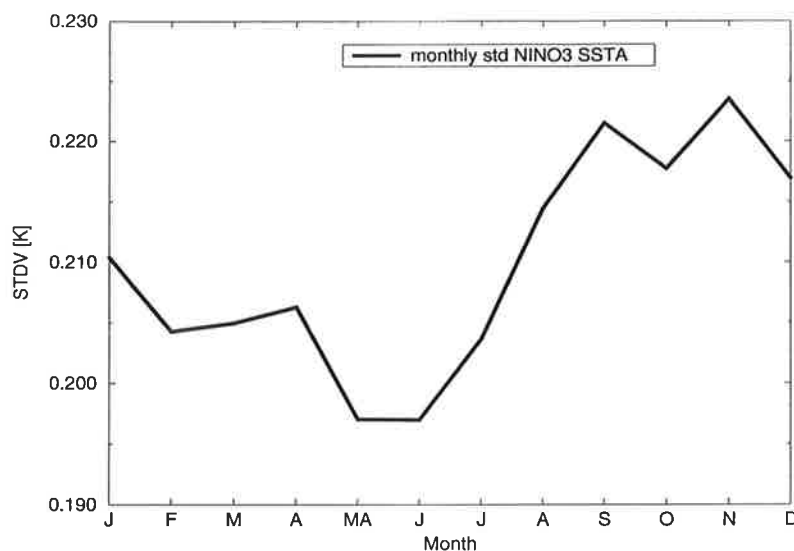


Figure 3.5: Standard deviation of the SSTA in the Niño 3 region as a function of the calendar month.

cycle.

### 3.5 ENSO modulation

In order to study the low-frequency modulation of ENSO, a wavelet analysis on the Niño 3 SSTA is performed. As in the studies of Gu and Philander (1995) and Knutson et al. (1997) a Morlet wavelet decomposition is performed.

Recent studies (Meyers et al. 1993,1994, Weng et al. 1994, Gu and Philander 1995, Mak 1995, Knutson et al. 1997, Torrence and Compo 1998) demonstrate the broad spectrum of possible wavelet applications in climate research. In contrast to Fourier analysis, wavelets provide the appropriate framework to analyze non-stationary and transient signals in an optimal phase space resolving manner. For a review on wavelet theory see Kumar et al. (1994). Wavelets as well as evolutionary Fourier spectra provide a kind of time resolving variance and phase spectra. The result of the wavelet analysis is depicted in Fig.3.6. In order to avoid energy leakage the time series is buffered on both ends by a fitted AR(2) process, which yields rather stable wavelet spectra for the full time-range. Enhanced spectral power is found in the range 3-8 years. During some epochs there is a preference of the time scales from 6-8 years, whereas during other periods the 4-6 year range is the dominating periodicity. In order to obtain the variance modulation of interannual (2-8 years) energies, we compute the absolute square of the wavelet transform and integrate the result over the interannual time-scale range of 2-8 years using a weight factor of the inverse square of the scale parameter. Interdecadal and centennial modulations of the interannual Niño 3 variance are obvious (Fig.3.7). These features are resolved more properly in Fig.3.8 showing the discrete Fourier spectrum of the time series shown in

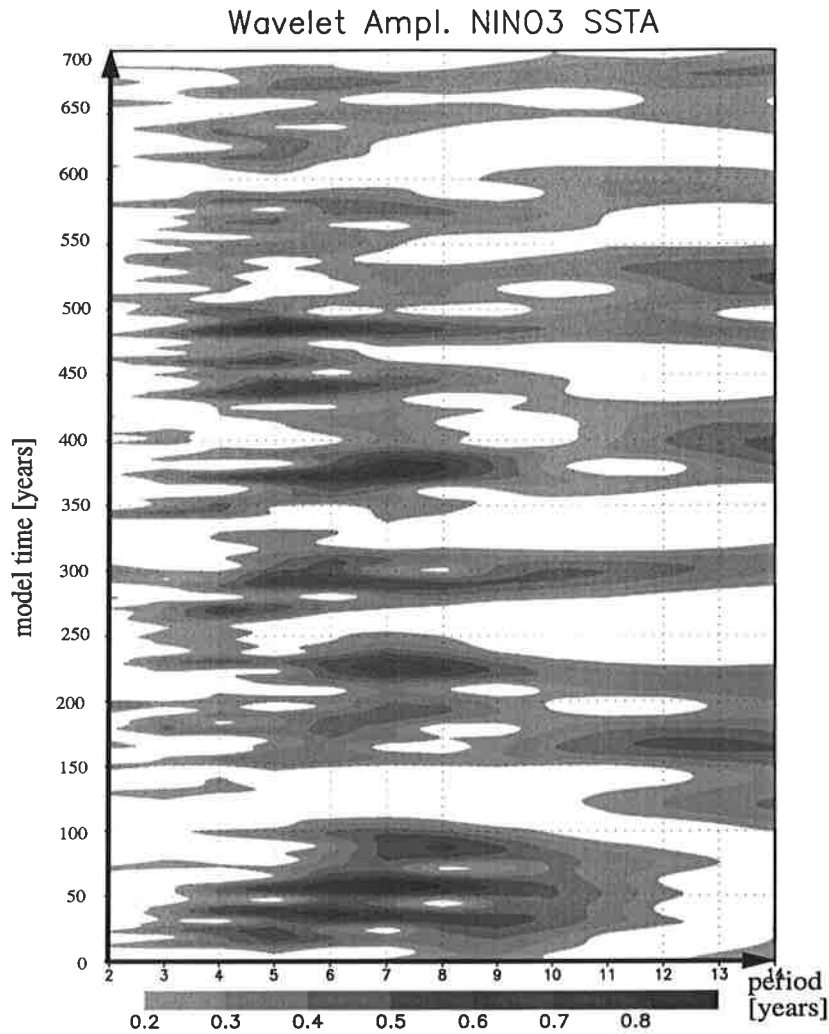


Figure 3.6: Amplitude of a Morlet wavelet decomposition of the Niño 3 SSTA. Units are arbitrary. The x-axis denotes the time scale in years. The y-axis is the time evolution axis of the spectrum for 700 integration years.

Fig.3.7. This spectrum clearly shows two interdecadal peaks at periods of 22 and 35 years. Furthermore, enhanced spectral power is found at a period of about 100 years. In order to test whether these modulations of the interannual variance are just the expression of the stochastic nature of ENSO or whether they reflect some possible deterministic oscillatory influence of other system components, a set of AR(2) surrogates ( $100 \times 1000$  samples) is generated and analyzed in the following way. The surrogates are wavelet transformed using the Morlet mother wavelet. The wavelet transform is then integrated over the time-scale range of 2-8 years and the resulting time series is then Fourier transformed. Each of the 100 Monte Carlo sets is subject to this procedure, and one obtains a mean spectrum and confidence intervals for these spectra. Apparently, the interannual energy

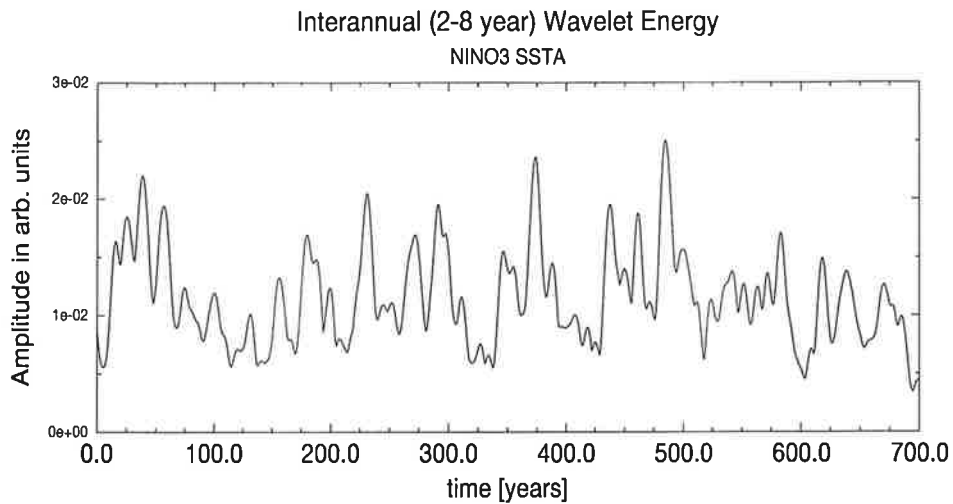


Figure 3.7: Interannual Wavelet energy of Niño 3 SSTA index.

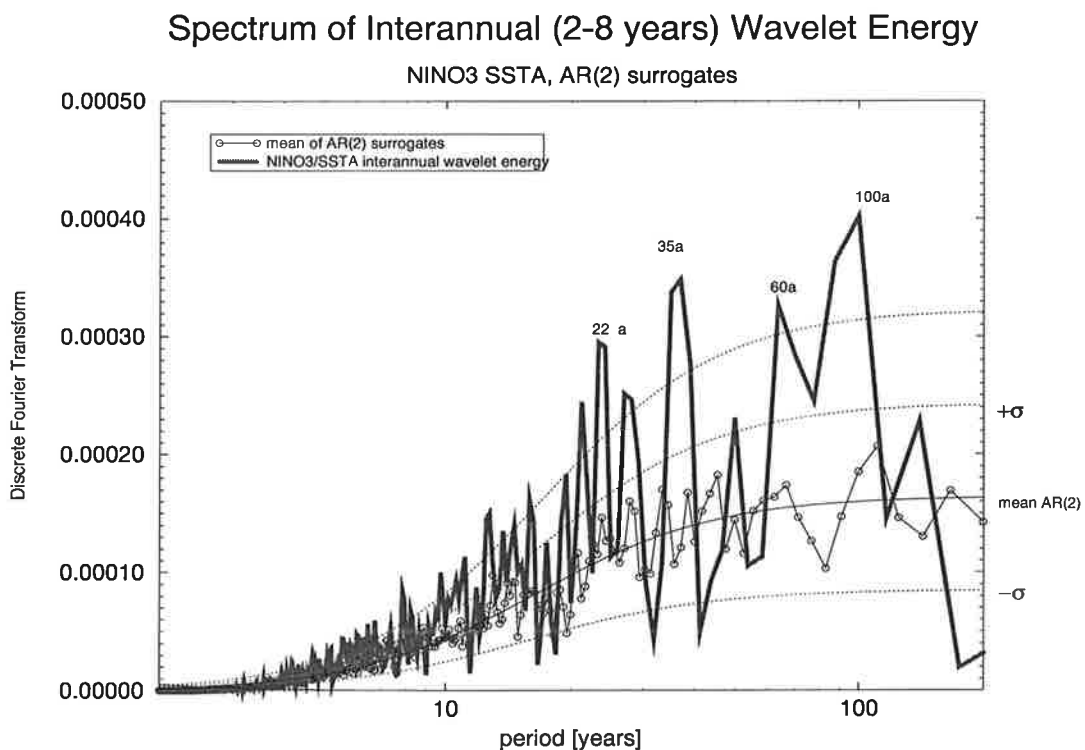


Figure 3.8: Discrete power spectrum of the time series shown in Fig.3.7 using a Bartlett window. The confidence intervals for a set of AR(2) surrogates is obtained from a Monte Carlo simulation.

modulations on the 22-, 35- and 100-year time scales deviate substantially from the  $2\sigma$  confidence interval of the AR(2) surrogates. A very simple explanation of the 22 year ENSO modulation can be provided by the superposition of the two distinct ENSO time scales with periods of 5.8 and 8 years (Fig.3.1b).

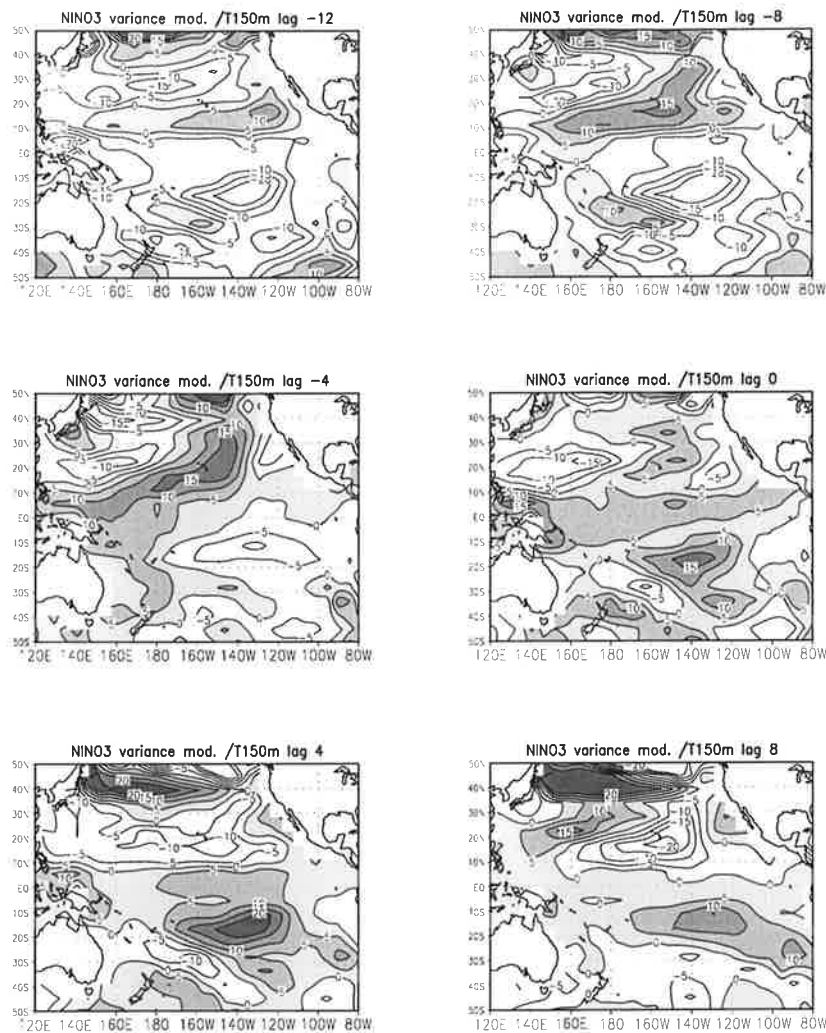


Figure 3.9: Lagged regressions of the interannual wavelet energy time series (Fig.3.7) upon the anomaly field of temperature at 150m depth. Prior to the analysis all data were detrended and the time series of Fig.3.7 was bandpass filtered around 30-50 years. The figures depict lag regressions for lags -12,-8,-4,0,4,8 years. Units are  $^{\circ}\text{C}$  per one unit of wavelet energy. Typical fluctuations of interannual wavelet energy are in the order of 0.005.

The second interdecadal modulation of the local ENSO energy with a characteristic time scale of 35 years is investigated by regressing the interannual wavelet energy time series of Fig.3.7 upon the subsurface temperature field at 150m depth at various lags (Fig.3.9). 12 years prior to the maximum variance a positive subsurface temperature anomaly is found between  $10^{\circ}\text{N}$  and  $20^{\circ}\text{N}$  with a maximum near the west coast of North America. This anomaly propagates southwestward, reaching the warm pool region at lag -4 years. Eventually it penetrates into the equatorial thermocline at lags 0 and 4 years. There is

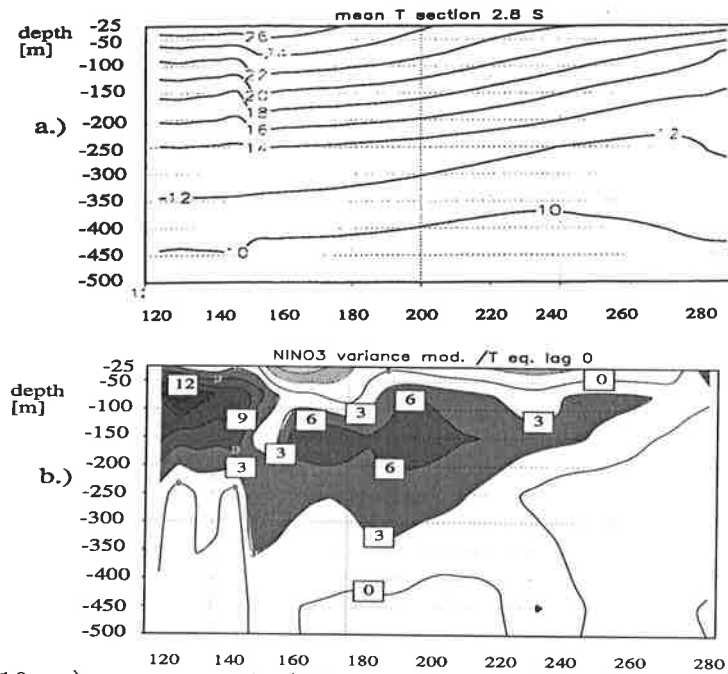


Figure 3.10: a.) mean vertical temperature profile along  $2.8^{\circ}\text{S}$ . b.) Lag 0 regression of the interannual wavelet energy time series (Fig.3.7) upon the anomaly field of temperatures along a section at  $2.8^{\circ}\text{S}$ . Prior to the analysis all data were detrended and the time series of Fig.3.7 was bandpass filtered around 30-50 years. Units are  $^{\circ}\text{C}$  per one unit of wavelet energy. Typical fluctuations of interannual wavelet energy are in the order of 0.005.

also evidence of a positive subsurface temperature anomaly which propagates in from the Southern Hemisphere into the tropical Pacific. One possible and very effective mechanism for changing the magnitude of ENSO fluctuations is to perturb the temperature structure across the equatorial thermocline (Stone et al. 1998, Timmermann et al 1998). The overall equatorial temperature structure (Fig.3.10a) in our model is rather diffusive and a pronounced thermocline is hardly detectable. Furthermore, the strongest upwelling signal can be seen slightly east of the dateline, rather than close to the South American coast as in reality<sup>1</sup>. During the time of maximum variability a positive temperature anomaly affects the mean temperature stratification along the equator (Fig.3.10 b). Since the mean thermocline is not well pronounced, it is difficult to assess whether the thermocline becomes sharper or not. However, given the rather diffusive thermocline in our model the warm anomaly is likely to strengthen the thermocline, which would explain the enhanced ENSO variability at this stage. The 35 year time scale of this modulation is reminiscent of the interdecadal Northern Hemisphere mode described chapter 5 and by Timmermann et

<sup>1</sup>Thus, our results and conclusions regarding the mechanisms which change ENSO variability have to be taken with some caution.

al. (1998b). Additional statistical analyses of heat content anomalies (not shown) reveals that the 35 year Northern Hemispheric mode is in fact associated with modulations of ENSO variance on the same time scale<sup>2</sup>.

### 3.6 ENSO response to greenhouse warming

In the last section we investigated natural changes of ENSO variability which occur at preferred periods of 22, 35 and 100 years. We analyze also a global warming scenario run with the ECHAM3/LSG CGCM forced by the IPCC greenhouse gas forcing scenario IS92a (IPCC 1992) for the equivalent CO<sub>2</sub> concentrations. Fig.3.11 displays the probability distributions of the simulated Niño 3 SSTA for the control and the greenhouse warming simulation. A small change of variance can be detected for the probability distribution of the last 100 years as compared to the control run. F-test analysis yields a significance level for rejecting the hypothesis of constant variance of about 90%. Furthermore, an indication of bimodality in the CO<sub>2</sub> run can be seen, which is due to a sudden jump of the Niño 3 SST to another state during the last 10 years of the scenario simulation.

In a recent study by Timmermann et al. (1998) the issue of ENSO response to greenhouse warming was addressed by analyzing a global warming simulation which was conducted with the higher resolution CGCM ECHAM4/OPYC3. This simulation showed a remarkable sensitivity to greenhouse warming. Some of the changes found can be regarded as expressions of a nonlinear and nonstationary response to external forcing. The most important change in the greenhouse warming simulation with the ECHAM4/OPYC3 model was a sharpening of the thermocline. In our coarse resolution model ECHAM3/LSG the thermocline sharpness is strongly underestimated as compared to the ECHAM4/OPYC integration. This might explain the relative insensitivity of ENSO to global warming in the ECHAM3/LSG model.

### 3.7 Summary

It is shown that in this CGCM the complex interactions between the tropical Pacific Ocean and the atmosphere are captured in a reasonable manner. Although, the simulated ENSO variability is too weak as compared to observations and the associated time scale too long, fundamental features of observed ENSO dynamics are reproduced in the ECHAM3/LSG simulation:

- Alternation of down- and upwelling signals in the equatorial thermocline, providing the memory of ENSO, consistent with the delayed action oscillator concept.

---

<sup>2</sup>The identified interannual-interdecadal scale interactions were confirmed also by other independent methods. Bispectrum and bicoherence analyse (Hasselmann and Munk 1963) yield significant scale interactions in the Niño 3 SSTA time series for the period dupletts (6,40) and (8,20) years.

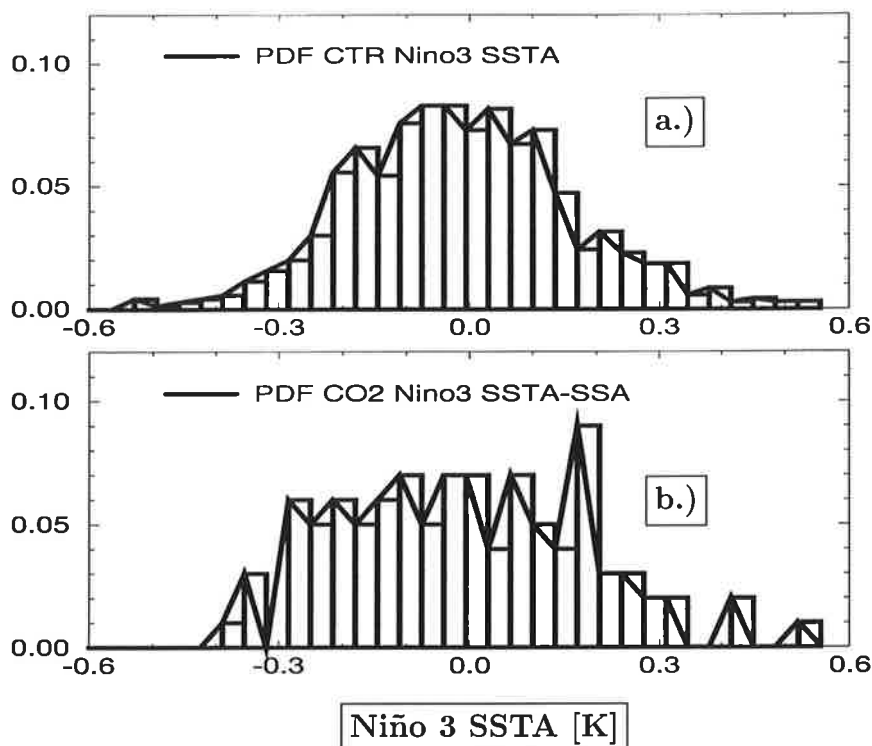


Figure 3.11: Normalized frequency distribution of annual SST anomalies in the Niño 3 region for the 700 year control integration and the greenhouse warming simulation. Prior to the analysis the first SSA mode (describing the trend) is subtracted from the data. a.) Niño 3 histogram as obtained from the control run. b.) estimated histogram for the last 100 years of the CO<sub>2</sub> run.

- Realistic teleconnections.
- Phase locking of ENSO to the annual cycle (although too weak).

Furthermore, we discussed the origin of variance modulations in the simulated ENSO behaviour. The identified 22 years amplitude modulation arises possibly from a linear superposition of the 5.8 and 8 year peak in the ENSO spectrum.

The 35 year amplitude modulation results from an interaction with a 35 year climate mode of the Northern Hemisphere which is described in Timmermann et al. (1998a). Subsurface temperature anomalies are generated in the eastern subtropical Pacific and propagate southwestwards. After 8 years these anomalies penetrate into the equatorial thermocline and change the statistics of ENSO-like fluctuations. Warm anomalies tend to be followed by strong variability whereas cold anomalies are accompanied by low ENSO energy. Direct mean wind forcing does not play a key role in triggering changes in the level of ENSO variability. This study can be seen as an attempt to highlight time scale interactions in the climate system, namely the interaction between interdecadal climate

variability and ENSO and greenhouse warming and ENSO. Greenhouse warming, however seems to have only a minor impact on the ENSO statistics in this particular model.

### 3.8 References

Barnett, T.P., D. Pierce and M. Latif, 1998: Interdecadal Interactions Between the Tropics and Midlatitudes in the Pacific Basin. submitted to *Science*.

Battisti, D.S., and A. C. Hirst, 1989: Interannual Variability in a Tropical Atmosphere-Ocean system: Influence of the Basic State, Ocean Geometry and Nonlinearities. *J. Atmos. Sci.*, **46**, 1687-1712.

Benzi, R., A. Sutera, A. Vulpiani, 1982: Stochastic resonance in climatic change. *Tellus*, **34**, 10-16.

Berlage, H.P., 1957: Fluctuations in the general atmospheric circulation of more than one year, their nature and their prognostic value. *K. Ned. Meteor. Inst. Meded. Verh.*, **69**, 152 pp.

Blanke, B., J.D. Neelin, and D. Gutzler, 1997: Estimating the Effect of Stochastic Wind Stress Forcing on ENSO irregularity. *J. Climate*, **10**, 1473-1486.

Chang, P., B. Wang, T. Li, and L. Ji, 1994: Interactions between the seasonal cycle and ENSO-frequency entrainment and chaos in a coupled atmosphere-ocean model. *Geophys. Res. Lett.*, **21** No. 25, 2817-2820.

Cubasch, U., Hegerl G.C., Voss R., Waszkewitz J. and Crowley T. J., 1997: Simulation of the influence of solar radiation variations on the global climate with an ocean-atmosphere general circulation model. *Clim. Dyn*, **13**, 757-767.

Eckert, C. M. Latif, 1997: Predictability of a Stochastically Forced Hybrid Coupled Model of El Niño. *J. Climate*, **10**, 1488-1504.

Frankignoul, C., and K. Hasselmann, 1977: Stochastic climate models, II, Application to sea-surface temperature variability and thermocline variability. *Tellus*, **29**, 284-305.

Grötzner, A., M. Latif, A. Timmermann and R. Voss, 1998: Interannual to Decadal Predictability in a Coupled Ocean-Atmosphere General Circulation Model. *J. Climate* submitted.

- Gu D., S.G.H. Philander, 1995: Secular Changes of Annual and Interannual Variability in the Tropics during the Past Century. *J. of Climate*, **8**,864-876.
- Gu D., S.G.H. Philander, 1997: Interdecadal Climate Fluctuations That Depend on Exchanges Between the Tropics and Extratropics. *Science*, **275**, 805-807.
- Hasselmann, K., W. Munk and G. MacDonald, 1963: Bispectra of ocean waves. *Time Series Analysis*, Rosenblatt, Ed. J. Wiley, 125-139.
- Hasselmann, K.,1976: Stochastic climate models, Part I: Theory. *Tellus*, **28**, 473-485.
- Hasselmann, K., Bengtsson L., Cubasch U., Hegerl G.C., Rodhe H., Roeckner E., v. Storch H., Voss, R. and Waskewitz J. (1995): Detection of anthropogenic Climate Change using a fingerprint method. In: *Proc. Modern Dynamical Meteorology, Symposium in Honor of Aksel Wiin-Nielsen*, (P. Ditlevsen ed.), (ECMWF press), 203-221.
- Hegerl, G.C., H.v. Storch, K. Hasselmann, B.D. Santer, U. Cubasch, P.D. Jones, 1996: Detecting Greenhouse Gas induced Climate Change with an Optimal Fingerprint method. *J. Climate*, **9**, 2281.
- IPCC, 1992: Climate Change 1992. The Supplementary Report to the IPCC Scientific Assessment. Edited by J. T. Houghton, B. A. Callander and S. K. V. Varney. Cambridge University Press, 200 pp.
- Jin, F.-F., J.D. Neelin, and M. Ghil, 1994: El Niño on the Devil's Staircase: Annual subharmonic steps to chaos. *Science*, **264**, 70-72.
- Knutson, T.R., S. Manabe and D. Gu 1997: Simulated ENSO in a Global Coupled Ocean Model: Multidecadal Amplitude Modulation and CO<sub>2</sub> Sensitivity. *J. Climate*, **10**, 138-161.
- Kumar P., Foufoula-Georgiou E., Wavelet Analysis in Geophysics: An Introduction; in *Wavelets in Geophysics* E. Foufoula-Georgiou, P. Kumar (eds.), 1-43, Academic press 1994.
- Latif M. and coauthors, 1998: The El Niño simulation intercomparison project (ENSIP). in preparation.
- Lau, N.C., S.G.H. Philander and M.J. Nath, 1992: Simulation of ENSO-like phenomena

- with a low resolution coupled GCM of the global ocean and atmosphere. *J. Climate*, **5**, 284-307.
- Lysne, J., P. Chang and B. Giese, 1997: Impact of the Extratropical Pacific on Equatorial Variability. *Geophys. Res. Lett.*, **24**, 2589-2592.
- Mak M., Orthogonal Wavelet Analysis: Interannual Variability in the Sea Surface Temperature. *Bull. of Am. Met. Soc.*, **76**, 2179-2186, 1995.
- Meehl, G.A., 1990: Seasonal cycle forcing of El Niño-Southern Oscillation in a global ocean-atmosphere model. *J. Climate*, **3**, 72-98.
- Meehl, G.A., G.W. Branstator and W.M. Washington, 1993: Tropical Pacific interannual variability and CO<sub>2</sub> climate change. *J. Climate*, **6**, 42-63.
- Meyers S.D., Kelly B.G., O'Brien J.J., 1993:, An introduction to Wavelet Analysis in Oceanography and Meteorology: With Application to the Dispersion of Yanai Waves. *Mon. Weath. Rev.*, **121**, 2858-2866.
- Meyers S.D., O'Brien J.J., 1994: Spatial and temporal 26-day SST variations in the equatorial Indian Ocean using wavelet analysis. *Geophys. Res. Lett.*, **21**, 777-780.
- Münnich, M., M. A. Cane and S. E. Zebiak 1991: A Study of Self-excited Oscillations of the Tropical Ocean-Atmosphere System, Part II: Nonlinear Cases. *J. Atm. Sci.*, **48**, 1238-1248.
- Nicolis, C. 1982: Stochastic aspects of climatic transitions – response to a period forcing. *Tellus*, **34**, 1-9.
- Rajagopalan, B., U. Lall, and M. Cane, 1997: Anomalous ENSO Occurrences: An Alternate View. *J. Climate*, **10**, 2351-2357.
- Ropelewski, C.F.: 1992: Predicting El Niño events. *Nature*, **356**, 476-477.
- Schopf, P.S., and M.J. Suarez, 1990: Ocean Wave Dynamics and the Time Scale of ENSO. *J. Phys. Oceanogr.*, **20**, 629-645.
- Stone, L., P.I. Sagarin, A. Huppert and C. Price 1998: El Niño Chaos: The potential role of noise and stochastic resonance on the ENSO cycle. *Geophys. Res. Letters*, **25**, 175-178.

- M.J. Suarez, and Schopf, P.S. 1988: A delayed action oscillator for ENSO. *J. Atmos. Sci.*, **45**, 3283-3287.
- Tett, S., 1995: Simulation of El Niño-Southern Oscillation-like variability in a global AOGCM and its response to CO<sub>2</sub> increase. *J. Climate*, **8**, 1473-1502.
- Timmermann, A., J. Oberhuber, A. Bacher, M. Esch, M. Latif, E. Roeckner, 1998a: ENSO response to greenhouse warming. submitted to *Nature*.
- Timmermann, A., M. Latif, R. Voss, A. Grötzner, 1998b: Northern Hemispheric Interdecadal Variability: A coupled air-sea mode. *J. Clim.* **11**, 1906-1931.
- Timmermann, A., 1998: Detecting the Nonstationary Response of ENSO to Greenhouse Warming, *J. Atmosph. Sc.*, accepted.
- Torrence, C., G.P. Compo, 1998: A Practical Guide to Wavelet Analysis. *Bull. of the Am. Meteorolog. Soc.*, **79**, 61-78.
- Trenberth K. and T. Hoar, 1996: The 1990-1995 El Niño-Southern Oscillation event: Longest on record. *Geophys. Res. Lett.*, **23**, 57-60.
- Trenberth K. and T. Hoar, 1997: El Niño and climate change. *Geophys. Res. Lett.*, **24**, 3057-3060.
- Tziperman, E., L. Stone, M. A. Cane and H. Jarosh 1994: El Niño Chaos: Overlapping of Resonances Between the Seasonal Cycle and the Pacific Ocean-Atmosphere Oscillator. *Science*, **264**, 72-74.
- Voss, R., R. Sausen, U. Cubasch, 1998: Periodically synchronously coupled integrations with the atmosphere-ocean general circulation model ECHAM3/LSG. *Climate Dyn.*, **14**, 249-266.
- Weng H., Lau K.-M., Wavelets, Period Doubling and Time-Frequency Localization with Application to Organization of Convection over the Tropical Western Pacific. *J. of Atmos. Sc.*, **51**, 2523-2541, 1994.
- Xie, S.-P., 1995: Interaction between the annual and interannual variations in the equatorial Pacific. *J. Phys. Oceanogr.*, **25**, 1930-1941.

# 4 Decadal Climate Variability in the North Atlantic

“Entities should not be multiplied unnecessarily.” (William of Occam, Quodlibeta, 1320.)

## 4.1 Abstract

On the basis of a multi-century integration conducted with the coupled general circulation model ECHAM3/LSG we investigate the dynamics of decadal North Atlantic climate variability. A climate mode with a period of 14-18 years is identified, which has a signature both in the atmosphere and the ocean. This mode can be understood in terms of the coupled air-sea mode concept. The long time scale is provided by oceanic processes which involve the subtropical and subpolar gyres. The atmosphere is sensitive to mid-latitude sea surface temperature anomalies and serves as an amplifier for oceanic temperature anomalies. Furthermore, the atmospheric response has the potential to change the Sverdrup balance in the ocean gyres, thereby forcing a delayed negative feedback. Overall this mode is characterized by a tripole-like pattern in the ocean and the North Atlantic Oscillation in the atmosphere. Decadal sea ice fluctuations in the North Atlantic are forced by anomalous cold and warm air advection. They contribute only marginally to the dynamics of the decadal climate mode.

## 4.2 Introduction

Rigorous analysis of the physics of North Atlantic climate variability started with the pioneering work of Bjerknes (1964). In this early work Bjerknes discovered the main physical processes which are responsible for the generation of interannual and interdecadal climate variability<sup>1</sup> in the North Atlantic region. Interannual sea surface temperature

---

<sup>1</sup>“Interannual”, “decadal” and “interdecadal” variability denote the time scale ranges 2-8, 8-20, 20-70 years, respectively.

(SST) variability is considered to result from atmospheric heat flux variations. This result is supported by recent investigations (Wallace et al 1993, Zorita and Frankignoul 1997 and Delworth 1996). The interannual climate variations in the North Atlantic are associated with a characteristic atmospheric pattern – the North Atlantic Oscillation (NAO)<sup>2</sup>. Furthermore, Bjerknes showed on the basis of a very short and sparse dataset that interdecadal climate variability in the North Atlantic region appears to be largely governed by ocean dynamics. The important role of ocean dynamics in this context is also emphasized by Deser and Blackmon (1993) and Kushnir (1994) on the basis of almost century-long observational datasets and on the basis of a CGCM simulation by Delworth et al. (1993) and Timmermann et al. (1998).

The observational study of Deser and Blackmon (1993) reveals further that apart from interannual and interdecadal variability pronounced decadal climate variability can be found in the North Atlantic involving both atmospheric and oceanic dynamics. In their investigation a time scale of approximately 9 years is identified in North Atlantic SST anomalies during the pre-war period, whereas in the post-war era significant variability in the SST anomaly fields with a 12 year period is observed. Deser and Blackmon (1993) speculate that one possible origin of the decadal-scale oscillation in the North Atlantic might be the presence of a positive atmosphere-ocean feedback. In this scenario mid-latitude SST anomalies are not just passive but have also the potential to change the atmosphere in such a way that on the one hand the initial SSTA is reinforced and on the other hand a delayed negative feedback via ocean dynamics can be initiated. However, observations are rather sparse and not sufficient to fully explore the physical mechanisms being responsible for the generation of decadal-scale climate variability. Coupled general circulation modelling studies might help to shed some light on the relevant physical processes.

In order to explain decadal variability in the North Atlantic climate system, Grötzner et al. (1998) analyze a 100 year present day climate integration performed with the CGCM ECHO1. This model simulates a quasi-decadal North Atlantic mode which, as far as SLP and SST anomalies are concerned, is very similar to that described in Deser and Blackmon (1993). The study of Grötzner et al. (1998) suggests that the decadal North Atlantic mode can be interpreted as a slightly modified counterpart of the North Pacific decadal mode described in Latif and Barnett (1994,1996). Unstable air-sea interactions associated with anomalous oceanic temperatures and an anomalous NAO as well as the slow oceanic adjustment processes due to changes in the wind stress curl are crucial constituents of this North Atlantic mode. However, it should be noted that in the modelling studies of Latif and Barnett (1994) and Grötzner et al. (1998) a relaxation towards observed climatological boundary values is applied poleward of 60°S and 60°N. This attenuates the

---

<sup>2</sup>The NAO can be regarded as a seesaw that modulates the mean pressure gradient between the Icelandic Low and the Azores High. The NAO governs e.g. the winter climate over Europe and Greenland.

high latitude internal variability of the model and in particular the processes which are associated with changes of the thermohaline circulation (THC).

In a recent modelling approach (Selten et al. 1998) a simplified coupled atmosphere-ocean model (ECBILT) is used in an investigation of decadal climate dynamics in the North Atlantic. In a series of experiments the authors explore the physical mechanisms which are responsible for the generation of a distinct decadal mode. The signature of this mode can be identified in both the atmosphere and the ocean. Their results can be summarized as follows. A positive temperature anomaly south of Greenland is associated with anomalously weak deep convection. Furthermore, this temperature anomaly creates a local geostrophic anticyclonic circulation in the upper ocean which leads to an enhanced horizontal transport of saline water into the convection region. After a lag of a few years the enhanced salinity strengthens the convective activity south of Greenland thereby generating a negative subsurface temperature anomaly. The atmosphere has a stabilizing effect by reinforcing the temperature anomalies south of Greenland. It is argued that such temperature anomalies are responsible for shifting the probability for the NAO regime to occur, and hence imprinting the decadal signal also on the atmosphere. Some elements of this mechanism have been described in an earlier paper by Delworth et al. (1993), who investigated the interdecadal variability in the GFDL model.

### 4.3 Identification of the decadal climate mode

In order to gain further insight into the mechanisms that generate decadal climate variability in the North Atlantic we analyze atmospheric and oceanic fields obtained from the multi-century integration conducted with the coupled general circulation model ECHAM3/LSG. Further information on the simulation of the climate mean state and the climate variability in the North Atlantic can be found in Voss et al. (1998) and Timmermann et al. (1998). A simulation of 700 years length was available for analysis. The decadal climate variability in the North Atlantic is most pronounced during the last 200 years, whereas during other periods it is somehow weaker relative to the other variability modes in the North Atlantic and in particular to the 35 year mode described in Timmermann et al. (1998). Thus, in order to obtain high signal to noise ratios we limit the analysis to the model years 500-700.

A POP analysis (Hasselmann 1988) of the oceanic heat content anomalies<sup>3</sup> is performed. The upper ocean heat content used in this analysis is obtained by integrating the ocean temperatures of the upper 200m. Heat content is an appropriate variable to analyze upper ocean dynamics and in particular slow Rossby waves. Furthermore, it captures also variations of the mixed layer and the thermocline, the later being associated with sea level changes. Prior to the POP analysis the heat content anomalies (the data basis

---

<sup>3</sup>The domain chosen for the analysis is the North Atlantic as depicted in Fig.4.1

consists of annual mean values) are detrended and smoothed with a 3 year running mean filter. The POP analysis yields two dominant modes with estimated oscillation periods of 18 and 40 years, explaining 21% and 14% of the variance of the filtered data, respectively. The 40 year mode (not shown), with a characteristic monopole-like pattern is described in more detail in Timmermann et al. (1998) and Chapter 5. We focus our attention here on the (quasi-)decadal POP mode with a period of 18 years. The period estimate, however, is subject to some uncertainties. The imaginary and real part of the decadal mode are depicted in Fig.4.1.

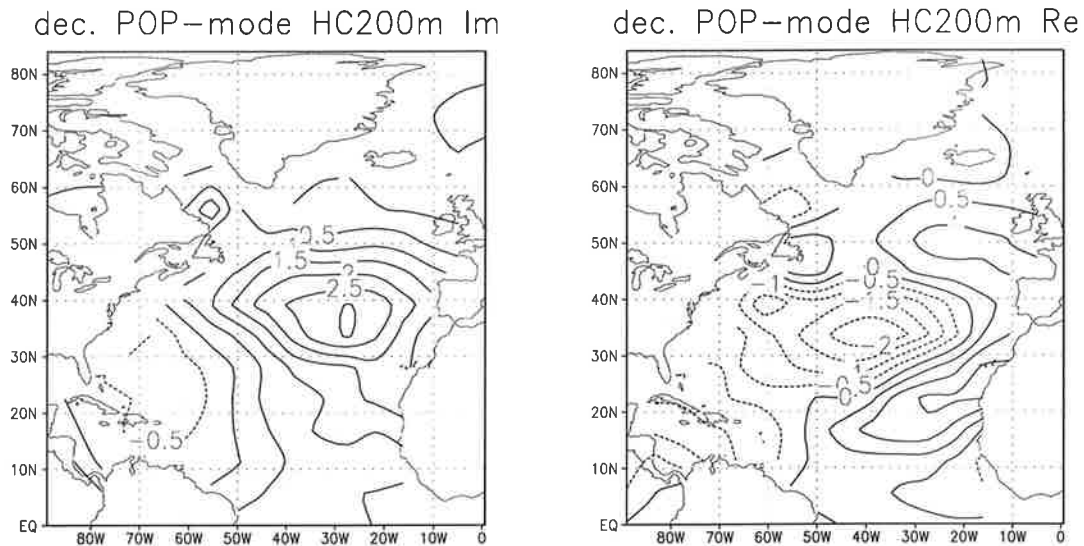


Figure 4.1: POP analysis of the upper ocean heat content anomalies (anomaly field of the temperatures integrated over the upper 200m). Prior to the analysis the data were detrended and smoothed with a 3 year running mean filter. The POP analysis yields a decadal POP mode with an estimated period of 18 years and an e-folding time of 9 years. It explains 21 % of the variance of the detrended and smoothed heat content anomaly field. The left and right panels show the imaginary and real parts of the POP mode respectively.

The evolution of the heat content anomalies according to a single POP mode can be understood as a cyclic sequence of patterns.

$$Im \rightarrow Re \rightarrow -Im \rightarrow -Re \rightarrow \dots \quad (4.1)$$

The imaginary part (Fig.4.1, left side) shows a dipole like pattern. The negative pole is located in the western Sargasso Sea near Florida. A quarter of the rotation period later, during the real-part phase, the negative heat content anomaly has propagated into the middle North Atlantic (Fig.4.1, right side). In the meanwhile, the positive anomaly of

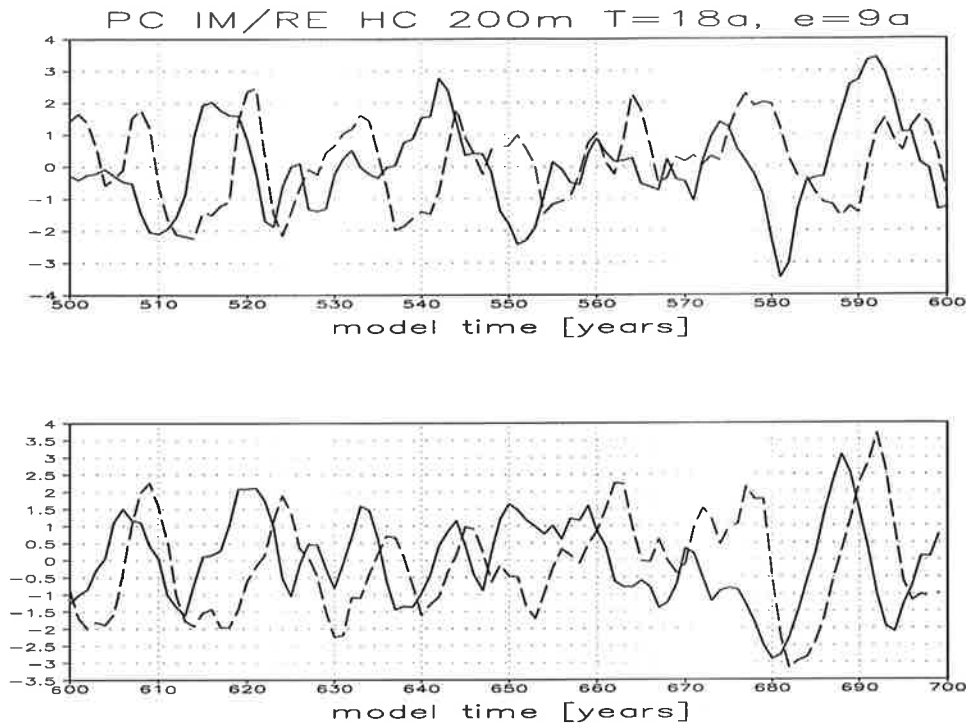


Figure 4.2: POP coefficients of the real and imaginary parts of the POP mode shown in Fig. 4.1. The solid and dashed lines correspond to the imaginary and real parts, respectively.

the imaginary part has split into a southern and a northern branch, creating a tripole like heat content pattern. The amplitudes of both positive branches are somewhat weakened as compared to the imaginary part. The next phase is given by the negative real part of Fig.4.1. A westward propagation of the positive anomaly in the subtropics is simulated. This behaviour and also the deformation of the positive anomaly with latitude is reminiscent of Rossby wave propagation (see e.g. Grötzner et al. 1998, Münnich et al. 1998). A more thorough analysis on this issue will be given below.

In order to validate the POP results it has to be shown that the real and imaginary POP coefficients<sup>4</sup> (shown in in Fig.4.2) are in quadrature with each other at the POP period. A cross spectral analysis of the POP coefficients was performed for this purpose (see Fig.4.3). In the vicinity of the estimated POP period of about 18 years the POP time series are highly coherent. The squared coherence exceeds the the 99% confidence level of zero coherence and the phase amounts to about  $-90^\circ$ . Furthermore, a spectral peak in the variance spectrum of the real part is found. This peak exceeds the 95% confidence level for a red-noise null hypothesis (not shown). The spectral analysis yields a variance maximum at a period of 14-16 years, somewhat smaller than the estimated POP period of 18 years. These results give us confidence that the POP analysis extracted a decadal

<sup>4</sup>which can be obtained by projecting the original data onto the adjoint POP pattern

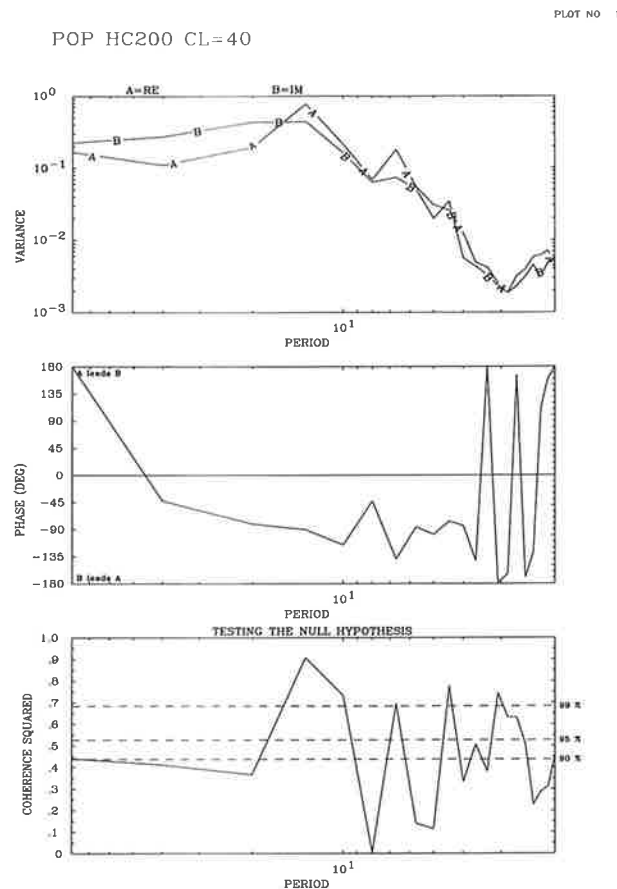


Figure 4.3: Cross spectral analysis of the real (A) and imaginary (B) POP coefficients shown in Fig.4.2. The analysis is performed by applying the Bartlett procedure with a chunk length of 40 years, i.e. 5 chunks. The upper panel displays the variance spectrum of the POP coefficients as a function of period [years]. The middle panel shows the phase spectrum. The lower panel depicts the squared coherency of A and B and also the estimated 90%,95% and 99% confidence levels for zero coherence.

mode with a time scale of 14-18 years, which is distinct from a simple mixed-layer response to atmospheric white-noise forcing.

In order to study whether this mode can also be detected in the atmosphere and in order to derive the characteristic patterns of atmosphere-ocean interactions, we performed a canonical correlation analysis between the detrended sea level pressure (SLP) and sea surface temperature (SST) anomalies. The analysis is based again on annual mean values. Canonical Correlation Analysis (CCA) (Hotelling 1936) yields the joint multivariate correlation structure of a pair of random vectors. The first CCA mode with a canonical correlation of 0.83, accounting for 18% of variance of the SST anomaly field and 52% of the SLP anomaly field is depicted in Fig.4.4. A characteristic tripole pattern in SST and

the typical North Atlantic Oscillation (NAO) dipole pattern in SLP anomalies are simulated, consistent with the observations described by Deser and Blackmon (1993). These two patterns can be understood simply in terms of the ocean mixed layer responding to atmospheric (NAO-like) forcing. Experiments performed with the ECHAM3 model and a mixed layer ocean (not shown here) show not only the same patterns but also a similar level of variability.

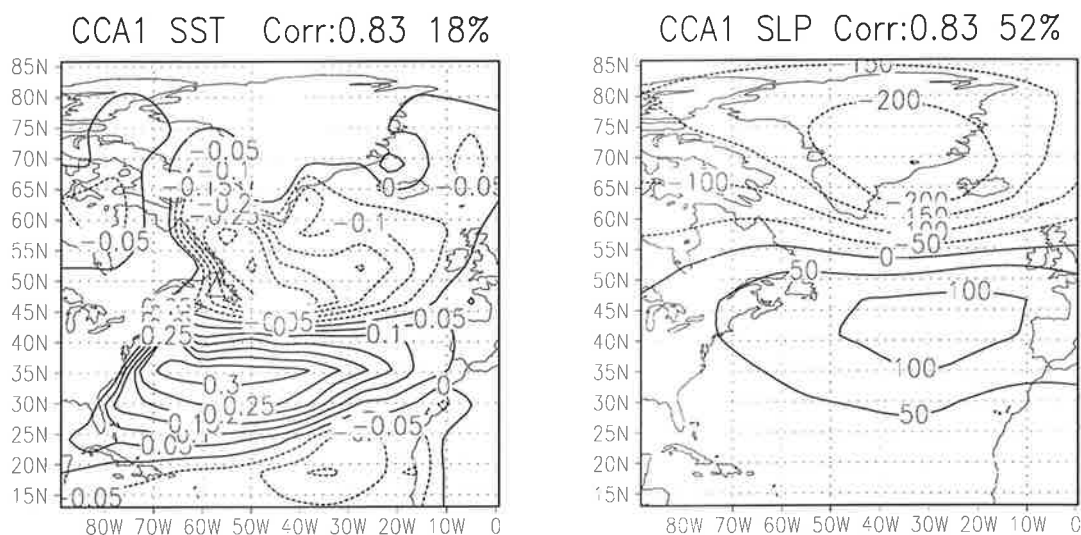


Figure 4.4: The patterns of the leading CCA mode of SST and sea level pressure in the North Atlantic: a) SST pattern [ $^{\circ}\text{C}$ ], b.) sea level pressure pattern [Pa].

Evidence for hidden ocean dynamics, associated e.g. with a characteristic decadal time scale, can be extracted from the principal components of the leading CCA mode (Fig.4.5). In order to highlight the decadal components a 5 year running-mean filter is applied. This figure shows also the real POP coefficient from Fig.4.2. All time series co-vary in phase with each other. Without spectral analysis, just by visual inspection, it becomes clear that both the atmosphere and the ocean are part of the same joint decadal climate mode with a period of 14-18 years. Whether it is the ocean forcing the atmosphere or vice versa, or whether the oscillation can only be generated by the interplay of both climate components, is discussed below.

## 4.4 Decadal ocean dynamics

As mentioned in the introduction of this chapter a paradigm to explain the dynamics of decadal North Atlantic climate variability is the so called “gyre hypothesis” (Grötzner et al. 1998), a slightly modified version of the mechanism proposed for decadal North

## Relationship between POP HC200m and CCA SLP,SST

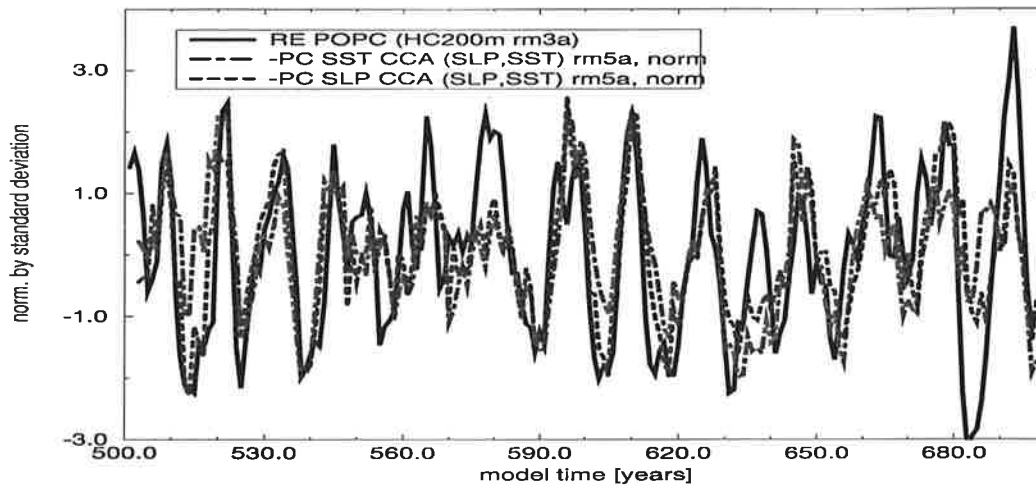


Figure 4.5: Relationship between the principal components of the leading SSTA-SLPA canonical correlation mode (corresponding patterns are shown in Fig.4.4) and the POP coefficient of the real part of the decadal heat content POP mode. The CCA time series are smoothed with a 5 year running mean filter, whereas POP time series is obtained by smoothing the heat content data prior to the POP analysis with a 3 year running mean filter.

Pacific variability by Latif and Barnett (1994). Grötzner et al. (1998) hypothesize that changes in the oceanic temperature structure in mid-latitudes modify the atmospheric baroclinicity, thereby changing also the transient eddy statistics. Averaging over these processes leads to an overall atmospheric response which not only amplifies the initial ocean temperature anomaly but initiates also a delayed negative feedback by perturbing the oceanic Sverdrup balance via an anomalous atmospheric vorticity supply. The gyre adjustment involves Rossby wave propagation and advection of temperature anomalies by the mean ocean circulation. These slow processes are regarded as providing the long-term memory of the decadal climate mode analyzed in the study of Grötzner et al. (1998). The interplay of the positive and delayed negative feedbacks gives rise to a coupled decadal climate oscillation. However, it is still controversial whether the atmosphere responds at all to mid-latitudinal SST anomalies.

The aim here is to understand how far the concepts of Grötzner et al. (1998) can be transferred to the decadal North Atlantic mode simulated with the global climate model ECHAM3/LSG.

The analysis presented here is based on the results of the POP analysis. The associated patterns for the imaginary and real part of the decadal POP mode are determined by

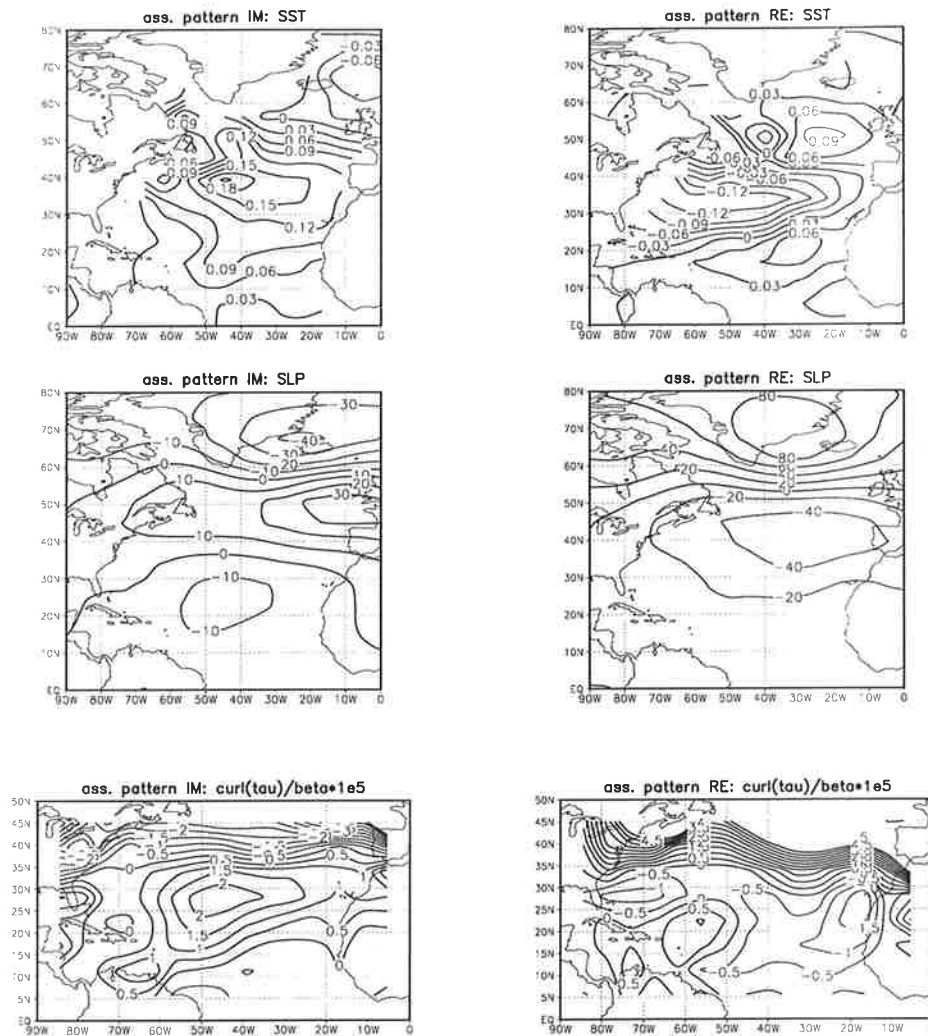


Figure 4.6: Associated imaginary and real patterns of SST, SLP,  $\nabla \times \tau / \beta$ . These patterns are obtained by regressing the imaginary and real part of the decadal POP (see Fig.4.2) with the anomaly fields given above at lag 0.

regressing the POP coefficients (see Fig.4.2) linearly upon the anomaly fields of SST, SLP, and also the wind stress curl divided by the meridional derivative of the Coriolis parameter<sup>5</sup> (Fig.4.6). The left panels show the associated imaginary parts, the right panels the corresponding real parts of the decadal POP mode. The imaginary phase characterizes an intermediate stage in SST of the decadal oscillation. The imaginary part SLP pattern does not project onto the SLP pattern of the leading CCA mode (see Fig.4.4), the NAO. The same is true for the associated imaginary SST pattern, which shows a monopole like structure with maximum anomalies of about 0.18 ( $^{\circ}\text{C}$ /per standard deviation of the POP coefficient) at  $40^{\circ}\text{N}$  and  $50^{\circ}\text{W}$ . The wind stress curl pattern for the

<sup>5</sup>The corresponding units are  $^{\circ}\text{C}$ , Pa,  $\text{Pa} \times \text{s}$  per standard deviation of the POP coefficients, respectively.

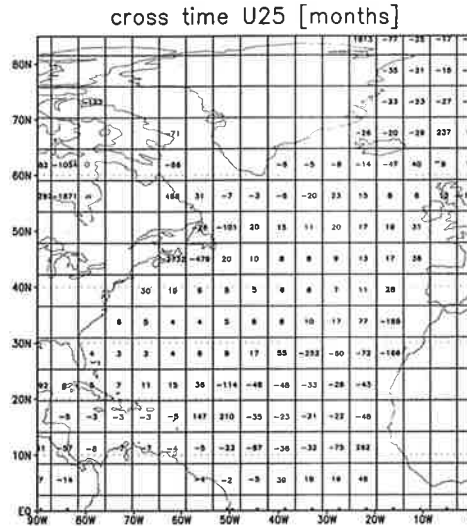


Figure 4.7: Mean zonal crossing time for tracer particles per grid box. Unit is months.

imaginary part is characterized by large negative values north of  $35^{\circ}\text{N}$ , associated with downwelling. The wind stress curl north of  $35^{\circ}\text{N}$  is important for anomalous Ekman pumping, however in terms of Rossby wave dynamics these wind stress curl anomalies provide Rossby wave traveling times which exceed the time scale of the decadal climate mode under consideration.

The real phase of the POP mode (Fig.4.6, right panels) is characterized by weak westerlies (negative NAO index) across the North Atlantic and Europe and an anomalous negative wind stress curl in the subtropics near the northwest coast of Africa. As already discussed by Grötzner et al. (1998) such conditions may lead to the initiation of westward propagating downwelling Rossby waves in the subtropics. A typical signature of these downwelling Rossby waves is a positive heat content anomaly, which crosses the ocean with a typical latitudinal deformation. Such an anomaly structure is shown in Fig.4.1 (right panel). The temporal evolution of the patterns, as obtained from the POP analysis (real part  $\rightarrow$  negative imaginary part) illustrates the westward propagation of the positive heat content anomaly. Another mechanism which might lead to the westward propagation of heat content anomalies in the subtropics is the advection of temperature anomalies within the subtropical gyre. Grötzner et al. (1998) show that the Rossby wave propagation and the mean advection in the subtropics yield similar time scales, both contributing to the delayed negative feedback.

It is known from Timmermann et al. (1998) that the subtropical gyre in the North Atlantic as simulated in the CGCM ECHAM3/LSG is rather weak as compared to that of the ECHO model (see also Chapter 2). Thus, one might think that the mean advection time scale of the subtropical gyre recirculation yields much longer time scales. The mean time for “virtual” tracer particles to cross one oceanic grid box at the surface is calculated

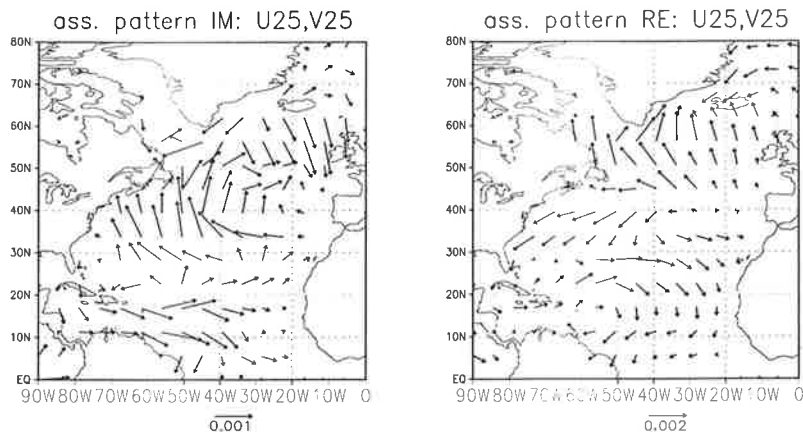


Figure 4.8: Associated imaginary and real patterns for the upper ocean currents.  
Units are m/s per POP standard deviation

and the result for the surface currents is shown in Fig.4.7. It is found that along subtropical latitudes ( $10^{\circ}$ - $30^{\circ}$ N) the tracer crossing time for the entire Atlantic basin exceeds significantly the hypothesized delay time scale of the decadal mode under consideration, which is roughly half a POP period i.e. 9 years. Thus, we can exclude mean advection in the subtropics as being an important process in the generation of the decadal climate mode. It is concluded that Rossby-type wave propagation in the subtropics is the likely candidate to provide the long-term memory of this climate mode.

Now, let us consider the mechanisms which are responsible for the generation of mid-latitude SST anomalies. The wind pattern associated with the SLP field in Fig.4.6 (middle right) leads to an anomalous northward directed Ekman transport north of  $50^{\circ}$ N and a southward directed Ekman transport between  $25^{\circ}$ N- $40^{\circ}$ N. This is consistent with Fig.4.8 showing the associated imaginary and real patterns of the upper ocean current anomalies. The southward Ekman currents in mid-latitudes subsequently lead to the generation of a cold SST anomaly (real part). Lagged cross correlations are calculated between a mid-latitude SSTA index (SSTA averaged over the region  $30^{\circ}$ - $50^{\circ}$ N,  $20^{\circ}$ - $70^{\circ}$ W) and the zonal, meridional and vertical components of the surface current anomalies averaged over the same region. Additionally the lagged cross correlation between the SSTA index and the corresponding net heat flux is calculated. The result is shown in Fig.4.9. The strongest lag 0 correlation can be seen for the meridional surface current anomalies, suggesting that anomalous surface transport across the mean meridional temperature gradient is an important factor for the generation of SST anomalies. Furthermore, one should note that this correlation of about 0.5 is roughly symmetric around lag 0, which might be an expression of bilateral atmosphere-ocean interactions, constituting a positive feedback. A significant anticorrelation becomes apparent between the vertical velocity anomaly and

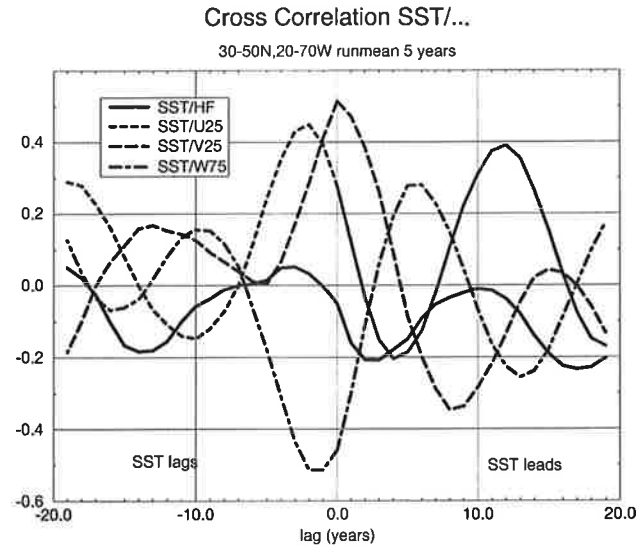


Figure 4.9: Cross correlations between a SST anomaly index (obtained by averaging the detrended SST anomalies over the region  $30^{\circ}$ - $50^{\circ}$ N,  $20^{\circ}$ - $70^{\circ}$ W) and the corresponding indices for the net heat flux, upper ocean horizontal current and upper ocean vertical velocity anomalies. Prior to the analysis the data were smoothed with a 5 year running mean filter.

the SSTA, with a tendency for the vertical velocity to lead. This is an indication for anomalous Ekman pumping contributing also to the development of SST anomalies. The net heat flux/SSTA cross correlation is marginal and no sign of a positive atmosphere-ocean feedback involving heat flux variations is found. Furthermore, the zonal current anomalies lead the surface temperature changes.

The real patterns characterize the stage of maximum air-sea interactions (Figs.4.4 and 4.6 (right panels)). The crucial question is now whether these interactions act bilaterally or whether there is only a one way forcing either from the atmosphere to the ocean or vice versa.

One key factor in the hypothesis of a coupled air-sea mode is the atmospheric response to mid-latitude SST anomalies. In order to prove this link, two Atlantic SSTA response experiments were performed with the ECHAM3 atmosphere model at T21 resolution with positive and negative SST anomalies superimposed on the annual cycle as simulated by the coupled model integration ECHAM3/LSG. The experiments are compared with a control run in which the mean seasonal SST cycle of the 700 year ECHAM3/LSG integration is prescribed<sup>6</sup>. It is found that the atmospheric circulation response to negative mid-latitude SSTA (not shown) is characterized by a weakened subtropical jet, negative

<sup>6</sup>A more thorough analysis of these experiments is presented in a forthcoming paper by Merkel, Timmermann and Latif.

NAO and positive PNA indices, and hence the reversed Arctic Oscillation. These findings reveal that not only the atmosphere forces the ocean as discussed in the previous section but that also the resulting SST anomalies change the atmospheric dynamics in such a way that enables a positive atmosphere-ocean feedback.

## 4.5 Decadal sea ice variability

It has long been recognized (Häkkinen 1993, Yang and Neelin 1993) that sea-ice dynamics can become an important contributor to decadal and interdecadal climate variability in the North Atlantic region. In fact, evidence is also reported from observations (Agnew 1991, Deser and Blackmon 1993) that the sea-ice extent in the Labrador Sea oscillates on a pronounced 11 year time scale. Only little is known about the role of sea-ice dynamics to generate decadal climate variability in the North Atlantic. Deser and Blackmon (1993) show that sea ice variations lead the decadal temperature fluctuations in the North Atlantic. In our model simulation sea ice can be created only locally by anomalous heat

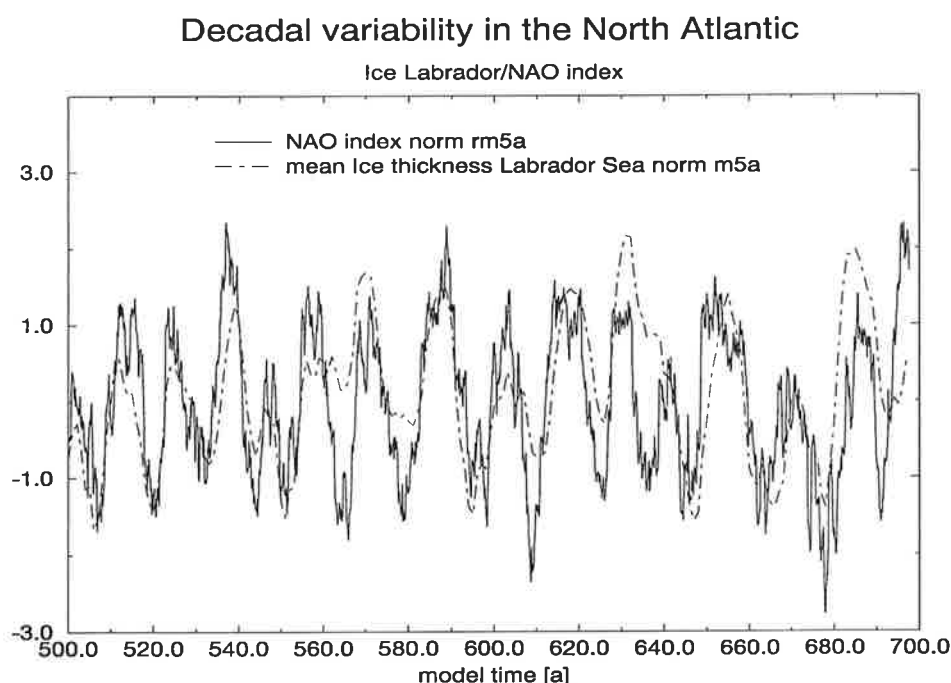


Figure 4.10: Time series of the normalized North Atlantic Oscillation index and the spatially averaged normalized ice thickness in the Labrador Sea. Both time series are smoothed with a 5-year running mean filter. The NAO index is obtained from the difference of the grid points closest to the Azores and to Iceland. The time series are based on annual mean values.

fluxes while ice drift and ice dynamics are not considered. In Fig.4.10 the relation between

spatially averaged ice thickness in the Labrador Sea and the simulated North Atlantic Oscillation index is illustrated. The atmosphere and the ice vary in phase, which can be explained simply just in terms of the NAO forcing the sea ice fluctuations by anomalous cold air advection. Thus, the results of Deser and Blackmon (1993) indicating that sea ice leads temperature on a decadal time scale are not consistent with our results which might be due to the crude ice representation in our model.

## 4.6 Discussion and Summary

One of the key questions in the context of decadal climate variability in the North Atlantic is the question as to whether the atmosphere responds in a linear way to typical subtropical or mid-latitude SST anomalies. This problem was addressed in a recent study by Venzke et al. (1998) in a very elegant way. These authors calculate the joint spatio-temporal structure of SLP anomalies within an ensemble of 6 atmospheric integrations which were forced by observed SSTA. The methodology used in this study is related to the optimal fingerprinting technique (Hasselmann 1979) and the pre-whitening transformation (Allen and Smith 1997). The part of atmospheric variability in the North Atlantic region which, after subtraction of the ENSO signal, is shared by all atmospheric ensemble members is expressed by the detection variable. This variable is obtained by projecting the observed (or simulated) SLP anomalies onto the optimal fingerprint pattern, which is constructed by maximizing the signal to noise ratio. Venzke et al. (1998) find that a joint decadal signal with a time scale of roughly 14 years exists within the atmospheric ensemble, which is coherent with an oceanic signal found by Sutton and Allen (1997). The main detectable atmospheric response to SST anomalies is located in the subtropics. This gives us some confidence that bilateral ocean-atmosphere interactions are crucial in generating North Atlantic decadal variability.

The fundamental findings of this chapter are summarized with a schematic diagram of the relevant feedbacks (Fig.4.11). Starting with a negative SSTA in mid-latitudes, one could argue that the atmospheric baroclinicity is changed in such a manner that the overall response is a weakened North Atlantic Oscillation. A weakened NAO is associated with a further cooling of the initial SSTA. These processes together provide the positive feedback of the coupled air-sea mode. On the other hand a weakened NAO generates downwelling in the subtropics near the African coast by negative wind stress curl anomalies (Fig.4.6, lower right panel), initiating Rossby waves which cross the subtropical North Atlantic from east to west with a typical latitudinal deformation structure (Fig.4.1). Reaching the western boundary of the North Atlantic these Rossby waves readjust the subtropical gyre leading to an enhanced Gulf stream transport. Subsequently the strengthened transport across the mean temperature generates a positive SST anomaly in mid-latitudes, completing one half of the feedback loop.

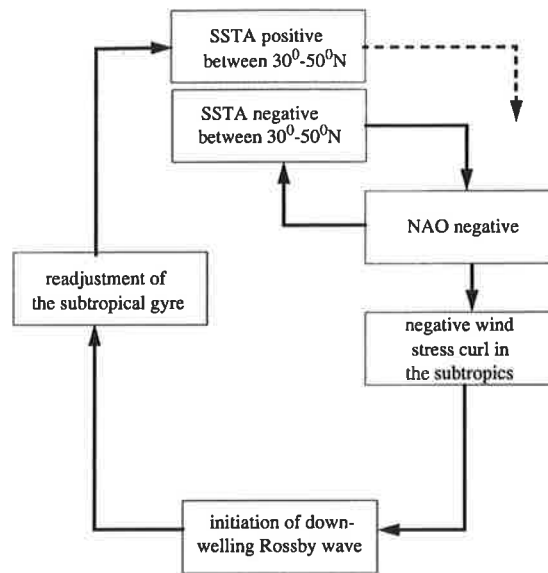


Figure 4.11: Schematic view of the feedback loop for the decadal North Atlantic mode.

Apart from this deterministic view of the decadal climate mode, one has to consider also the role of atmospheric noise. As suggested by the POP analysis the climate mode can be understood as a damped harmonic oscillator. Thus, processes are necessary that help to overcome the inherent damping. Such excitations are provided by the internal noise of the coupled atmosphere-ocean system, namely by random weather fluctuations. Hence, the decadal climate mode can be regarded as a stochastically forced eigenmode of the coupled atmosphere-ocean system.

## 4.7 References

Agnew, T., 1991: Simultaneous winter sea ice and atmospheric circulation anomaly patterns, Preprints, *Fifth AMS Conference on Climate Variations*, Amer. Meteor. Soc., Denver, 362-365.

Allen, M.R., and L. A. Smith, 1997: Optimal filtering in singular spectrum analysis. *Phys. Lett.*, **234**, 419-428.

Bjerknes, J., 1964: Atlantic air-sea interaction. *Adv. Geophys.*, **10**, 1-82.

Delworth, T.L., S. Manabe, R.J. Stouffer, 1993: Interdecadal Variations of the thermohaline circulation in a Coupled Ocean-Atmosphere Model. *J. Climate*, **6**, 1993-2011.

- Delworth, T.L., 1996: North Atlantic interannual variability in a coupled ocean-atmosphere model, *J. Climate*, **9**, 2356-2375.
- Deser, C., Blackmon M.L., 1993: Surface Climate Variations over the North Atlantic Ocean during Winter: 1900-1989. *J. Climate*, **6**, 1743-1753.
- Grötzner, A., M. Latif, T.P. Barnett, 1998: A decadal climate cycle in the North Atlantic Ocean as simulated by the ECHO coupled GCM. *J. Climate*, in press.
- Häkkinen, S., 1993: An Arctic Source for the Great Salinity Anomaly: A Simulation of the Arctic Ice-Ocean System for 1955-1975. *J. Geophys. Res.*, **98**, C9, 16,397-16,410.
- Hasselmann, K. 1979: On the signal-to-noise problem in atmospheric response studies. In: "Meteorology over the Tropical Oceans", Shaw, D.B. (Ed.), Roy. Met. Soc., **251-259**.
- Hasselmann, K., 1988: PIPs and POPs: The reduction of complex dynamical systems using Principal Interaction and Oscillation Patterns, *J. Geophys. Res.*, **93**,D9, 11015-11021.
- Hotelling, H., 1936: Relations between two sets of variants, *Biometrika*, **28**,321-377.
- Kushnir, Y., 1994: Interdecadal Variations in the North Atlantic Sea-Surface Temperature and Associated Atmospheric Conditions. *J. Climate*, **7**, 141-157.
- Latif, M. and T.P. Barnett, 1994: Causes of decadal climate variability over the North Pacific and North America. *Science*, **266**, 634-637.
- Latif, M. and T.P. Barnett, 1996: Decadal variability over the North Pacific and North America: Dynamics and predictability. *J. Climate*, **9**, 2407-2423.
- Münnich, M., M. Latif, St. Venzke and E.Maier-Reimer 1998: Decadal oscillations in a simple coupled model, *J. Climate*, accepted.
- Selten, F.M., R.J. Haarsma, J.D. Opsteegh 1998: On the mechanism of North Atlantic decadal variability. *J. Climate*, submitted.
- Sutton, R.T. and M.R. Allen, 1997: Decadal predictability in Gulf Stream sea surface temperatures, *Nature*, **388**, 563-567.

- Timmermann, A., M. Latif, R. Voss and A. Grötzner, 1998: Northern Hemispheric interdecadal climate variability: A coupled air-sea mode, *J. Climate*, **11**, 1906-1931.
- Venzke, S., M.R. Allen, R.T. Sutton, D.P. Rowell 1998: The atmospheric response over the North Atlantic to changes in sea surface temperature. *J. Climate*, submitted.
- Voss, R., R. Sausen, U. Cubasch, 1998: Periodically synchronously coupled integrations with the atmosphere-ocean general circulation model ECHAM3/LSG. *Climate Dyn.*, **14**, 249-266.
- Wallace, J.M., Y. Zhang and K.-H. Lau, 1993: Structure and seasonality of interannual and interdecadal variability of the geopotential height and temperature fields in the Northern Hemisphere troposphere. *J. Climate*, **6**, 2063-2082.
- Yang, J. and J.D. Neelin, 1993: Sea-ice interaction with the thermohaline circulation. *Geophys. Res. Lett.*, **20**, 217-220.
- Zorita, E., and C. Frankignoul, 1997: Modes of North Atlantic decadal variability in the ECHAM1/LSG coupled ocean-atmosphere model, *J. Climate*, **10**, 183-200.

# 5 Interdecadal Climate Variability in the Northern Hemisphere

*“If your experiment needs statistics, you ought to have done a better experiment.” Rutherford, Ernest (1871-1937), In N. T. J. Bailey the Mathematical Approach to Biology and Medicine, New York: Wiley, 1967.*

## 5.1 Abstract

We describe in this chapter a coupled air-sea mode in the Northern Hemisphere with a period of about 35 years. The mode was derived from a multi-century integration with a coupled ocean-atmosphere general circulation model and involves interactions of the thermohaline circulation with the atmosphere in the North Atlantic and interactions between the ocean and the atmosphere in the North Pacific.

This chapter focusses on the physics of the North Atlantic interdecadal variability. If, for instance, the North Atlantic thermohaline circulation is anomalously strong, the ocean is covered by positive sea surface temperature (SST) anomalies. The atmospheric response to these SST anomalies involves a strengthened North Atlantic Oscillation (NAO), which leads to anomalously weak evaporation and Ekman transport off Newfoundland and in the Greenland Sea and the generation of negative sea surface salinity (SSS) anomalies. These SSS anomalies weaken the deep convection in the oceanic sinking regions and subsequently the strength of the thermohaline circulation. This leads to a reduced poleward heat transport and the formation of negative SST anomalies, which completes the phase reversal.

The Atlantic and Pacific Oceans seem to be coupled via an atmospheric teleconnection pattern and the interdecadal Northern Hemispheric climate mode is interpreted as an inherently coupled air-sea mode. Furthermore, this chapter investigates the origin of the Northern Hemispheric warming observed recently. We compare the observed temperatures with a characteristic warming pattern derived from a greenhouse warming simulation with

our coupled general circulation model and also with the Northern Hemispheric temperature pattern which is associated with the 35 year climate mode. It is shown that the recent Northern Hemispheric warming projects well onto the temperature pattern of the interdecadal mode under consideration.

## 5.2 Introduction

The aim of the section is to shed light on the role of the atmosphere-ocean interactions on interdecadal time scales. Our attention will be focussed on the physical mechanisms that lead to interdecadal oscillations in the Northern Hemisphere and in particular in the North Atlantic region.

Interdecadal climate variability is considered to be important in masking the greenhouse warming signal in the present climate record. Hence it is necessary to understand the mechanisms that generate interdecadal climate variability, particularly in the Northern Hemisphere.

A very important goal of climate research is the identification of climate modes and the understanding of the underlying physical processes. Recently, strong scientific interest has focused on the detection of decadal up to secular climate time scales in observational records by means of sophisticated mathematical techniques. Schlesinger and Ramankutty (1994) perform a singular spectrum analysis (SSA) of the detrended surface temperature record for several geographical locations over the period of 1858-1992. In the North Atlantic region their analysis yields an oscillation of 76 years. Recently, Mann et al. (1995) performed a multivariate singular value decomposition in the frequency domain of historical and climate proxy records and evidence is reported for interdecadal and century-scale oscillations. A wavelet analysis of the Northern Hemispheric surface temperature record (Lau and Weng 1995) reveals a time scale of 35-60 years. However, Lau and Weng (1995) do not address the question as to whether their results are significant against the hypothesis of a first order autoregressive process. Since the ocean and sea ice can integrate high frequency noise, yielding an approximately red noise climate spectrum (Hasselmann 1976), the results of statistical methods should be tested against this null hypothesis.

The available observations are too sparse to identify the mechanisms that lead to long-term climate changes. However, it is known from paleo-climatology (Broecker et al. 1985, Duplessy et al. 1992) and from model simulations (e.g. Maier-Reimer and Mikolajewicz 1989, Mikolajewicz and Maier-Reimer 1990, Mysak et al. 1993, Winton and Sarachik 1993, Delworth et al. 1993, Weaver et al. 1991,1993,1994, Greatbach and Zhang 1994) that long-term variability and abrupt climate changes (e.g. Manabe and Stouffer 1995, Schiller et al. 1997) in the climate system may originate from changes in the thermohaline circulation (THC). In this context North Atlantic deep water (NADW) formation plays a crucial role. One prominent example of such a climate change in this century was the Great Salinity

Anomaly (GSA) – a freshwater anomaly that originated in the Greenland Iceland Norway Sea (GIN) in the late 1960s and moved with the East Greenland current southward. It passed the regions of deep-water formation reducing the deep water formation temporarily (Lazier 1988) and its trajectory turned northeastwards in 1971/72. The GSA supports the idea that atmosphere-ocean interactions north of  $50^{\circ}\text{N}$  play a crucial role in the generation of interdecadal variability as suggested by Dickson et al. (1975,1988). Dickson et al. (1975,1988) argue that a persistent intensification of northerly winds over the Greenland Sea led to an increased injection of polar waters into the East Greenland current. This was accompanied also by a shift in the sea-ice conditions (see Mysak et al. 1990), contributing significantly (Häkkinen 1993) to the polar freshwater excess during the GSA. An interdecadal feedback loop explaining the GSA was proposed by Wohllleben and Weaver (1995) which involves the Labrador-Sea convection, the subpolar gyre, the atmosphere and the freshwater-transport through the Fram-Strait. This mechanism is supported by observations and in particular by the conditions associated with the GSA. The feedback loop is based on the idea that on interdecadal time scales the atmosphere responds to SST anomalies in the subpolar gyre system. Our study follows the same philosophy.

Further evidence for the existence of interdecadal variability is reported by Bjerknes (1964). He describes a climate shift between the late 1890s and the mid-1920s in the North Atlantic. The positive sea surface temperature trend observed during this period, with maximum anomalies at about  $40^{\circ}\text{N}$  is explained by a strengthened atmospheric circulation, which stimulated the subtropical ocean gyre. However, the physics of the long-term temperature fluctuations within the Gulf Stream cannot be explained adequately in this study. On interannual time scales, which we shall not address here, the wind speed south of  $50^{\circ}\text{N}$  and the sea surface temperatures (SST) are negatively correlated, confirming that interannual variability in the North-Atlantic is determined by air-sea flux variations. In contrast, on interdecadal time scales the correlation is positive indicating that ocean dynamics (in particular the dynamics of the subtropical and subpolar gyres) plays an active role.

Bjerknes' (1964) ideas are partially supported by the analysis of a century long SST dataset by Kushnir (1994). But Kushnir (1994) argues that the THC rather than the ocean gyres plays the important role for the North Atlantic interdecadal variability. This is underscored by the fact that maximal SST anomalies can be found in the regions of North Atlantic deep water formation (the Labrador and GIN-seas). Thus, active coupling between the atmosphere and the THC may be a crucial feature of the interdecadal variability in the North Atlantic. Deser and Blackmon (1993) discuss on the basis of a 90 year dataset that the interdecadal sea level pressure (SLP) pattern leads to a damping of the corresponding extratropical SST anomalies, which is in agreement with Kushnir's findings. This was also Bjerknes' (1964) argument to attribute the generation of interdecadal variability to ocean dynamics, with the atmosphere responding to changes in the

ocean circulation.

Regarding the physical origin of the interdecadal variability it has not been clarified yet whether the THC (as proposed by Delworth et al. 1993 analyzing a multi-century CGCM integration) or the wind-driven ocean circulation or both provide the memory for interdecadal oscillations. In particular, it was argued by Latif and Barnett (1994) and by Grötzner et al. (1998) that decadal variability in the North Pacific and North Atlantic Oceans can be generated by an unstable interaction between the atmosphere and the wind-driven subtropical ocean gyres. One should note, however, that a restoring in their modeling experiments to observed climatology north of  $60^{\circ}\text{N}$  attenuates internal variability and thus may underestimate the role of the THC in their coupled model.

In order to separate the interdecadal fluctuations from the greenhouse warming signal, Hegerl et al. (1996) calculate projections of observed 15-, 20- and 30-year trends onto a fingerprint pattern which carries the characteristic greenhouse warming signal, as inferred from greenhouse warming simulations with coupled general circulation models (CGCMs) in an optimized way. The optimal fingerprint (Hasselmann 1993) consists of a first guess greenhouse pattern rotated in the direction of maximum signal to noise ratio. One of its characteristics is a relative cooling in the North-Atlantic, with maximum cooling around  $40^{\circ}\text{N}$ - $50^{\circ}\text{N}$ . This is the region which exhibited remarkable variability on long time scales in Bjerknes' (1964) analysis. The projection (called detection variable) of the observed 30-year trends onto the optimal fingerprint leaves the 95%-confidence limit just for a few years around 1945 and again around 1990 as shown in Hegerl et al. (1996).

The aim of our study is to shed light on the role of the atmosphere-ocean interactions on interdecadal time scales. Our attention will be focussed on the physical mechanisms that lead to interdecadal oscillations in the Northern Hemisphere and in particular in the North Atlantic region.

This chapter is organized as follows. In Section 5.3 we shall analyze the simulated northern hemispheric variability with spectral methods in order to identify the characteristic time scales in our model simulation. The physical mechanism which leads to the interdecadal oscillations in the Atlantic is described in Section 5.4. In Section 5.5 we discuss the pan-oceanic connection between the Atlantic and Pacific Oceans. In Section 5.6 we discuss the role of the interdecadal climate mode in masking the greenhouse warming signal. This chapter is concluded with a summary and discussion of the results in Section 5.7.

### 5.3 Interdecadal time scales

The search for climate modes with a distinct period which can be explained by a consistent physical mechanism is a major goal of climate research. Spectral methods help as a mathematical tool to infer characteristic periods.

Fig.5.1 shows the temporal evolution of the maximum of the meridional overturning in

the Atlantic. The same index was also used by Delworth et al. (1993). Also shown is

### Max. meridional overturning

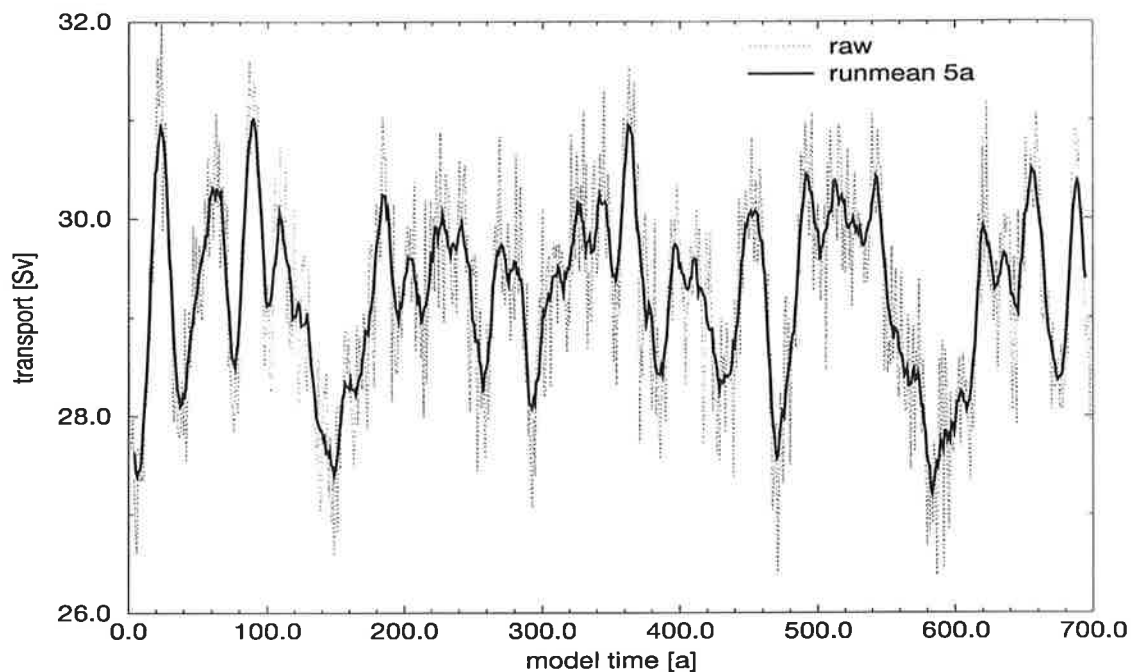


Figure 5.1: Detrended time series of the maximum of the Atlantic meridional overturning (Sv).

a low-pass filtered (5 year running-mean) version of the time series to highlight the low-frequency variability. The model simulates interdecadal fluctuations of approximately 10% ( $\sim 2-3$  Sv) of the mean transport, which might have important consequences for the climate in the North Atlantic region. Thus, Fig.5.1 is used in the subsequent analyses as a reference time series.

Fig.5.2 shows a Fourier spectrum of the maximum of the meridional model overturning in the Atlantic. The spectrum was obtained using a Bartlett window and 15 degrees of freedom. It is tested against the hypothesis that the signal is generated by a first order autoregressive process (yielding a red noise spectrum), and the 95% confidence limit for the rejection of the red noise hypothesis is also displayed. The appropriate spectrum of the red noise process was obtained by calculating the first order maximum entropy spectrum of the THC index. The THC index shows enhanced spectral density at a frequency of about 0.03 cycles/year (period of about 35 years) and at about 0.008 cycles/year (period of 125 years). Both peaks leave the 95% confidence level of the first order autoregressive process, indicating that other processes than just the integration of synoptic weather noise (in the sense of the stochastic climate model of Hasselmann 1976) are involved. The THC spectrum is robust against reasonable changes of the window width. The spectral characteristics of the overturning time series are consistent neither with a first nor a

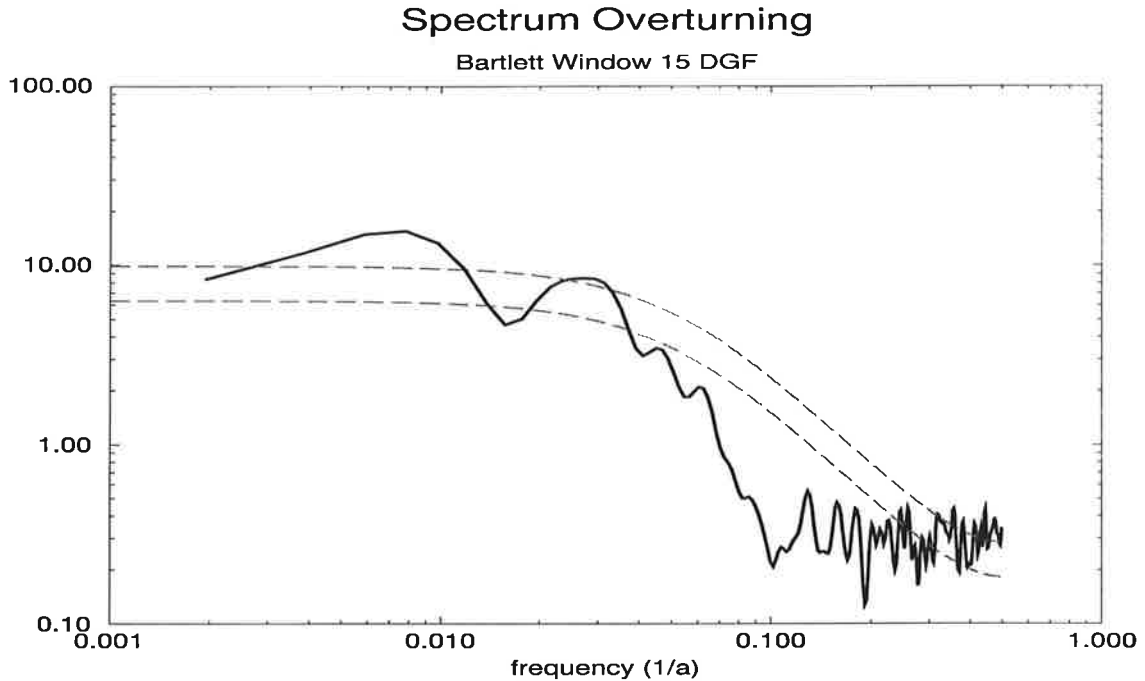


Figure 5.2: Power spectrum [ $\text{Sv}^2\text{a}$ ] of the meridional overturning index calculated using a Bartlett window and 15 degrees of freedom. The power spectrum of a fitted AR(1) process and its 95% confidence limit are displayed by the dashed lines.

second order autoregressive process. The sharp drop of the spectrum at periods around 10-15 years implies that the thermohaline circulation has the properties of a low pass filter. This feature is different to the findings of Griffies and Tziperman (1995) who argue that the thermohaline circulation in the GFDL CGCM can be understood as a noise driven oscillator. Our goal is to understand which climate processes are participating in the generation of interdecadal Northern Hemispheric climate variability associated with the 35 year period. An index of the Labrador Sea sea ice volume and the THC index show no coherence on interdecadal time scales (not shown here). Thus, we conclude that sea ice effects do not play an important role in the 35 year mode. Fig.5.3a displays a spectrum of a North Atlantic sea surface temperature anomaly (SSTA) index. The averaging region ( $70^{\circ}\text{W}$ - $20^{\circ}\text{W}$ ,  $30^{\circ}\text{N}$ - $50^{\circ}\text{N}$ ) represents the area where maximum variance is explained by the interdecadal mode. The spectrum was calculated using normalized annual data and a Bartlett window with a width of 140 years (15 degrees of freedom). It shows a significant peak at about 0.03 cycles/year (period of  $\sim 35$  years). Thus, interdecadal fluctuations in the THC are related to North Atlantic SST anomalies. This relationship is also underscored by the high coherence (not shown) between the SSTA in this region and the overturning index which exceeds the 95% limit at this frequency.

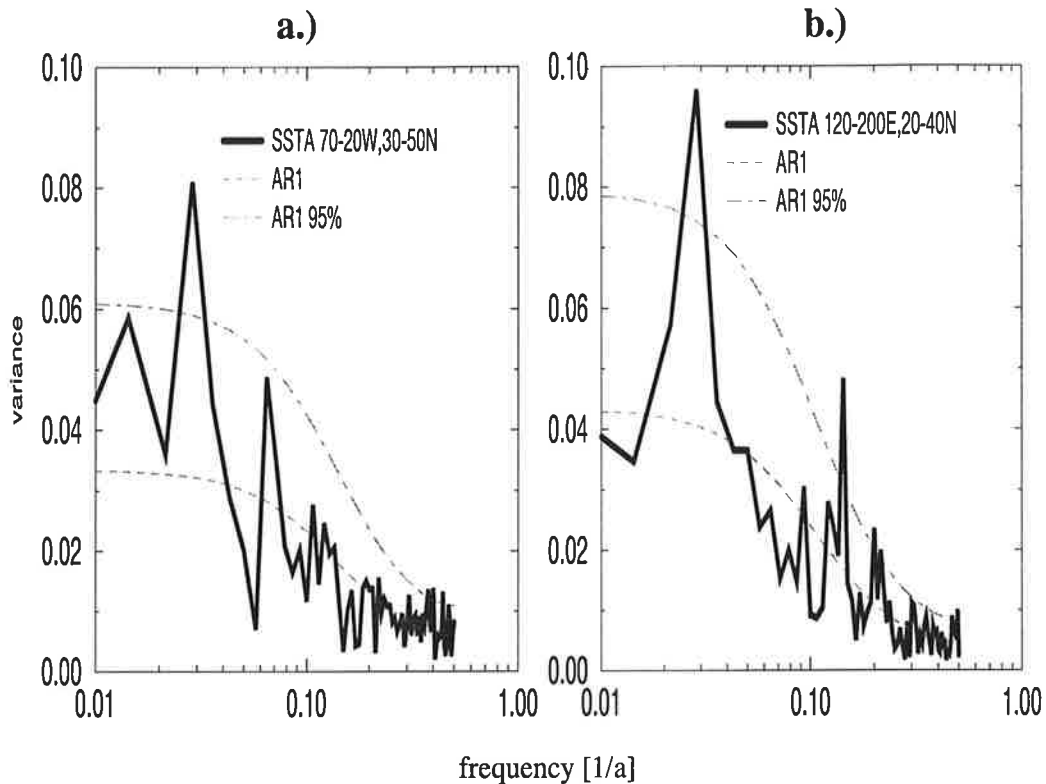


Figure 5.3: (a): Power spectrum of the detrended and normalized SST anomalies averaged over the North Atlantic index region  $30^{\circ}\text{N}$ - $50^{\circ}\text{N}$ ,  $70^{\circ}\text{W}$ - $20^{\circ}\text{W}$ . The spectrum was obtained by using annual data and a Bartlett window with 15 degrees of freedom. It is tested against a first order autoregressive process (dashed line). The 95% confidence limit is represented by the dash-dotted line. (b): Same as in (a) but for the North Pacific index region  $20^{\circ}\text{N}$ - $40^{\circ}\text{N}$ ,  $120^{\circ}\text{E}$ - $160^{\circ}\text{W}$ .

Fig.5.3b shows the spectrum of a North Pacific SSTA index ( $120^{\circ}\text{E}$ - $160^{\circ}\text{W}$ ,  $20^{\circ}\text{N}$ - $40^{\circ}\text{N}$ ). The spectrum was calculated in the same way as the spectrum of the Atlantic SST index. The significant 35 year peak found in the North Atlantic can also be seen in the North Pacific SSTA spectrum. Thus, the North Atlantic and the North Pacific Oceans seem to be coupled on interdecadal time scales. Since both ocean basins have different geometries and therefore time scales, we believe that the most reasonable explanation for the pan-oceanic connection is an atmospheric coupling of the two oceans.

The atmospheric coupling of the two oceans is confirmed by an EOF expansion of the Northern Hemispheric ( $20^{\circ}\text{N}$ - $85^{\circ}\text{N}$ ) 500 hPa geopotential height anomalies. The leading EOF, which explains 26% of the total variance is shown in Fig.5.4a. The dominant pattern shows that the weakened subtropical anticyclones go along with a weakened Icelandic low. The pattern in the Atlantic region represents the negative phase of the North At-

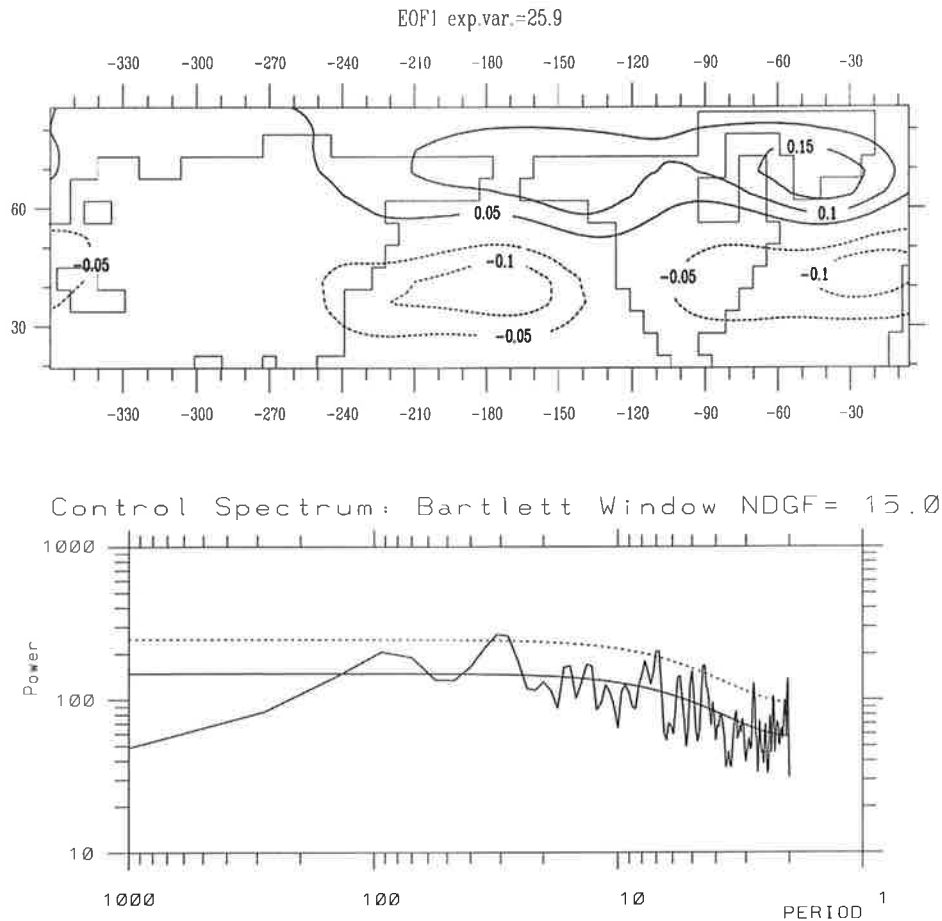


Figure 5.4: (a): 1. EOF of annual Northern Hemispheric 500 hPa height anomalies. (b): Power spectrum of the corresponding first principal component. The x-axis denotes the period in years. The spectrum was obtained using a Bartlett window and 15 degrees of freedom and is tested against a red noise spectrum. The 95% confidence limit is represented by the dotted line.

lantic Oscillation (NAO). The spectrum of the corresponding first principal component (Fig.5.4b) shows a clear interdecadal peak at a period near 30-35 years.

In order to verify that Atlantic and Pacific SST anomalies oscillate synchronously with a period of 35 years, a cross spectral analysis was performed between the two SSTA indices shown in Figs.5.3a and 5.3b. The corresponding phase and the squared coherence spectra are displayed in Figs.5.5a and 5.5b, respectively. For frequencies of about 0.03 cycles/year (35 year period) the Pacific and the Atlantic vary in phase. The atmosphere only can provide an instantaneous coupling mechanism between the two oceans. The squared coherence for periods of 35 years reaches the 99% level, as can be inferred from Fig.5.5b. It is unlikely that this kind of temperature synchronization is due to pure ocean processes, because time scales, (either associated with wave or advective processes) are

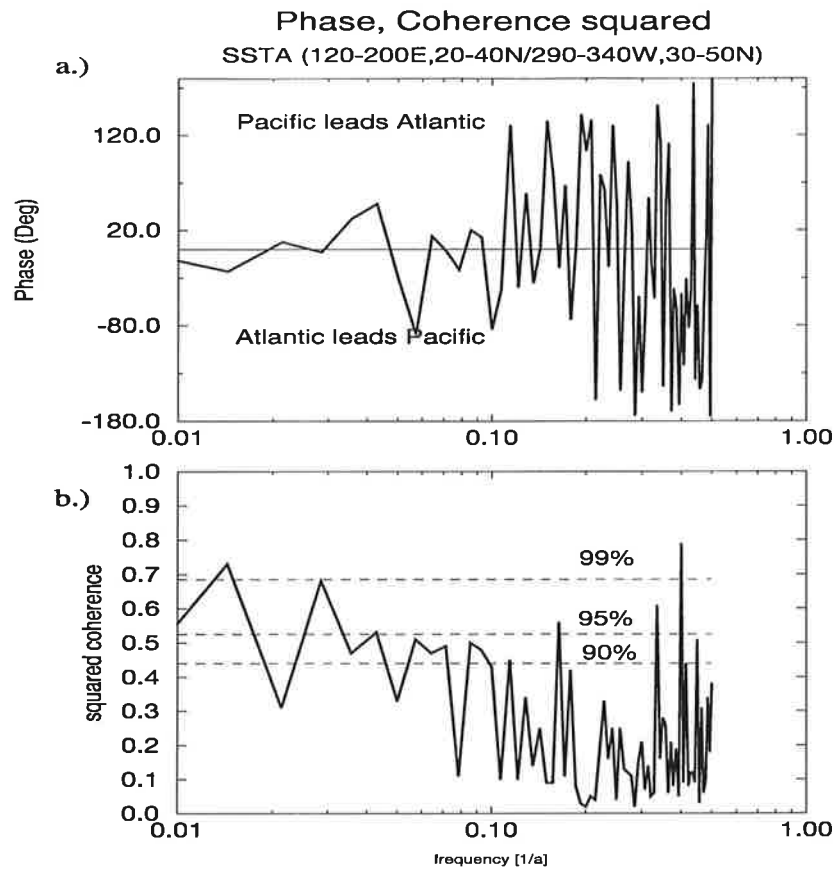


Figure 5.5: (a): Phase spectrum between the normalized and detrended SSTA indices shown in Figs.5.3 a and b. The Bartlett procedure was applied with a chunk width of 140 years. (b): Squared coherence spectrum of the Pacific and Atlantic indices. The 90%, 95% and 99% confidence limits for nonzero coherence are displayed as dashed lines.

of the order of many years. The decadal and interdecadal peaks discussed in this section are very stable features which show up also by applying other spectral methods such as wavelet and maximum entropy techniques.

Thus, we have identified a Northern Hemispheric interdecadal climate mode with a period of 35 years. Fig.5.6 summarizes the different hypotheses that were proposed to explain the interdecadal variability in the Northern Hemisphere. Delworth et al. (1993) analyzing a multi-century integration with the GFDL CGCM argue that atmospheric forcing as well as the atmospheric response to SST anomalies are of minor importance (Delworth, personal communication, 1996). They explain the interdecadal variability in the North Atlantic mainly in terms of ocean dynamics. From this viewpoint no synchronous pan-oceanic connections can arise. Analyzing also the GFDL CGCM, Griffies and Tziperman (1995) investigate the role of atmospheric noise for the generation of the Delworth-mode. They argue that the THC variability may be understood within the framework of a noise

<b>paradigma for interd. variability</b>	<b>atmospheric &amp; oceanic peak</b>	<b>panoceanic connection</b>
noise driven ocean oscillator (Delworth et al., Griffies et al.)	<b>no</b> atmospheric feedback not crucial	<b>no</b> different timescales of Pacific and Atlantic
coupled mode (this study)	<b>yes</b> memory resides in the ocean	<b>yes</b> atmosphere is the coupling device
atmospheric mode (James and James)	<b>yes</b> internal atmospheric memory	<b>yes</b> forcing oceans with one frequency

Figure 5.6: Table of different hypotheses that can explain interdecadal variability.

driven linear oscillator. In contrast, our findings, in particular the pan-oceanic connection and the existence of an atmospheric peak at 30-35 years, imply the existence of a coupled atmosphere-ocean mode. However, it should be noted that the hypothesis of James and James (1989) who identify long-term internal variability in a simple atmospheric model could explain our findings also. The James and James-hypothesis cannot be simply rejected by our findings. Only atmospheric or coupled atmosphere-mixed layer experiments can clarify whether the atmosphere is able to generate interdecadal eigenmodes.

## 5.4 Physics of the North Atlantic interdecadal mode

We have shown that the meridional overturning exhibits a characteristic oscillatory behaviour on time scales of about 35 years. In order to study how the ocean and the atmosphere interact on this time scale, we analyze several oceanic and atmospheric variables in relation to the meridional overturning strength.

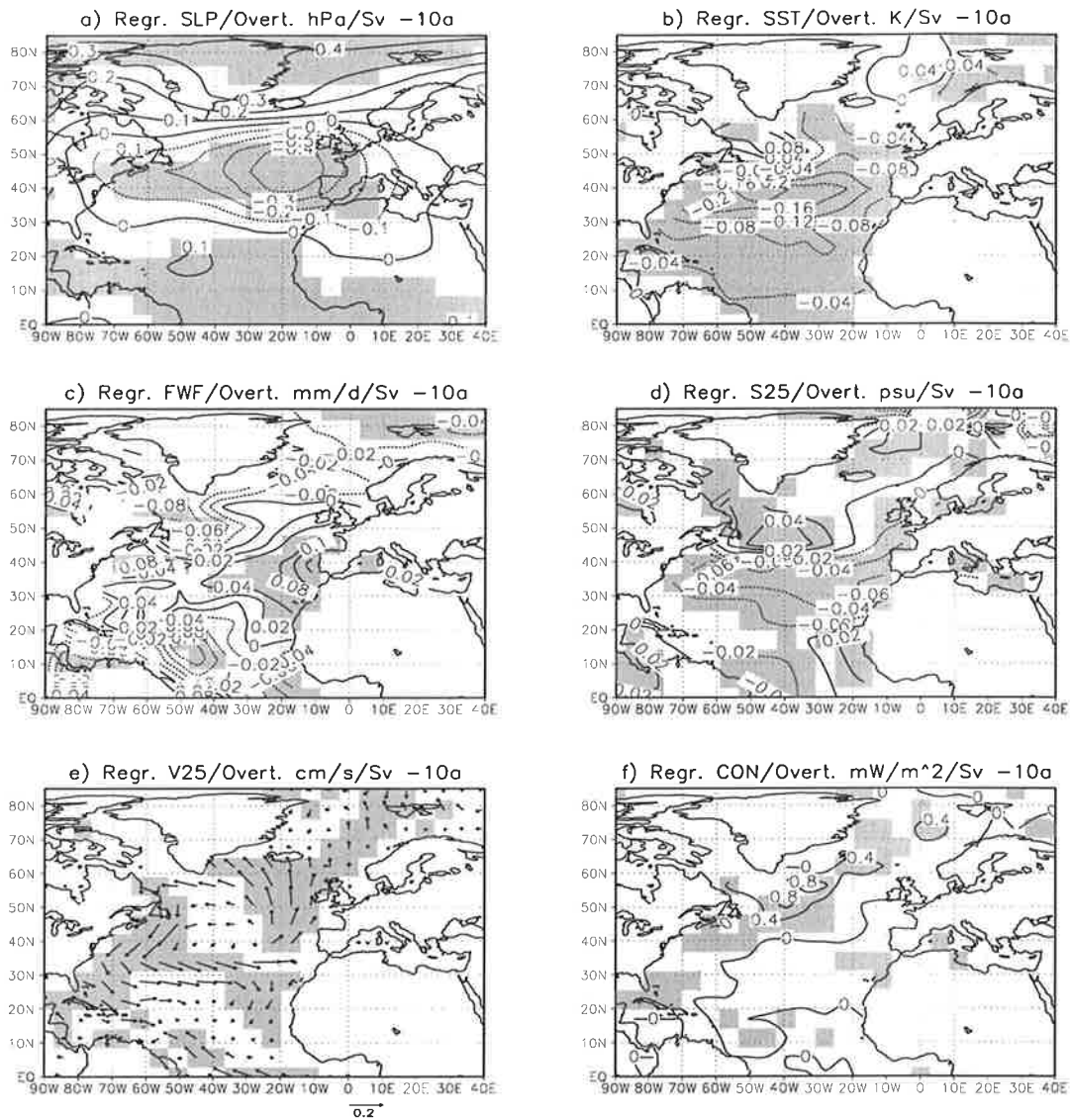


Figure 5.7: Lag regressions of a) SLP [hPa/Sv], b) SST [K/Sv], c) freshwater flux gain of the ocean [mm/d/Sv], d) SSS [psu/Sv], e) surface currents [cm/s/Sv] and potential energy loss by convection [mW/m<sup>2</sup>/Sv] to the band-pass filtered THC index. Annual mean values were used and prior to the analysis all time series were detrended. The results are shown for a lag of -10 years.

### 5.4.1 Atlantic air-sea interactions

For the following discussion lag regression plots between the bandpass filtered THC index and annually averaged atmospheric and oceanic fields are calculated. The THC index was bandpass filtered retaining variability with periods between 25-45 years. The filtering window is buffered at both ends by cosine tails in order to suppress secondary maxima that might occur for a pure rectangular filter. Figs.5.7-5.10 show the conditions at lags -

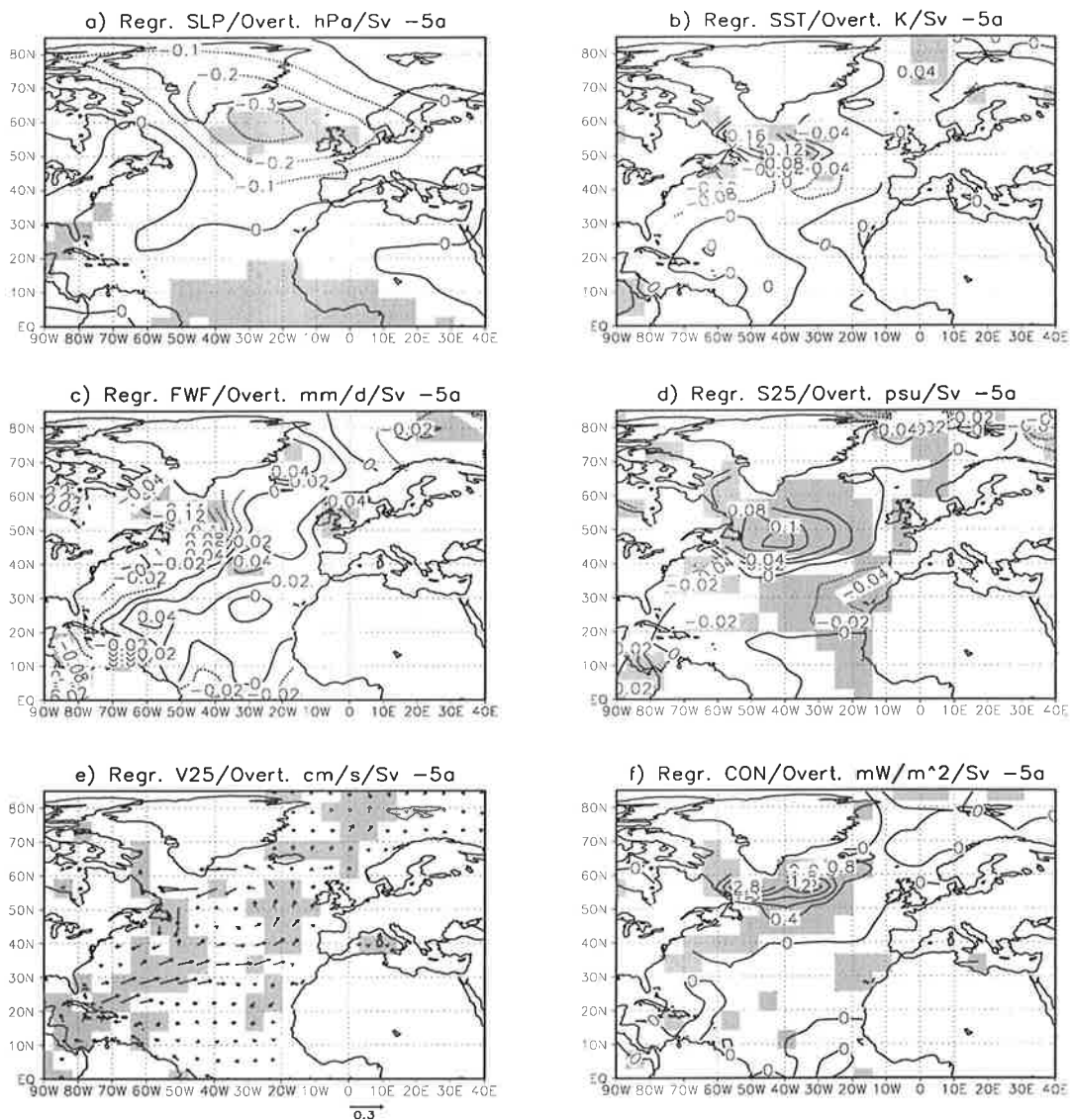


Figure 5.8: Same as Fig.5.7, but for lag -5 a.

10 (10 years prior to the maximum overturning), lag -5, lag 0 and lag +5 for the anomalies of SLP, SST, surface freshwater flux (including also the river runoff), SSS, oceanic surface velocity and the oceanic potential energy loss by convection. The shading indicates the regions in which the regressions exceed the 95% confidence limit of rejecting the hypothesis of zero regression.

At lag -10 (Fig.5.7) anomalous conditions are characterized by a strong negative SSTA (b) and a weakened NAO (a). The negative temperature anomaly is associated with anomalous southward advection of cold subpolar waters (e) especially into the region off the North American coast. The meridional current anomalies in the western Atlantic north of 30°N are highly correlated (about -0.7) with the zonal wind stress anomalies

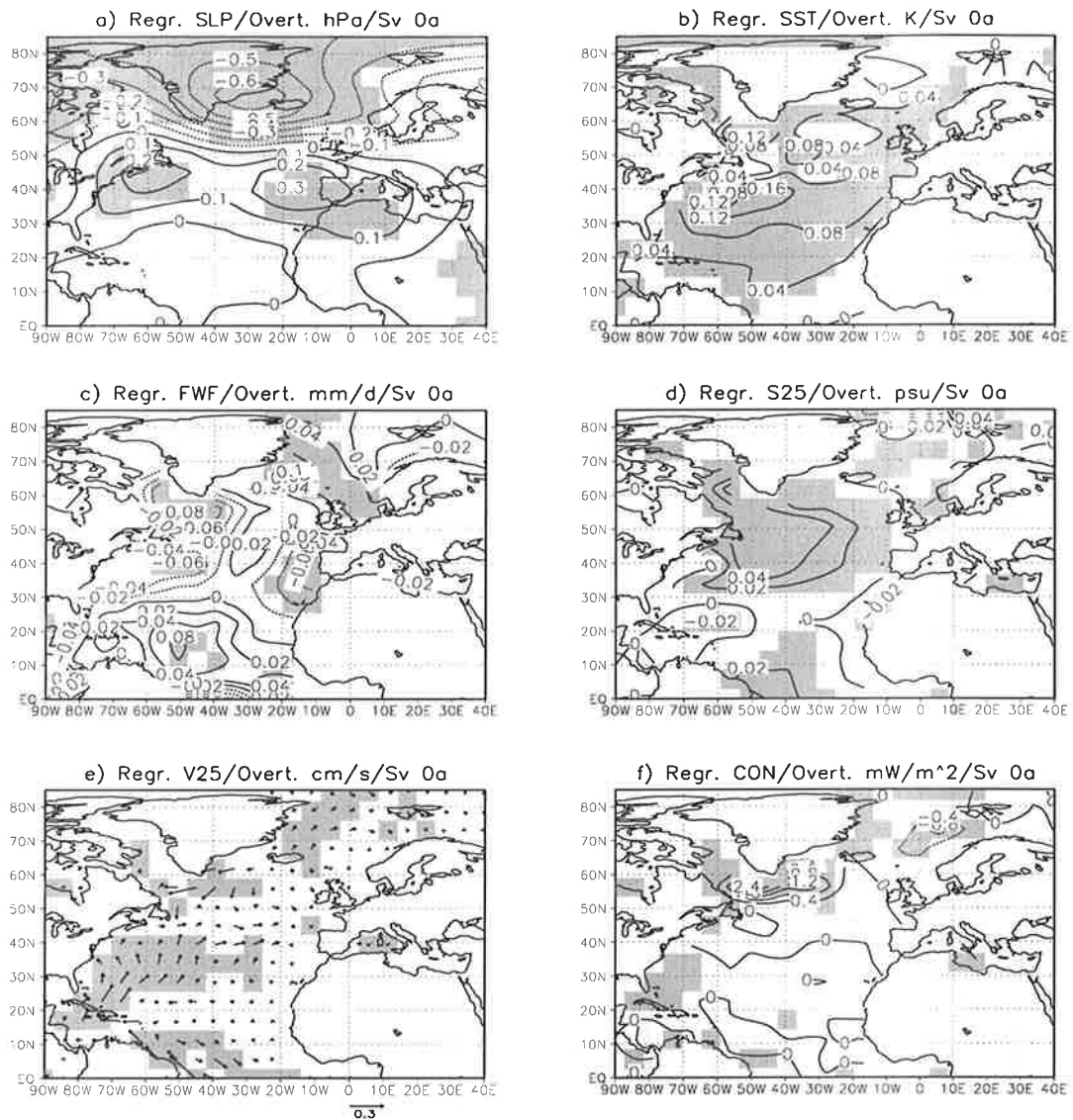


Figure 5.9: Same as Fig.5.7, but for lag 0 a.

(after removing high frequencies by applying a 11 year running mean filter), which is typical for anomalous Ekman currents. A similar regression pattern of the heat flux (not shown) does not show any correspondence to the SST pattern (Fig.5.7 b). Hence, the surface heat flux does not contribute to the generation of mid-latitude SST anomalies on these time scales. The SSS anomalies (d) exhibit a dipole-like structure. In the region  $30^{\circ}\text{N}$ - $40^{\circ}\text{N}$  negative SSS anomalies are created mainly by an anomalously positive freshwater flux<sup>1</sup>. This can be inferred from the close correspondence between Figs.5.7 c and 5.7 d. Of particular importance are the relatively small positive SSS anomalies off

<sup>1</sup>A negative value of the freshwater flux regressions is equivalent to a net freshwater removal from the ocean

Newfoundland and east of Greenland which – after amplification – are going to play a crucial role for the phase reversal in the climate mode under consideration. The positive salinity anomalies are partly due to reduced freshwater supplies from the atmosphere to the ocean. A moderate increase in the convection can be seen at this time (f), which can be attributed to the positive salinity anomalies. The mechanisms that generate the subpolar SSS anomalies are discussed in more detail below. It should be noted that the SLP (a) and the temperature anomaly patterns (b) shown here are rather similar to those shown in Bjerknes' (1964) study, for the interdecadal change which was observed during 1890-1925.

The various oceanic and atmospheric anomaly fields associated with the conditions 5 years prior to the maximum overturning are depicted in Figs.5.8 a-h.

The regression pattern for the anomalous SLP shows an intermediate phase of the NAO. The pressure anomalies near Iceland changed their signs (compared to lag -10 years), which is associated with an enhanced cold air advection over the Northwest Atlantic. The SST anomalies in this region are positive, which leads to a strong heat loss of the ocean (not shown). The enhanced oceanic convection at lag -5 brings warmer water masses from below to the surface, supporting further heat loss of the ocean. This intermediate phase of the NAO reduces further the atmospheric freshwater flux (c) south of Greenland, resulting in an amplification of the initial positive SSS anomaly which was first simulated at lag -10 years. The northerly winds along the west coast of Greenland have an additional effect on the surface salinities through anomalous Ekman transport (Fig.5.8 e) off Newfoundland (not shown). According to the mean salinity gradients (Fig.2.1) this means that the anomalous ocean currents advect more saline waters into this region, thereby amplifying the positive salinity anomaly further. The effect of this positive salinity anomaly is a destabilization of the water column south of Greenland leading to enhanced deep convection. At lag -5 years the strongest anomalies in the convection are simulated, indicating a lag between the convection and the maximum meridional overturning of about 5 years (Fig.5.8 f).

A striking resemblance between the interdecadal mode in our model and that of Delworth et al. (1993) can be found by comparing the corresponding SST, SSS and SLP patterns. The SST and SSS composites of Delworth et al. (1993) calculated by taking SST and SSS differences between four decades with anomalously large THC index and four decades of anomalously small THC index values (shown in Figs.6a,c of their study) have a close correspondence to the regression patterns we obtain at lag -5 years (Figs. 5.7 b,d).

Fig.5.9 shows the regression patterns to the THC index for time lag 0.

The SLP-pattern at lag 0 in our model (see Fig.5.9 a) agrees extremely well with that found in the GFDL model (see their Fig.20), which is also true for the magnitudes. During the maximum phase of the meridional overturning the NAO is anomalously strong, associated with anomalously strong westerlies centered near  $55^{\circ}\text{N}$  and anomalous easterlies at about  $35^{\circ}\text{N}$ . The SSTA pattern is now characterized by a positive anomaly covering the whole

North Atlantic. During the maximum phase of the THC an increased northward heat transport contributes to the generation of the positive SSTA. This SSTA seems to be amplified by the atmosphere via anomalous winds and Ekman transport. Comparing Fig.5.9 b with Fig.5.7 b we find that although the atmospheric conditions have almost changed to their reverse, there is still a positive SSTA in the Labrador Sea, whereas south of  $50^{\circ}\text{N}$  the temperature pattern has changed its sign. This is a hint that the atmospheric response to SST anomalies is mainly active in the region  $30^{\circ} - 50^{\circ}\text{N}$ . The salinity anomaly (d) at lag 0 attains a magnitude of 0.04 psu/Sv, and it has spread relative to lag -5a, covering now the whole North Atlantic. The anomalous atmospheric freshwater flux (c) favours still the generation of positive salinity anomalies in the region  $30^{\circ}\text{N}-55^{\circ}\text{N}$ . Thus there are several opposing mechanisms at lag 0. There is an atmospheric tendency to amplify the salinity anomaly and also anomalous currents south of Greenland still promote further salinity import into the Northwest Atlantic. On the other hand the horizontal diffusion of the salinity anomaly becomes apparent and parts of the salinity anomaly are removed from the surface by deep convection south of Greenland. This indicates that – regarding air-sea interactions – we are in an intermediate phase. Fig.5.9 h demonstrates that oceanic convection south of Greenland is still anomalously strong, while reduced convection is found in the GIN sea (Fig.5.9h). There is also evidence from observations (Dickson et al. 1996) that deep convection in the GIN Sea and the Northwest Atlantic were out of phase during the postwar period. Five years after the maximum of the THC the anomalous climate conditions (Fig.5.10) are basically given by the mirror images of those shown at lag -10 years thereby completing one half cycle.

Let us consider now the processes that are responsible for the generation of the surface salinity anomalies off Newfoundland. Fig.5.11 depicts a collection of lag correlations of salinity anomalies in the oceanic sinking region in the Northwest Atlantic ( $60^{\circ}-20^{\circ}\text{W}$ ,  $45^{\circ}\text{N}-65^{\circ}\text{N}$ ) and anomalous evaporation, sea ice thickness, precipitation, zonal and meridional surface currents averaged over this region, respectively. The lag correlations were obtained by removing high frequencies applying a 11-year running mean filter. Fig.5.11 demonstrates that the evaporation and the salinity anomalies in the sinking region vary in phase – although an in phase relationship is expected for the *time-integrated* fluxes and the salinity anomaly. This feature has to be clarified. The physical time constant for the upper ocean salinity anomalies being created by fluxes is rather short and of the order of a few months. We use in our analysis annual data and some low-pass filtering. Hence, the difference between the freshwater flux and its time integral (on the basis of short data sampling) is smeared out and we obtain an in phase relationship between the freshwater fluxes and the salinity anomalies. The correlations indicate that SSS anomalies are forced locally in the sinking region by anomalous evaporation and anomalous zonal surface currents. As mentioned above, the latter are mainly due to anomalous wind stress over the sinking region. The roles of area averaged sea-ice thickness and precipitation for the generation of salinity anomalies in the sinking region are negligible. It should be

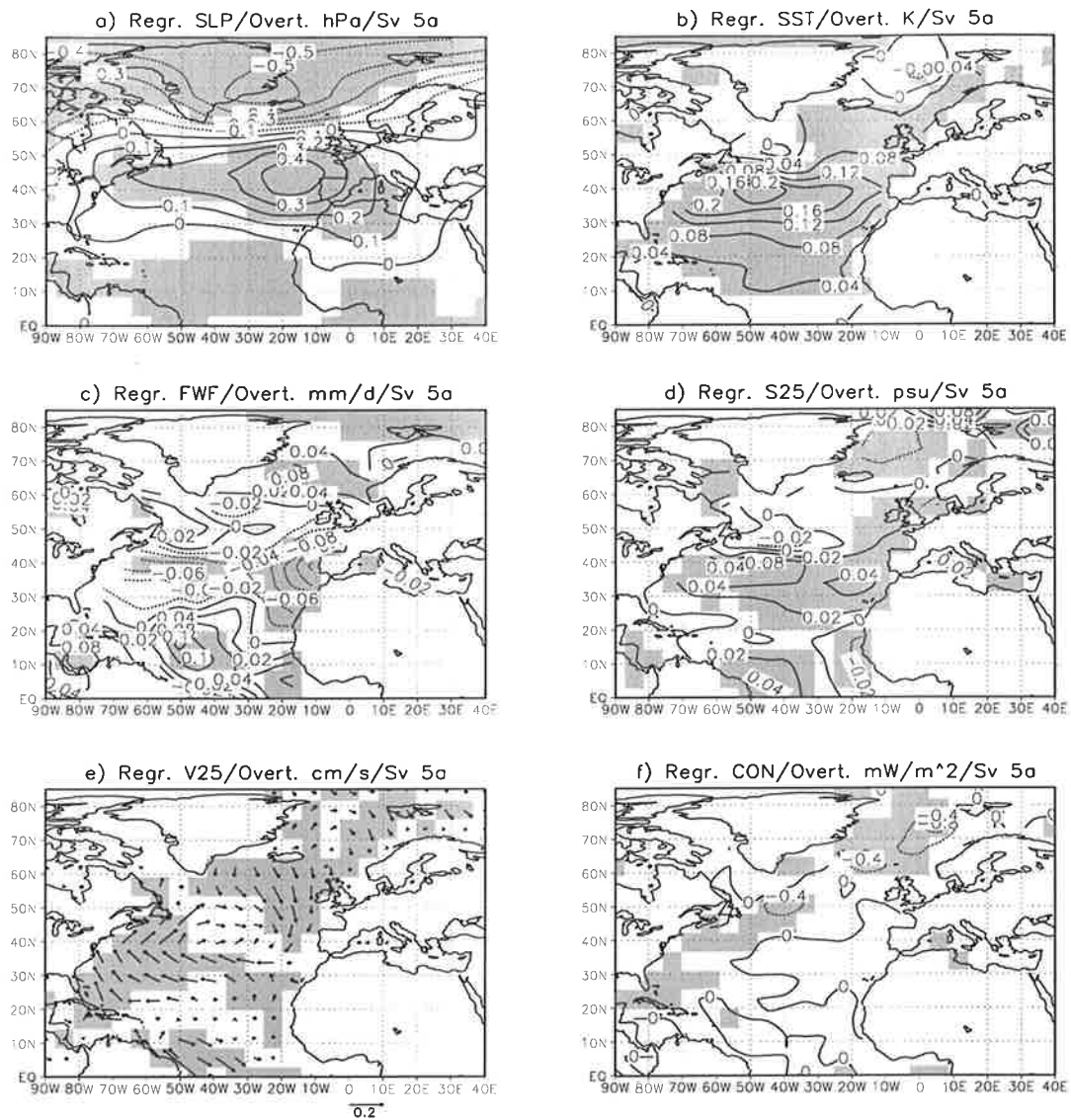


Figure 5.10: Same as Fig.5.7, but for lag +5 a.

noted that in our model version there is no free sea-ice drift included. Instead, sea-ice is created and destroyed locally by thermal processes. Thus, the direct comparison of the averaged sea ice thickness anomalies with the salinity anomalies is justified and hence also the conclusion that sea ice does not play an important role.

In order to gain further insight into the generation of salinity anomalies, we investigate the vertical structure of the zonally averaged salinity anomalies in the North Atlantic. Fig.5.12 displays a lag regression for lag -5 between the bandpass filtered THC index and the zonally averaged salinity anomalies as a function of depth and latitude. Lag -5 represents the conditions when maximum positive salinity anomalies can be observed in the North West Atlantic and also when deep convection south of Greenland is at its maximum

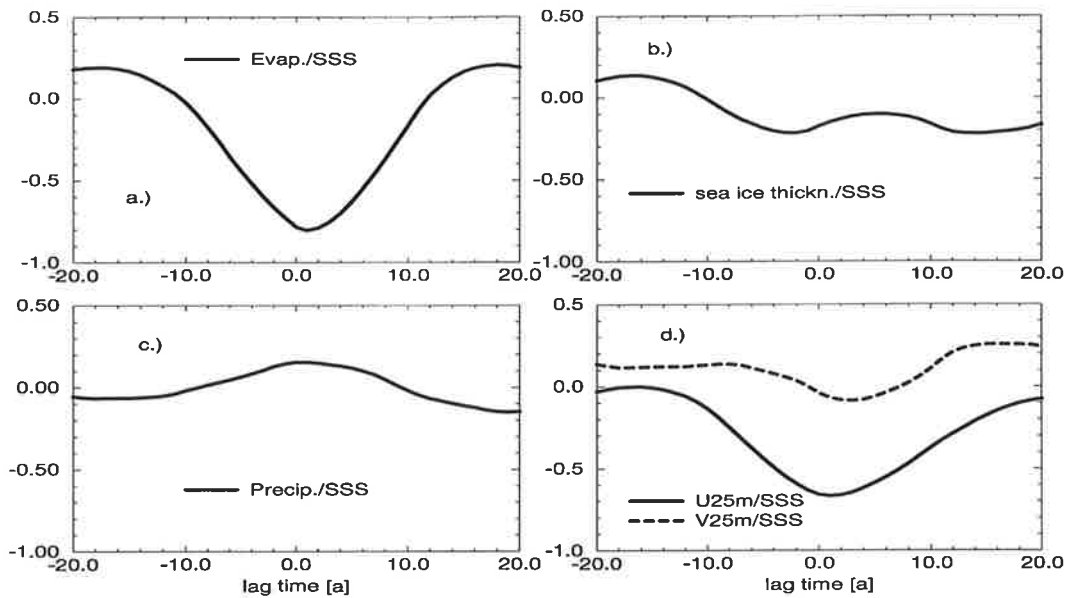


Figure 5.11: Cross correlations between the SSSA averaged over the sinking region ( $60^{\circ}$ - $20^{\circ}$ W,  $45^{\circ}$ N- $65^{\circ}$ N) and the corresponding fields of evaporation (a), sea ice thickness (b), precipitation (c) and the zonal and meridional components of the surface velocities (d), respectively. Positive lag times are associated with the field (evaporation, sea ice thickness, precipitation, and surface velocities) leading the SSS anomaly.

(Fig.5.8). Fig.5.12 demonstrates that the strong positive salinity anomalies of about 0.1 psu/Sv are surface-trapped which indicates that they are generated by surface processes (such as evaporation and Ekman currents). This surface-trapped salinity anomaly sets up the conditions (in particular a vertical density gradient) for deep convection in the sinking region. The relative roles of thermal and haline forcing for the variability of the THC shall be discussed in the next section.

### 5.4.2 The dynamics of the THC

Salinity is one of the key variables for long-term climate variability, since it governs partly the intensity of the thermohaline overturning. It was shown in Spall (1993) that the variances of salinity anomalies are proportional to the square of the freshwater flux amplitudes in the case of small advective and diffusive time scales. The local integration of a white noise freshwater forcing in the Labrador Sea can lead to decadal low-frequency

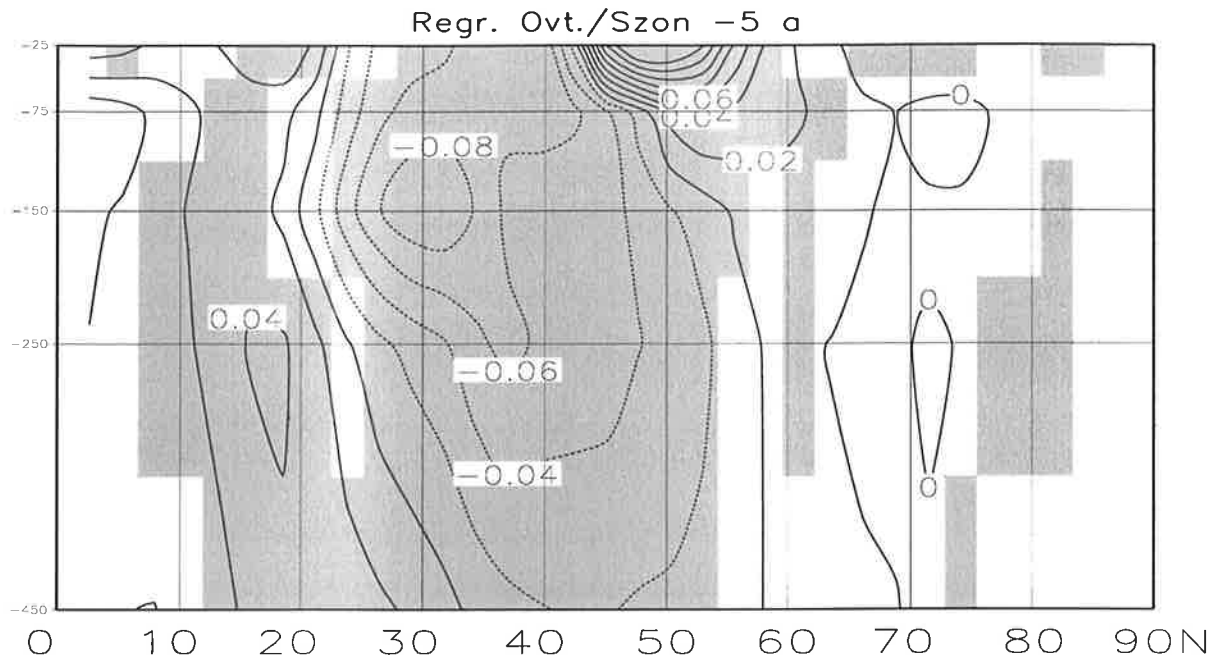


Figure 5.12: Lag regression pattern between the bandpass filtered THC index anomaly and the detrended field anomalies of the zonally averaged salinities in the North Atlantic for lag -5 years as a function of depth in the upper 450 m. Units are psu/Sv. Shading indicates non-zero regression at the 95% significance level.

variability of the North Atlantic Ocean, as was shown in Weisse et al. (1994)<sup>2</sup>.

In the previous sections we have shown that the THC is crucial in generating the interdecadal coupled climate oscillation discussed here. It was argued that the salinity anomalies are essential in destabilizing the North Atlantic Ocean. In order to understand whether changes in the THC are mainly triggered by thermal or haline processes, the density anomalies (obtained from the zonally averaged salinities and temperatures in the North Atlantic) are split into their thermal and haline contributions using the full non-linear equation of state. These density contributions are set in relation to the THC again by calculating lag regressions of the field anomalies and the bandpass filtered THC index. These regressions are then integrated over the full depth range of our ocean model and over the sinking region 45°N-65°N. The result is shown in Fig.5.13. We see that salinity dominates the evolution of density anomalies in the sinking region.

However, it is the complex interplay between the thermal and the haline density parts which is responsible for the time lag of about 3 years between the total density and the THC index. Thus, although the temperature contribution is much smaller than the

<sup>2</sup>In this context the mechanism of stochastic resonance (Benzi 1982) which represents the constructive influence of noise in e.g. bistable systems has to be investigated further.

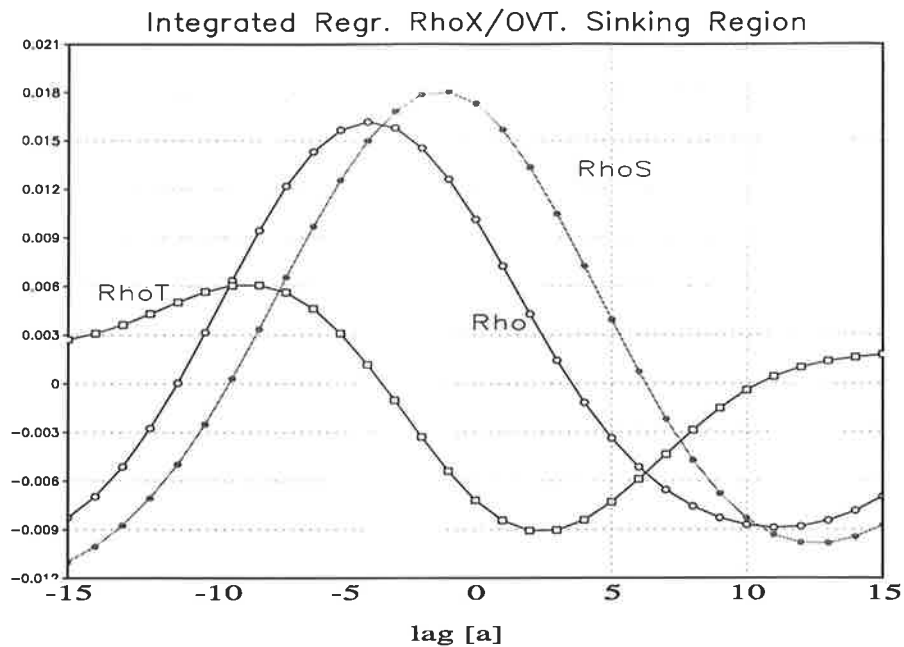


Figure 5.13: Over the sinking region ( $45^{\circ}\text{N}$ - $65^{\circ}\text{N}$ ) volume-integrated regressions of the bandpass filtered THC index anomaly and the detrended field anomalies of the zonally averaged haline (RhoS) and thermal (RhoT) density contributions and the total (Rho) density. Units are  $\text{g}/\text{m}^3/\text{Sv}$ .

salinity contribution the contribution of the temperature anomalies for lags -7 to +5 years is a crucial part of our 35 year climate mode. Regarding the role of density in the sinking region Delworth et al. (1993) reach similar conclusions (see their Figs. 8 and 10). However, one crucial difference between our findings and those of Delworth et al. (1993) is that in our model the dominant haline density anomalies are created by surface processes which include strong air-sea interactions in mid-latitudes.

In order to illustrate the vertical structure of the oscillations in the THC, lag regressions between the filtered THC index (see above) and the meridional streamfunction are calculated (Fig.5.14). Positive values of the streamfunction anomalies indicate a clockwise circulation. At lag -10 years (Fig.5.14a) the meridional overturning is in a negative phase, associated with reduced northward mass and heat transports. This is linked to a negative temperature anomaly in the North Atlantic, as shown in Fig.5.7b. Five years prior to the maximum meridional overturning a positive anomaly in the meridional circulation develops (Fig.5.14b). The anomalous density conditions at lag -5 lead to the destabilization of the water column in the sinking region, thus generating enhanced overturning in the North Atlantic. As can be seen in Fig.5.14c, the whole meridional overturning cell in the

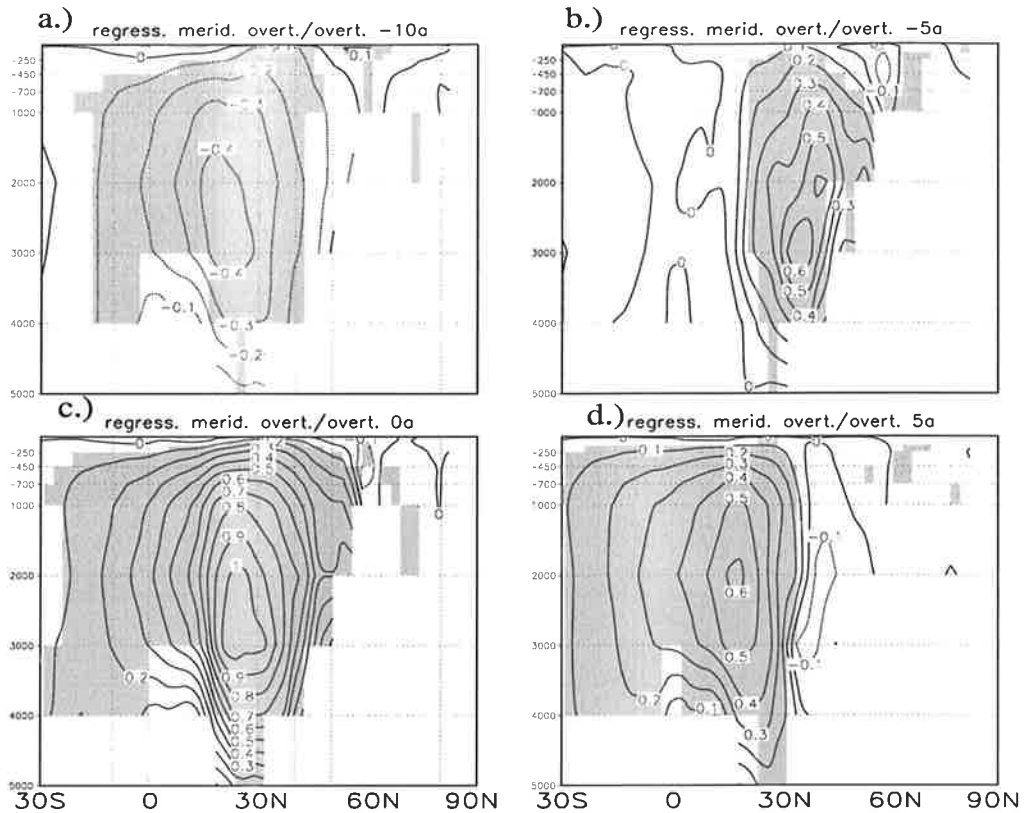


Figure 5.14: Lag regression between the bandpass filtered (transparent for periods between 25-45 years) THC index anomaly and the meridional stream-function anomalies for lag -10, -5, 0 and +5 years. Units are [Sv/Sv].

North Atlantic needs about 5 years to adjust to these new density conditions<sup>3</sup>. This figure reveals that the new density conditions affect the Atlantic from 30°S-60°N at all depths. In summary, salinity anomalies are generated in the main sinking region during periods of strong ocean-atmosphere coupling via anomalous freshwater fluxes and Ekman transport. The salinity anomalies grow until they alter the deep convection. Subsequently, the strength of the THC is changed in a way which reverses the SST anomaly in the North Atlantic. It is concluded that air-sea coupling and the THC act in a feedback loop to generate the interdecadal 35 year cycle. A schematic of this feedback loop is presented in Fig.5.15.

<sup>3</sup>Two processes can be responsible for the adjustment time of 5 years. On the one hand the advection in the deep western boundary current can transfer the anomalous density signal southward. On the other hand baroclinic Rossby waves and in particular the fast topographic Rossby waves at the western continental slope in the North Atlantic can contribute to the adjustment time of the THC to density anomalies in the sinking region.

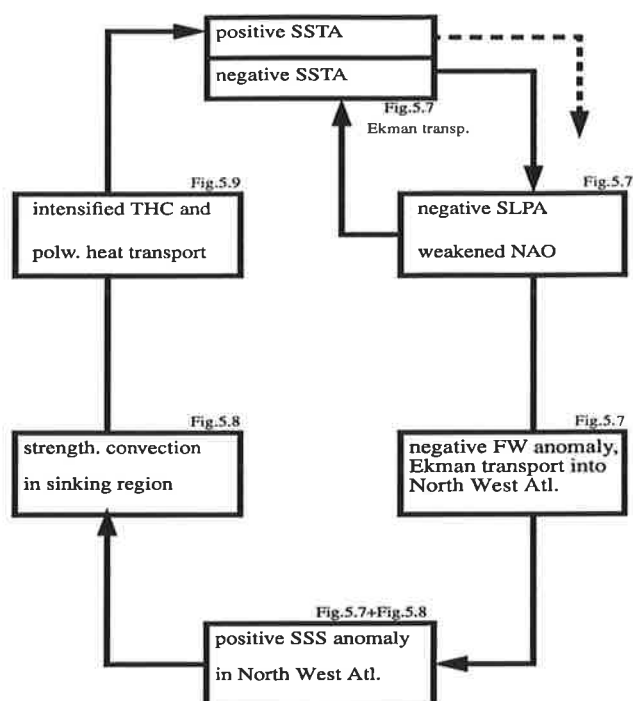


Figure 5.15: Schematic diagram of the interactions that lead to the interdecadal cycle: Consider a negative SSTA in the North Atlantic. The atmospheric response to this SSTA involves a weakened North Atlantic Oscillation (NAO) causing anomalous fresh water fluxes and Ekman transport off Newfoundland and in the Greenland Sea. This leads to the generation of positive SSS anomalies. These SSS anomalies enhance deep convection in the oceanic sinking regions and subsequently (after a lag of 5 years) the strength of the thermohaline circulation and the poleward heat transport. This leads to the formation of positive SST anomalies, which completes the phase reversal.

## 5.5 Northern Hemispheric interactions

It emerges from paleoclimate studies (Broecker et al. 1985) that strong changes in the THC may have global impacts. It is therefore tempting to study whether also small changes in the THC of approximately 10%, as found in our coupled GCM integration, force significant climate anomalies outside the North Atlantic. In order to illuminate a possible coupling between the North Atlantic and North Pacific oceans, we show lag regression plots of Northern Hemispheric upper ocean heat content (0-575m) with the bandpass filtered THC index (Fig.5.16). The heat content evolution demonstrates the existence of a common oscillatory behaviour in the Atlantic and Pacific Oceans.

The patterns in the North Pacific have some resemblance to the decadal climate mode that was described in the studies of Latif and Barnett (1994,1996) and Robertson (1996) using the ECHO1 and ECHAM1/LSG CGCMs, respectively. In their studies the hypothesis was formulated that a mode of decadal climate variability in the North Pacific (with a time scale of approximately 20 years) arises from an instability of the coupled ocean atmosphere system. They argue that e.g. a positive SSTA in the North Pacific ( the center of action in their study is located between  $30^{\circ}\text{N}$ - $50^{\circ}\text{N}$ ) changes the meridional temperature gradient, thereby changing the baroclinity of the atmosphere. The result is a weakened Aleutian low. In their concept the atmospheric response reinforces the SSTA by anomalous heat and momentum fluxes and by anomalous Ekman transport. They argue further that the Sverdrup balance in the subtropical gyre is changed by an anomalous wind stress curl. However, the ocean adjusts with some delay, and it is this transient response which can be expressed by Rossby wave propagation that is crucial to create the decadal oscillation.

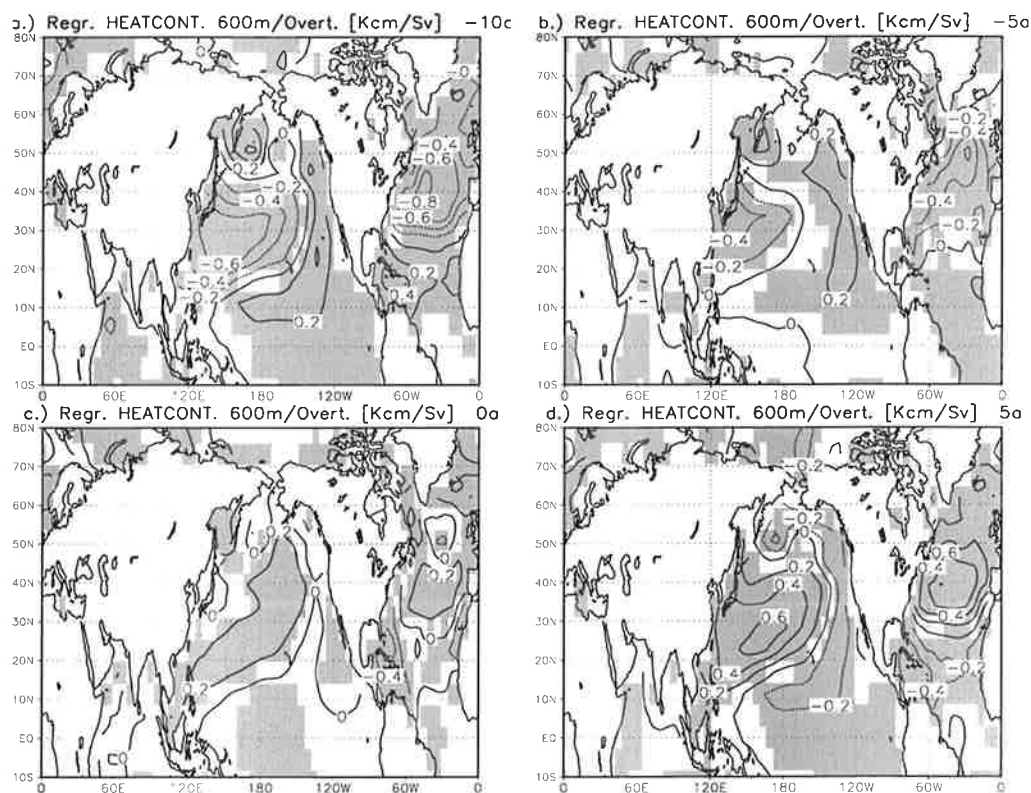


Figure 5.16: Lag regression patterns between the bandpass filtered THC index anomaly and the detrended field anomalies of the oceanic heat content of the upper 575m for lags -10, -5, 0, +5 years. Shading indicates nonzero regression with a 95% confidence limit.

Our model simulates at lag -10 a negative anomaly in the North Pacific which is embraced

by a positive anomaly (Fig.5.16). The center of action in our model is located between  $20^{\circ}\text{N}$ - $40^{\circ}\text{N}$  in the Pacific, whereas in the North Atlantic one finds the maximum anomalies between  $30^{\circ}\text{N}$ - $50^{\circ}\text{N}$ . The heat content signals in both oceans at lag -10 are associated with an anomalously strong (subtropical) jet stream (not shown) and anomalous low pressure systems between  $30^{\circ}\text{N}$ - $40^{\circ}\text{N}$  in the Pacific and between  $40^{\circ}\text{N}$ - $60^{\circ}$  in the North Atlantic. During the intermediate phase (lag -5) the North Pacific cold anomaly weakens

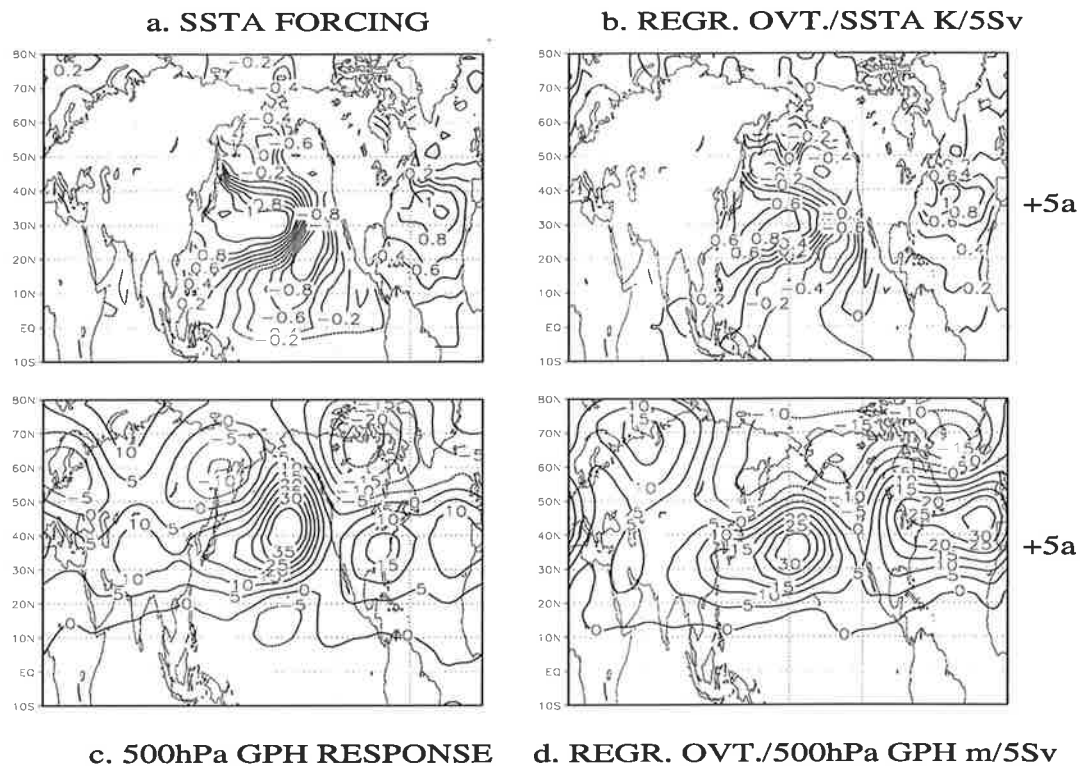


Figure 5.17: a): SSTA anomaly pattern which was added to the mean annual cycle for the atmosphere only response experiment. b.) Lag regression between the bandpass filtered THC index and the SSTA anomalies at lag +5 [K/5Sv] for a 5 Sv change in the THC. c.): Mean atmospheric 500 hPa geopotential height response to the SSTA pattern of a). This pattern is obtained by subtracting the mean of the control experiment (30 years annual cycle forcing) from the mean pattern of the response experiment (10 year annual cycle + anomaly forcing). d.) Lag regression between the bandpass filtered THC index and the 500 hPa geopotential height anomalies at lag +5 [m/5Sv] for a 5 Sv change in the THC.

and the corresponding upper tropospheric wind pattern (not shown) does not reveal much organization. At lag 0 a positive heat content anomaly develops in the Pacific. Five years later (lag +5) the model simulates basically the mirror image of the heat content anomalies

at lag -10, thereby completing one half cycle. Without going into detail, we note that the associated Pacific SST anomalies are primarily generated by anomalous Ekman currents. In contrast to the dynamics of the Latif and Barnett (1994,1996) mode which is associated with moving upper ocean heat content anomalies due to internal ocean gyre dynamics, the Pacific heat content patterns in our CGCM exhibit a standing oscillatory behaviour. This can be interpreted as an indication that the North Pacific is forced by the interdecadal mode in the North Atlantic via atmospheric teleconnections. However, it is possible that the North Pacific SST changes feedback onto the North Atlantic through changes in the large-scale atmospheric circulation. From our point of view the North Pacific gyre dynamics seem to play a minor role. At considerably longer periods than 20 years the North Pacific ocean is in equilibrium with the atmosphere which was shown by experiments which were performed with the oceanic general circulation model HOPE forced by prescribed low-frequency periodic wind stress forcing. The results of these experiments are described in Latif et al. (1996a).

In order to illustrate further the role of the panoceanic connections and to prove that the atmosphere is really responding to the mid-litudinal SST anomalies as hypothesized in the previous sections we performed atmosphere-only response experiments. A reference state was obtained by forcing the atmosphere model for 30 years with the SST annual cycle from the coupled control integration and a ten-year experiment was conducted in which a Northern Hemispheric SSTA is superimposed on the annual cycle. The SSTA forcing field used is shown in Fig.5.17 a. It has close resemblance with the Northern Hemispheric SSTA associated with our 35 year climate mode, as shown in its maximal phase (lag +5) in Fig.5.17 b for a 5 Sv change in the THC. The response of the 500 hPa height anomalies to the SSTA as simulated in the forced atmosphere-only experiment is depicted in Fig.5.17 c. The model simulates anomalous anticyclones in the Pacific (at 30°-60°N) and the Atlantic (at 20°-50°N). Over the North Atlantic and parts of Canada anomalous low pressure systems are simulated. This pattern would also contribute to a strong NAO index. Apart from minor differences the 500 hPa response pattern and the pattern of geopotential height differences at 500 hPa associated with the 35 year climate mode in the coupled run (d) are very similar. Differences between Fig.5.17 c and d might be due to the fact that the SSTA forcing field (a) is not exactly the same as the SSTA pattern in the coupled run (b). However, we believe that the close large-scale correspondence of the two atmospheric patterns is a very good proof that in our model the atmosphere responds to typical mid-litudinal SST anomalies in a linear manner. One can argue that the structures of the SST anomaly patterns in the North Atlantic and North Pacific are associated with changes in the meridional temperature gradients, which modify the atmospheric baroclinity over both basins. Subsequently this can change the transient eddy activity as shown in the modeling study of Palmer and Sun (1985). In their study an atmospheric model is forced by an SSTA located near the polar front (quite similar to our North Atlantic SSTA). The atmospheric response was found to be shifted

downstream of the SSTA. Overall they obtain an equivalent barotropic response. Their findings are consistent with our results shown in Figs.5.7a,5.7b and Figs. 5.10a,5.10b and Fig5.17. Unstable air sea interactions are therefore crucial constituents of our 35-year coupled air sea mode.

One should note that positive geopotential height anomalies in the subtropics are associated locally with positive SST anomalies and the anomalies in the Greenland/Iceland region appear to be always out of phase to the SST anomalies at 30<sup>0</sup>-50<sup>0</sup>N in the North Atlantic. This relationship can be found also in observations and shall be discussed in Section 5.7.

## 5.6 Interdecadal variability and greenhouse warming

In this section we return to one of the main questions mentioned in the introduction: The role of interdecadal climate modes in masking the anthropogenic greenhouse warming signal. In order to find the characteristic Northern Hemispheric pattern of 2m temperature associated with the interdecadal climate variability in our model, we performed an EOF analysis of the bandpass filtered (transparent for periods between 20-45 year) 2m temperatures from our 700 year integration. The first EOF explaining 27% of the variance of the filtered data is displayed in Fig.5.18a. The typical signature of this pattern is a warming over land and some adjacent areas and a cooling in the Aleutian area and in the Northwest Atlantic region. It can be regarded as a warming pattern (i.e positive pattern mean value) that is created by an anomalously strong Northern Hemispheric atmospheric circulation. In order to compare this pattern to the anthropogenic greenhouse warming pattern, we conducted an EOF analysis of the Northern Hemispheric 2m temperature obtained from a 205 year integration of our model forced by monotonically increasing atmospheric CO<sub>2</sub> concentrations (Voss et al. 1998). The CO<sub>2</sub> concentrations follow the observed concentrations up to the year 1985 (model year 105) and are subsequently extrapolated following the IPCC scenario A. The first EOF of this CO<sub>2</sub>-run (Fig.5.18 b) describes the characteristic warming pattern due to the increasing CO<sub>2</sub> concentrations. The corresponding principal component (not shown) exhibits an approximately linear warming trend after the model year 80 (referring to the CO<sub>2</sub> emissions of 1960). The warming pattern shows relative minima in the regions of the hemispheric low pressure systems and relative maxima over the continents and the western oceans. It is obvious that the overall structures of the interdecadal pattern and the greenhouse warming pattern are rather similar. In order to estimate which part of the observed 2m temperatures evolution can be explained by our interdecadal mode and which part is linked to the modeled anthropogenic greenhouse warming signal, we calculated the projections of the monthly Northern Hemispheric 2m temperatures observed since 1854 (Jones et al. 1991) onto the two EOF patterns. The results are displayed in Fig.5.19 a,b. In order to give an estimate of natural model climate

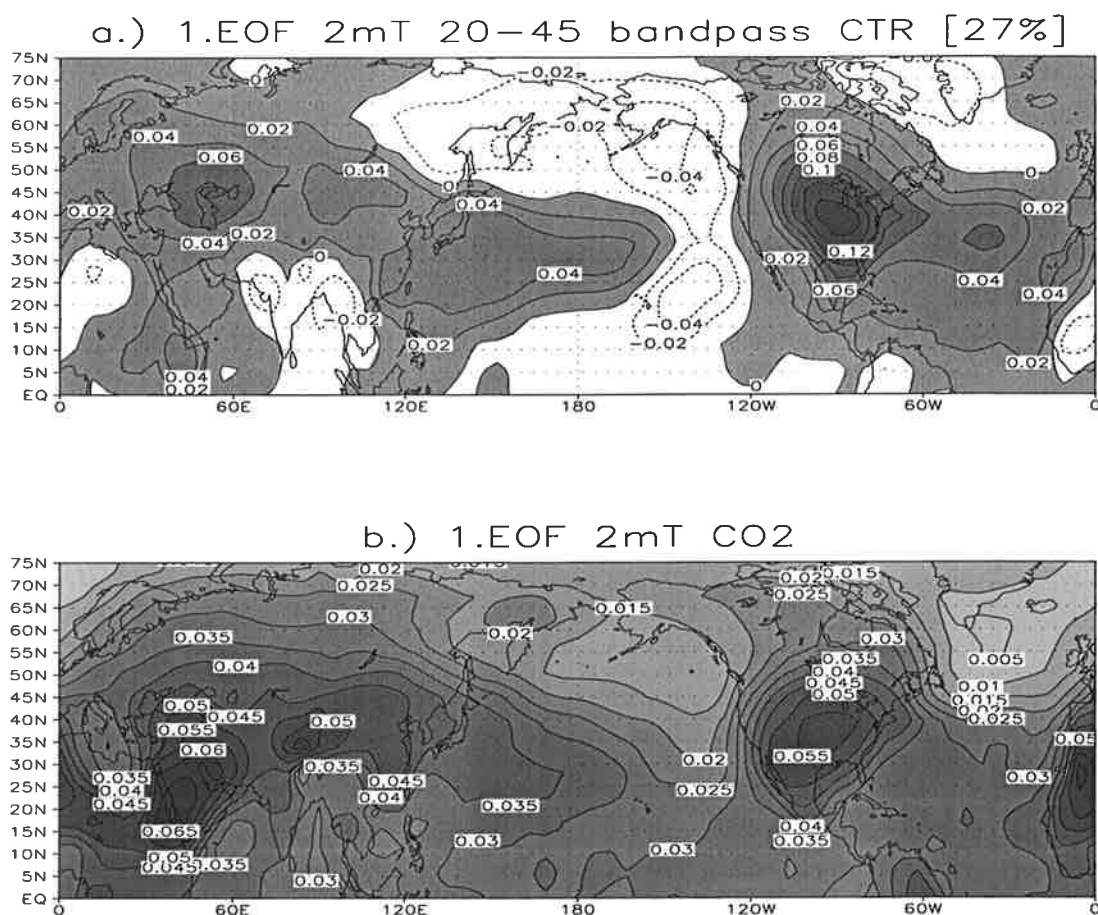


Figure 5.18: a): 1.EOF pattern of the bandpass filtered (20-45 year) 2m temperatures obtained from the 700 year control integration. b) 1.EOF pattern of the 2m temperatures obtained from a transient greenhouse warming simulation.

variability, the  $\pm 95\%$  model confidence limit is calculated from the projection of the 2m temperatures of our 700 year control integration onto the greenhouse warming pattern. The results reveal that from the late 1970s onwards the similarity between the observed temperature anomalies and the greenhouse pattern increased strongly, with a 9-year oscillation superimposed (Fig.5.19 a). Moreover, the projection of the observed temperatures onto the pattern of the interdecadal coupled atmosphere-ocean mode shows also an increasing tendency since 1970, which correlates extremely well with the wintertime values of the observed NAO index (Fig. 5.19 b). The 9 year oscillation is visible in all projections shown. Thus, a considerable part of the observed Northern Hemispheric warming is due to an intensification of the Northern Hemispheric circulation since the 1970s. A further

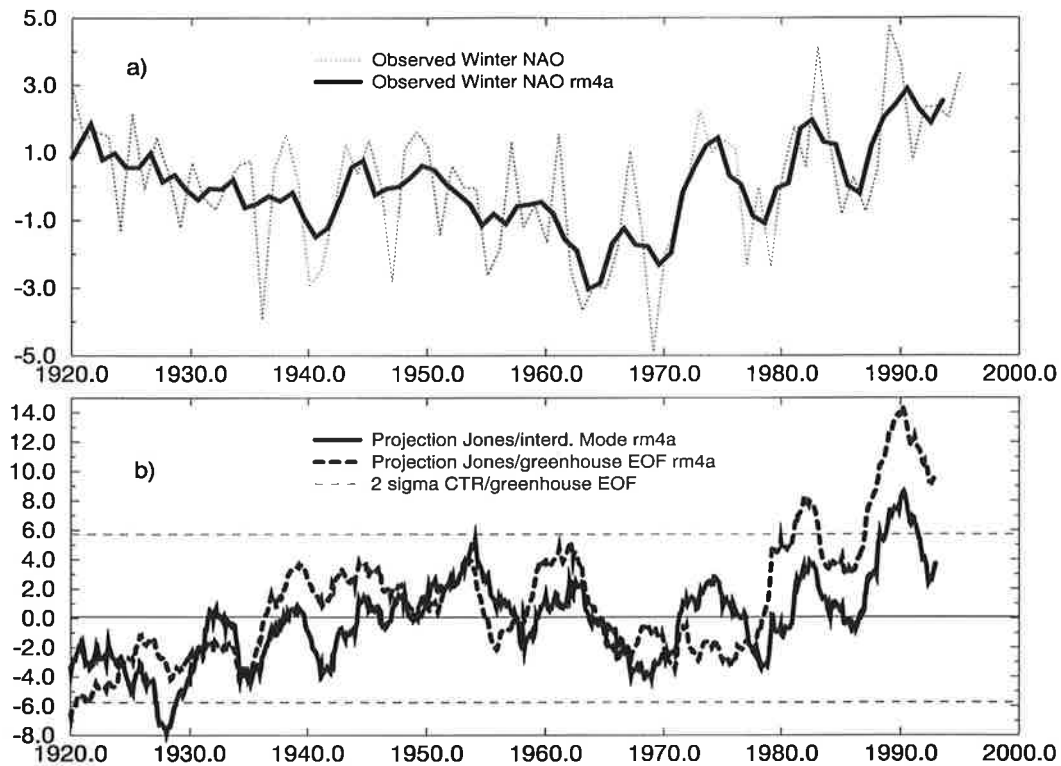


Figure 5.19: a.) Observed winter time North Atlantic Oscillation index (thin). The thick line represents the filtered NAO index. A 4 year running mean filter was adopted. b.) Projection of the observed Northern Hemispheric 2m temperatures on the EOFs displayed in Fig.5.18 a and b, respectively. The  $\pm 95\%$  confidence limit for the projection of the Northern Hemispheric control run 2m temperatures on Fig.5.18 b is marked by thin dashed lines.

amplification of the warming signal by a factor of two can be achieved by projecting the observations onto the pattern which is expected from a global warming simulation. Thus, about 50% of the recent warming can be explained by a pattern which is related to “natural model variability” and corresponds physically to an intensified Northern Hemispheric circulation. This is consistent with the findings of van Loon and Rogers (1978), Hurrell (1995) and Wallace et al. (1995). However, the fact that a strong coupling between the PNA and NAO patterns was observed in this century only during the last three decades could be understood also by assuming that anthropogenic greenhouse warming leads to an intensification of the circulation patterns. Changes in the meridional SST gradients as expected from global warming scenarios could lead to modifications in the global atmospheric circulation and hence to changes of the storm track characteristics. An analysis of

historical tree ring data, serving as proxy indices of the PNA and NAO could give further insights into this matter.

However, one should keep in mind that our model simulation has many caveats, e.g. the poor Gulf Stream representation, and the comparison between interdecadal variability and greenhouse warming made here should be interpreted with caution.

## 5.7 Summary and Discussion

This chapter represents an attempt to understand the mechanisms that generate interdecadal climate variability in the Northern Hemisphere by means of a coupled ocean-atmosphere general circulation model. Our results indicate that atmosphere-ocean interactions involving the thermohaline circulation in the North Atlantic and upper ocean in the North Pacific can generate a low-frequency climate oscillation with a dominant period of about 35 years. Our investigations focus mainly on the North Atlantic region. The analysis of the anomaly patterns of atmospheric pressure, SST, freshwater flux, SSS, oceanic surface currents and potential energy loss by convection provides the following physical picture of a coupled atmosphere-ocean mode in the North Atlantic. Salinity anomalies are forced through anomalous atmospheric freshwater fluxes and Ekman transport off Newfoundland and in the Greenland Sea. In the model's main sinking region south of Greenland the salinity anomalies are accumulated until the density conditions are favorable to initiate deep convection. With a lag of 5 years the meridional overturning cell of the North Atlantic adjusts to the new density conditions. An altered northward heat transport is the consequence, in association with the development of surface temperature anomalies in the entire North Atlantic which in turn change the atmospheric circulation. Consequently, freshwater flux anomalies (created mainly through evaporation) and anomalous Ekman transport force new salinity anomalies with signs just opposite to those simulated initially. This completes one half cycle of the 35-year climate mode in our CGCM.

However, the physical mechanisms that generate this kind of oscillation are more complex. A synchronous oscillatory behaviour of North Atlantic and North Pacific temperatures is simulated. This can be seen as a clear indication that the atmosphere is a necessary component of the interdecadal climate cycle. Unstable air-sea interactions in both oceans seem to play a key role for this oscillation.

It can be argued that some important time scales for this interdecadal mode are provided by the accumulation time for salinity anomalies, the response time of the meridional overturning to salinity anomalies and the time scale by which the thermal upper ocean structure lags the THC. Furthermore, the thermal memory of the Pacific can contribute to the time scale of the Northern Hemispheric mode. It is beyond the scope of this CGCM study to deduce whether both oceans provide the memory or whether one of the two

oceans only is responsible for the memory. This question is addressed in a forthcoming study.

We just started to conduct further experiments with our model components, focussing on the atmospheric response to Pacific and/or Atlantic SST anomalies. Another CGCM integration with our model is performed using only prescribed seasonally varying freshwater fluxes (including river runoff), so that the freshwater coupling which was shown to be a contributor to generate salinity anomalies is blocked in this experiment. We are confident that these experiments will shed more light on the interdecadal panoceanic connection found here and may help to determine whether the Atlantic forces the Pacific or vice versa, or whether they constitute a joint oscillator.

Observations seem to underscore also the importance of atmosphere-ocean coupling on interdecadal time scales. Fig.5.20 shows the normalized and detrended time series of the SLP in Stykkisholmur (Iceland) and of the SSTA averaged over the North Atlantic index region  $35^{\circ}\text{N}$ - $45^{\circ}\text{N}$  and  $95^{\circ}\text{W}$ - $0^{\circ}\text{E}$  (obtained from the GISST dataset of the UKMO). A running mean filter of 10 years was used in order to remove annual and interannual variability. Fig.5.20 shows an anticorrelation between the SLP in Stykkisholmur (Frich et al. 1995) and the SSTA index. This relation is consistent with our model results. Furthermore, there is evidence for a multidecadal time scale in both time series. Therefore, our coupled model feedback loop may explain some of the interdecadal variability observed in the NAO which was described by D'Arrigo et al. (1993) who analyzed tree ring proxy data. One further prominent example from observations for atmosphere-ocean interactions on interdecadal time scales is the GSA. Common features of our interdecadal model mode and the GSA are: a rather strong atmospheric forcing creates salinity anomalies in the polar and subpolar region which – after a lag of a few years – change the density conditions in the regions of NADW formation and modify subsequently the strength of the convective overturning. The studies of Greatbach et al. (1991) and Ezer et al. (1995) reveal that between 1955-1959 and 1970-1974 changes of the thermohaline structure occurred in the North Atlantic in association with the GSA. A very crucial difference between the GSA and the modeled salinity anomalies in the subpolar North Atlantic is the generation mechanism. Whereas in our study, anomalous freshwater fluxes as well as anomalous Ekman transport in the vicinity of a strong surface salinity gradient generate salinity anomalies, the GSA supports the picture that anomalous sea ice conditions (Häkkinen 1993) and enhanced injection of polar waters into the subpolar gyre (Dickson et al. 1988) are responsible for the birth of the salinity anomaly. However, multidecadal variations like that in our model can be found in nature e.g. in the North Atlantic and the polar climate system. This can be seen in the salinity and temperature time series shown by Dickson et al. (1988) (their Figs.1 and 29). Furthermore, the feedback loop of Wohllleben and Weaver (1995), explaining the GSA as a manifestation of a coupled air-sea mode is very similar to our findings. Thus, both the observations and our coupled GCM seem to support the idea that part of the interdecadal variability in the North Atlantic

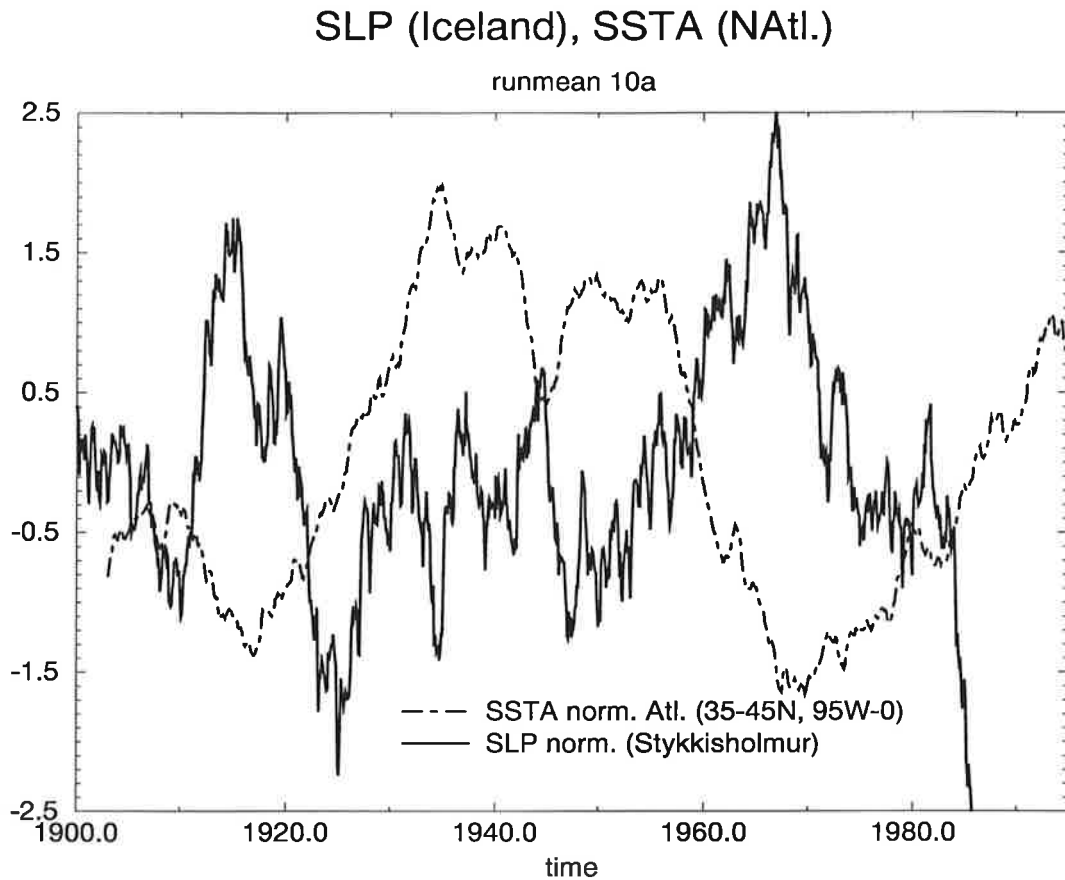


Figure 5.20: Normalized and detrended time series of the SLP in Stykkisholmur (Iceland) and the SSTA averaged over the region  $35^{\circ}\text{N}$ - $45^{\circ}\text{N}$  and  $95^{\circ}\text{W}$ - $0^{\circ}\text{E}$ . Both time series are smoothed with 10 year running mean filter.

originates from unstable air-sea interactions.

We have shown that the understanding of interdecadal climate variability may be very important to understand the recent observed temperature trends. Further insights into the mechanism of the PNA/NAO coupling and its natural occurrence is required to address the question as to whether the recently observed “dynamical” warming due to the intensified Northern Hemispheric atmospheric circulation is part of the anthropogenic climate change.

## 5.8 References

Benzi, R., A. Sutera, A. Vulpiani, 1982: Stochastic resonance in climatic change. *Tellus*, **34**, 10-16.

Bjerknes, J., 1964: Atlantic air-sea interaction. *Adv. Geophys.*, **10**, 1-82.

- Broecker, W.S., D.M. Peteet and D. Rind, 1985: Does the ocean-atmosphere system have more than one stable mode of operation ?, *Nature*, **315**,21-26.
- Chen F. and M. Ghil, 1995: Interdecadal Variability of the Thermohaline Circulation and High-Latitude Surface Fluxes, *J. Phys. Oceanogr.*, **25**, 2547-2567.
- D'Arrigo, R.D., E.R. Cook, G.C. Jacoby and K.R. Briffa, 1993: NAO and Sea Surface Temperature Signatures in Tree-Ring Records from the North Atlantic sector. *Quart. Sci. Rev.*, **12**, 431-440.
- Delworth, T.L., S. Manabe, R.J. Stouffer, 1993: Interdecadal Variations of the thermohaline circulation in a Coupled Ocean-Atmosphere Model. *J. Climate*, **6**, 1993-2011.
- Deser, C., Blackmon M.L., 1993: Surface Climate Variations over the North Atlantic Ocean during Winter: 1900-1989. *J. Climate*, **6**, 1743-1753.
- Dickson, R.R., H.H.Lamb, S.-A. Malmberg, J.M. Colebrook, 1975: Climate reversal in the northern North Atlantic. *Nature*, **256** 479-481.
- Dickson, R.R., J. Meincke, S.-A. Malmberg. A.J. Lee, 1988: The "Great Salinity Anomaly" in the Northern Atlantic 1968-1982. *Prog. Oceanogr.*, **20** 103-151.
- Dickson, R.R., Lazier J., Meincke J., Rhines P, 1996 in Decadal Climate Variability: Dynamics and Predictability (NATO ASI Series I: Global Environmental Change, Springer), 211-259.
- Duplessy, J.C., L. Labeyrie, M. Arnold, M. Paterne, J. Duprat and T.C.E van Weering, 1992: North Atlantic sea-surface salinity and abrupt climate changes. *Nature*, **358**, 485-488.
- Ezer, T., G.L. Mellor, R.J. Greatbach, 1995: On the interpentadal variability of the North Atlantic Ocean: Model simulated changes in transport, meridional heat flux and coastal sea level between 1955-1959 and 1970-1974. *J. Geophys. Res.*, **100**, 10,559-10,566.
- Frich, P., Alexandersson H., Ashcroft J., Dahlström B., Demaree G.R., Drebs A., van Engelen A.F.V., Førland E.J., Hansen-Bauer I., Heino R., Jonsson T., Jonasson K., Keegan L., Nordli P.Ø., Smith T., Steffensen P., Tuomenvirta H., Tveito O.E., 1995: North Atlantic Climatological Dataset (NACD)- Final National Reports 1993-1995. DMI Technical Report 95-16. Danish Meteorological Institute, Copenhagen, 1995.

- Greatbach, R.J., A.F. Fanning, A.D. Gouling and S. Levitus, 1991: A diagnosis of interpentadal circulation changes in the North Atlantic. *J. Geophys. Res.*, **96**, 22,009-22,023.
- Greatbach, R.J., S. Zhang, 1994: An interdecadal oscillation in an idealised ocean basin forced by constant heat flux. *J. Climate*, **8**, 81-91.
- Griffies, S.M., E. Tziperman, 1995: A linear Thermohaline Oscillator Driven by Stochastic Atmospheric Forcing. *J. Climate*, **8**, 2440-2453.
- Grötzner, A., M. Latif, T.P. Barnett, 1997: A decadal climate cycle in the North Atlantic Ocean as simulated by the ECHO coupled GCM. *J. Climate* in press.
- Häkkinen, S., 1993: An Arctic Source for the Great Salinity Anomaly: A Simulation of the Arctic Ice-Ocean System for 1955-1975. *J. Geophys. Res.*, **98**, C9, 16,397-16,410.
- Hasselmann, K., 1976: Stochastic climate models. Part I: Theory, *Tellus*, **28**, 473-485.
- Hasselmann, K., 1993: Optimal fingerprints for the detection of time dependent climate change. *J. Climate*, **6**, 1957-1971.
- Hegerl, G.C., H.v. Storch, K. Hasselmann, B.D. Santer, U. Cubasch, P.D. Jones, 1996: Detecting Greenhouse Gas induced Climate Change with an Optimal Fingerprint method. *J. Climate* (in press).
- Hurrell, J.W., 1995: Decadal Trends in the North Atlantic Oscillation: Regional Temperatures and Precipitation. *Science*, **169**, 676-679.
- James, I.N., P.M. James, 1989: Ultra-low-frequency variability in a simple atmospheric circulation model. *Nature*, **342**, 53-55.
- Jones, P.D., T.M. Wigley and G. Farmer (1991): Marine and Land Temperature Data Sets: A Comparison and a Look at Recent Trends. In *Greenhouse-Gas-Induced-Climatic Change: A Critical Appraisal of Simulations and Observations*, (Schlesinger ME ed.), 593-602, Elsevier Science Publishers, Amsterdam.
- Kushnir, Y., 1994: Interdecadal Variations in the North Atlantic Sea-Surface Temperature and Associated Atmospheric Conditions. *J. Climate*, **7**, 141-157.
- Latif, M. and T.P. Barnett, 1994: Causes of decadal climate variability over the North

Pacific and North America. *Science*, **266**, 634-637.

Latif, M. and T.P. Barnett, 1996: Decadal variability over the North Pacific and North America: Dynamics and predictability. *J. Climate*, **9**, 2407-2423.

Latif, M., A. Grötzner, M. Münnich, E. Maier-Reimer, S. Venzke, T.P. Barnett, 1996a: in Decadal Climate Variability: Dynamics and Predictability (NATO ASI Series I: Global Environmental Change, Springer), 264-292.

Lau, K.-M., Weng H., 1995, Climate Signal Detection Using Wavelet Transform: How to Make a Time Series Sing. *Bull. of Am. Met. Soc.*, **76**, 2391-2402.

Lazier, J.R.N., 1988: Temperature and salinity changes in the deep Labrador Sea, 1962-1986. *Deep-Sea Research*, **35**, 1247-1253.

Maier-Reimer, E. and U. Mikolajewicz, 1989: Experiments with an OGCM on the cause of the Younger Dryas, MPI Report No.39, Available from: Max-Planck-Institut für Meteorologie, Bundesstr.55, 20146 Hamburg, Germany.

Manabe, S., R.J. Stouffer, 1995: Simulation of abrupt climate change induced by freshwater input to the North Atlantic Ocean. *Nature*, **378**, 165-167.

Mann, M.E., J. Park and R.S. Bradley, 1995: Global interdecadal and century-scale climate oscillations during the past five centuries. *Nature*, **378**, 266-270.

Mikolajewicz, U., E. Maier-Reimer, 1990: Internal secular variability in an ocean general circulation model. *Climate Dyn.*, **4**, 145-156.

Mysak, L.A., D.K. Manak, R.F. Marsden, 1990: Sea-ice anomalies observed in the Greenland and Labrador Seas during 1901-1984 and their relation to an interdecadal Arctic climate cycle. *Climate Dyn.*, **5**, 111-133.

Mysak, L.A., T.F. Stocker, F. Huang, 1993: Century-scale variability in a randomly forced, two-dimensional thermohaline ocean circulation model. *Climate Dyn.*, **8**, 103-116.  
**8**, 1325-1342.

Palmer, T.N. and Z. Sun, 1985: A modelling and observational study of the relationship between sea-surface temperature anomalies in the north-west Atlantic and the atmospheric general circulation. *Quart. J. Roy. Meteor. Soc.*, **111**, 947-975.

- Robertson A.W., 1996: Interdecadal variability over the North Pacific in a multi-century climate simulation, *Climate Dyn.*, **12**, 227-241.
- Schiller, A., U. Mikolajewicz, R. Voss, 1997: The stability of the thermohaline circulation in a Coupled Ocean-Atmosphere General Circulation Model. *Climate Dyn.*, **13**, 325-347.
- Schlesinger, M.E., N. Ramankutty, 1994: An oscillation in the global climate system of period 65-70 years. *Nature*, **367**, 723-726.
- Spall, M.A., 1993: Variability of sea surface salinity in stochastically forced systems. *Climate Dyn.*, **8**, 151-160.
- van Loon, H. and J. Rogers, 1978: The seesaw in winter temperatures between Greenland and northern Europe. Part I: general description. *Mon. Wea. Rev.*, **106**, 303-309.
- Voss, R., R. Sausen, U. Cubasch, 1998: Periodically synchronously coupled integrations with the atmosphere-ocean general circulation model ECHAM3/LSG. *Climate Dyn.*, **14**, 249-266.
- Wallace, J.M., Y. Zhang and J.A. Renwick 1995: Dynamical Contribution to Hemispheric Mean Temperature Trends. *Science*, **270** 780-783.
- Weaver, A.J., E.S. Sarachik, 1991: Evidence for decadal variability in an ocean general circulation model: An advective mechanism. *Atmos.-Ocean*, **29**, 197-231.
- Weaver, A.J., J. Marotzke, P.F. Cummins and E.S. Sarachik, 1993: Stability and Variability of the thermohaline circulation. *J. Phys. Oceanogr.*, **23**, 36-90.
- Weaver, A.J., S.M. Aura and P.G. Myers, 1994: Interdecadal variability in an idealized model of the North Atlantic. *J. Geophys. Res.*, **99**, 12423-12442.
- Weisse, R., U. Mikolajewicz and E. Maier-Reimer, 1994: Decadal variability of the North Atlantic in an ocean general circulation model. *J. Geophys. Res.*, **89**, 12411-12421.
- Winton, M., E.S. Sarachik, 1993: Thermohaline oscillations induced by strong steady salinity forcing of ocean general circulation models. *J. Phys. Oceanogr.*, **23**, 1389-1410.
- Wohlleben, T.M.H. and A.J. Weaver, 1995: Interdecadal variability in the subpolar North Atlantic. *Climate Dyn.*, **11**, 459-467.

## 6 Outlook and Summary

*“Thus it is evident that the disturbed state of the sun’s surface affects the earth”, E. Walter Maunder, 1923 (The Sun and Sunspots 1820-1920, Smithsonian Report for 1923, Washington p.173).*

### 6.1 Climate predictability

As discussed in the introduction of this thesis, the existence of climate modes, which deviate significantly from the red noise null hypothesis of climate variability opens at least the theoretical possibility for climate forecasts with better skill than that of the damped persistence forecast. In a recent study by Grötzner et al. (1998) the predictability of the climate system on different time scales is investigated by means of ensemble forecast experiments, which were conducted with the CGCM ECHAM3/LSG. These experiments started from slightly different atmospheric initial conditions, whereas the oceanic initial conditions within one ensemble were identical and were obtained from the 700 year climate control integration. The general finding of Grötzner et al.’s study is that the existence of climate modes which deviate from an Ornstein Uhlenbeck process is not a sufficient condition for enhanced predictive skill. The predictive skill of the climate on different time scales (interannual to interdecadal) results from an interplay of the mean auto correlation function of the process, the ratio of high to low frequency variability in the spectrum of the process, and the initial conditions. The first two items are discussed thoroughly in the study of Grötzner et al. (1998), whereas the dependence on the initial state can only be evaluated by a large series of ensemble forecast experiments. However, one may ask, whether it is possible just by using statistics to quantify the *dynamics of climate predictability*. It is well known that nonlinear dynamical systems can be highly predictable for particular initialization states, whereas for others the trajectories diverge very quickly. Our aim here is to formulate a mathematical technique which quantifies the extent of predictability one can expect at a particular time during an integration. This technique should be able to determine appropriate ensemble initialization points for our forecast methodology mentioned above, which yield optimal predictability. On the other hand, it

should be possible with this methodology to attribute physical processes to eras of low or high predictability. The knowledge of physical conditions which perhaps favor bifurcations may be an essential point to explore the physical limitations of forecast schemes. For this purpose we start with a general information theoretical ansatz (Gelfand and Yaglom 1957, Palus 1993). The basic idea is to define a kind of moving nonlinear autocorrelation for a time series quantifying the local amount of information which is contained in the variable  $x$  at time  $t$  about the variable  $x$  at time  $t+\tau$ . Let  $X$  be a random variable with a set of values  $\chi$  and a probability density  $p(x), x \in \chi$ . The entropy  $H(X)$  of a random variable  $X$  is defined as

$$H(X) = - \sum_{x \in \chi} p(x) \ln p(x). \quad (6.1)$$

For a pair of random variables  $X, Y$  with a joint probability density  $p(x, y)$ , the joint entropy  $H(X, Y)$  is given by

$$H(X, Y) = - \sum_{x \in \chi} \sum_{y \in \psi} p(x, y) \ln p(x, y). \quad (6.2)$$

The average amount of information contained in the common dynamics of the variables  $X$  and  $Y$  is quantified by the mutual information  $I(X, Y)$ , which is defined as

$$I(X, Y) = H(X) + H(Y) - H(X, Y). \quad (6.3)$$

The amount of information contained in the variable  $X(t)$  about the variable  $X(t + \tau)$  – also sometimes referred to as the redundancy of  $X(t)$  and  $X(t + \tau)$  – can be regarded as a nonparametric measure of predictability. In this sense the mutual information can be regarded as a kind of nonparametric correlation for the prediction horizon  $\tau$ . Here, we compute the redundancy from the data under consideration and a set of surrogate data, which shall be seen as a representation of a null hypothesis model. A null-hypothesis model which we consider here is the first order autoregressive process, as proposed by the theory of the stochastic climate model (Hasselmann 1976). We analyze the statistical quantity which is computed from the absolute value of the difference between the redundancy value obtained from the data and a mean value of a set of surrogates in standard deviations of the latter. The predictability  $I[x(t), x(t + \tau)]$  and the related statistics are evaluated in sliding overlapping windows with a length of  $N_w$  samples and a window step of  $N_s$  samples. Our working hypothesis is step-wise stationarity and ergodicity for the time series. The resulting relative redundancy is expressed in standard deviations of the surrogate redundancy and as a function of model time. This technique is applied here for the time series of the meridional overturning strength as simulated by the multi-century integration of ECHAM3/LSG. The time series of the nonlinear relative redundancy is tested against red noise surrogates. We use a window length of  $N_w=128$  samples (years), a window step of  $N_s=8$  samples, and a prediction horizon of 5 years. The predictability of the strength of the meridional overturning for a 5 year forecast as compared to the red

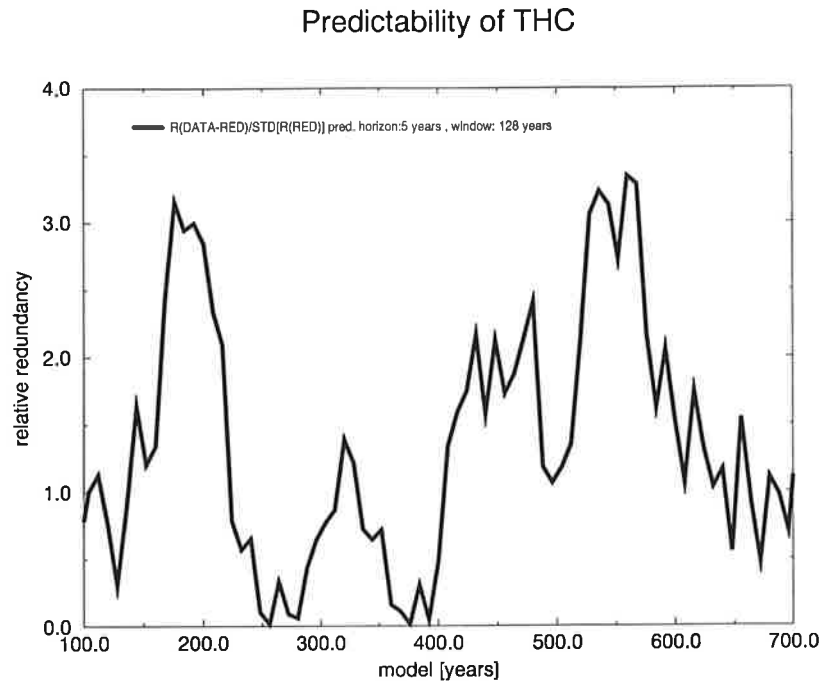


Figure 6.1: Relative redundancy of the strength of the meridional overturning in the North Atlantic tested against red noise. The analysis uses a sliding window with a window length of 128 years, a prediction horizon of 5 years and an overlapping interval of the windows of 8 years.

noise surrogates is shown in Fig.6.1. The deep ocean predictability is characterized by centennial variability, the origin of which shall be investigated in future work. As compared with the ensemble predictions of the thermohaline circulation described by Grötzner et al. (1998) (our model year 0 corresponds to their model year 149) the overall tendencies are reproduced quite well. Rather low predictability exists for the years 250-400 and rather high skill exists for the years 400-600, following our chronology. This information theoretical method has to be tested further by considering also other variables and prediction horizons. One of the big advantages of this method would be to determine just from long control integrations the patterns which exhibit highest predictability on different time scales. A determination of predictability limits of forecasting schemes is a crucial problem. An attribution of such limits to physical processes by means of information theoretical methods is a further step to improve climate forecasts.

## 6.2 External forcing and long-term climate variability

In a recent study by Cubasch et al. (1997), the ECHAM3/LSG was used to investigate to which extent long-term climate variability is influenced by anomalous solar forcing. Two

solar forcing experiments were conducted starting at year 1700 and ending in 1992. The solar forcing was obtained from the reconstruction of solar irradiance of Hoyt and Schatten (1993). As documented in this thesis, the North Atlantic Oscillation plays a major part in generating long-term climate variability in conjunction with ocean dynamics. The sensitivity of the NAO to anomalous solar forcing is another important question in order to determine the relative contributions of internally and externally forced long-term climate variability. The two experiments can be regarded as two realizations of the overall climate

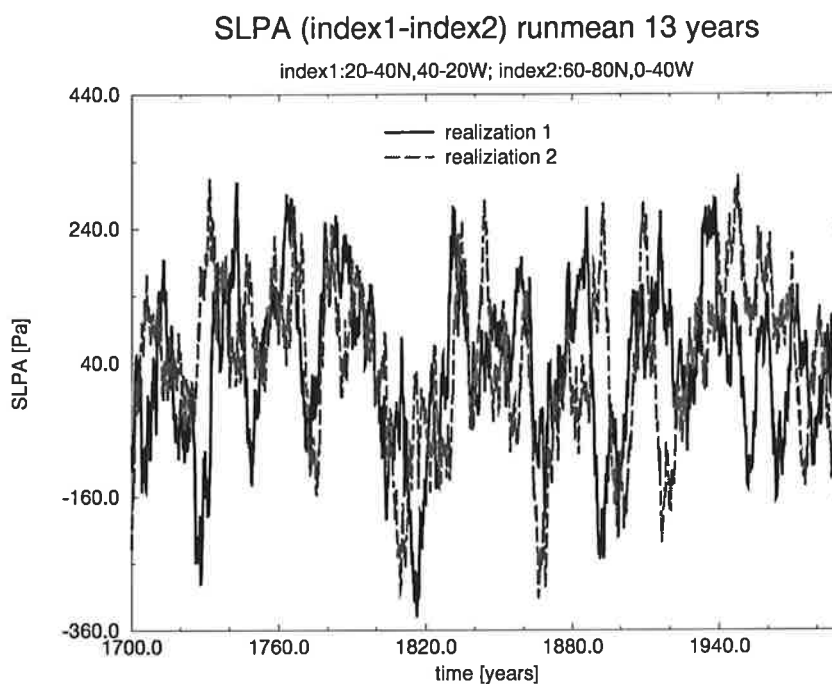


Figure 6.2: Atmospheric circulation indices from two realizations of a multicentury ECHAM3/LSG integration forced with the Hoyt and Schatten reconstruction of solar irradiance. Both time series are smoothed with a 13 year running mean filter. Data were provided by R. Voss.

trajectory over the past 300 years. An NAO-type index is calculated from these two simulations (Fig.6.2). Obviously the westerlies as quantified by the NAO-type atmospheric index are highly coherent on a 50-100 year time scale within the two realizations up to the model year 1900. Thereafter the correlation is lost. Without anomalous solar forcing it is expected that both realizations should decouple within a few weeks. The fact that Fig.6.2 shows coherence between the two realizations on much longer time scales is a clear illustration of solar forcing serving as a very effective pacemaker of long-term climate variability (Mann et al. 1998). It should be noted here that the Hoyt and Schatten index (1993) represents a rather conservative estimate. Accounting also for centennial changes in the UV-B radiation band, which might affect atmospheric ozone depletion, even a greater impact of solar forcing on long-term climate variability can be expected.

## 6.3 Future plans

The data analysis of the ECHAM3/LSG multi-century integration revealed also the existence of a decadal climate mode with a period of about 10 years in the Southern Hemisphere. This mode involves both the atmosphere and the ocean. Preliminary analysis, which shall be presented elsewhere indicates that this climate cycle arises from interactions between the Antarctic Circumpolar Current, the Southern Ocean gyres, and the Southern Hemispheric atmospheric circulation. This mode does not bear similarities with the Antarctic Circumpolar Wave (ACW) described in White and Peterson (1996), Christoph et al. (1997) and Weisse et al. (1997). In the ECHAM3/LSG simulation the atmosphere seems to play an interactive role in the Antarctic region rather than serving just as a noise generator for the ocean.

Furthermore, a centennial climate mode in the North Atlantic region with a time scale of about 180 years could be detected. This mode has also an atmospheric and oceanic signature. It is characterized by strong temperature and freshwater flux variations in the Greenland Sea, which trigger centennial changes of the thermohaline ocean circulation. Such changes are associated with anomalous oceanic temperatures in the North Atlantic region and anomalous atmospheric conditions, namely over Greenland. There is some evidence that this mode also can be described in terms of the coupled air-sea mode concept. A paper describing this long-term climate fluctuation is in preparation.

Apart from a more thorough analysis of the decadal mode in the Antarctic region and the centennial climate mode in the North Atlantic, my future research shall be devoted mainly to the issue of time scale interactions. The interaction of an interdecadal mode with the ENSO variance was discussed in Chapter 3. Furthermore, we scrutinized on the question how greenhouse warming might change the statistics of interannual climate variability in the tropics. In a recent paper (Timmermann 1998) the optimal fingerprint strategy is extended to higher order statistical moments, in order to determine detection horizons for anthropogenic changes of ENSO variability. The fundamental result of this investigation is that anthropogenic changes of ENSO variability are expected to exceed the natural background in about 20-30 years.

A very powerful tool to detect time scale interactions is bispectrum analysis. This technique exploits mainly the information of the third order cumulants. It is planned to apply this technique in future work in order to address the following problems:

- 1.) Are there multiple time scale interactions in the paleoclimatic record ?
- 2.) Are there significant bilateral interactions between intraseasonal and interannual climate variability in the tropical Pacific ?
- 3.) Is there a significant interaction of the different North Atlantic climate modes discussed in this thesis ?
- 4.) Which role does multiplicative noise play for the generation of long-term climate variability ?

5.) Which role does solar variability play to modify the statistics of long-term climate variability.

The last four questions shall be analyzed on the basis of multi-century CGCM integrations.

## 6.4 Summary

We discussed in this thesis an orchestra of climate modes with characteristic time scales of about 5, 16 and 35 years (see Fig.6.3).

Interannual variability in the Pacific is ENSO-like. This quasi-oscillatory mode can be understood as a coupled air-sea mode. We discussed the origin of ENSO variance modulations, which occur on time scales of 22 and 35 years. In particular the 35 year ENSO modulation arises from an interaction between ENSO and a 35 year Northern Hemispheric climate mode. Interdecadal wind stress curl anomalies in the subtropical Pacific initiate Rossby waves, which are associated also with subsurface temperature anomalies. These waves enter the equatorial region 8-12 years later. The subsequent changes in the mean equatorial temperature structure are considered to be important for the simulated interdecadal changes of ENSO variability. However, it was shown that the simulated ENSO cycle in the ECHAM3/LSG model is rather insensitive to global warming, whereas it is revealed from the scenario A integration performed with the more realistic CGCM ECHAM4/OPYC3 that global warming will increase the ENSO variability (Timmermann et al. 1998). This discrepancy in the sensitivities of these two climate models can be explained in terms of the mean thermocline structure, which in the ECHAM3/LSG model is highly diffusive, whereas in the ECHAM4/OPYC3 simulation it is relatively sharp.

In the North Atlantic, two climate modes are identified with time scales of 14-18 and 30-40 years, which can be understood in terms of the coupled air-sea mode framework. The wind-driven North Atlantic gyre system provides the memory of the decadal North Atlantic mode. The North Atlantic Oscillation is the atmospheric agent in this coupled air-sea mode, serving on the one hand as a stabilizer of oceanic temperature anomalies and on the other hand as an initiator of the temperature tendency which causes the phase reversal after some delay. The dynamics can be condensed within a feedback loop, which is shown in Fig.4.11. The 30-40 year North Atlantic mode (Timmermann et al. 1998a) involves interactions between the NAO and the North Atlantic thermohaline circulation. The generation of salinity anomalies plays a crucial role for the phase reversal. A feedback loop of the interdecadal oscillation in the North Atlantic is depicted in Fig.5.15. Thus, all climate modes discussed here fit into the coupled air sea mode concept.

We aimed to explore those physical processes which are relevant for the generation of climate modes on interannual to interdecadal time scales. Understanding the major processes and the space-time characteristics of long-term climate variability by means of



Figure 6.3: Schematic diagram of the climate modes simulated by the global climate model ECHAM3/LSG

CGCM experiments is not only of academic but also of direct interest for societies in the context of climate predictions (Grötzner et al. 1998). Due to the fact that the thermohaline circulation transports carbon dioxide into the deep ocean, changes of the thermohaline circulation as discussed in Chapter 5 can be linked also to the global carbon cycle. Furthermore the results presented in this thesis could give oceanographers some more indications on where to monitor the variability of the deep ocean. However, translating our results which were obtained from a coupled model to reality is a highly nontrivial task. *“Truth is much too complicated to allow anything but approximations”*, (John von Neuman).

## Acknowledgements

I am very grateful to Dr. habil. Mojib Latif and Prof. Dr. Klaus Hasselmann for supervising this thesis and for their overall support. I would also like to thank my colleagues Drs. Anselm Grötzner and Gerrit Lohmann for their neverending patience in discussing science with me. My particular gratitude to Dr. Reinhard Voss, for providing the ECHAM3/LSG output to me.

Finally, the inspiring encouragements of Dr. Lothar Weiss are acknowledged, who supported my scientific interest from the very beginning.

## 6.5 References

Christoph, M., T.P. Barnett, and E.Roeckner, 1997: The Antarctic Circumpolar Wave in a Coupled Ocean-Atmosphere GCM. *J. Climate* in press.

Cubasch, U., Hegerl G.C., Voss R., Waszkewitz J. and Crowley T. J., 1997: Simulation of the influence of solar radiation variations on the global climate with an ocean-atmosphere general circulation model. *Clim. Dyn.*, **13**, 757-767.

Gelfand I.M. and A.M. Yaglom, 1957: Computing information about a random function that is contained in another one. *Sov. Phys.-Uspekhi*, **12(1)**, 3-52, (in Russian).

Grötzner, A., M. Latif, A. Timmermann and R. Voss, 1998: Interannual to Decadal Predictability in a Coupled Ocean-Atmosphere General Circulation Model. *J. Climate* submitted.

Hasselmann, K.,1976: Stochastic climate models. Part I: Theory, *Tellus*, **28**, 473-485.

Hoyt, D.V., K.H. Schatten, 1993: A discussion of plausible solar irradiance variations, 1700-1992. *J. Geophys. Res.*, **98**, 18895-18906.

Mann, M.E., R.S. Bradley and M. K. Hughes, 1998: Global-scale temperature patterns and climate forcing over the past six centuries., *Nature*, **392**, 779-787.

Palus, M., 1993: Identifying and quantifying chaos by using information-theoretic functionals. In *Time Series Prediction: Forecasting the Future and Understanding the Past*, A.D. weigend and N.A. Gershenfeld, (eds.), Santa Fe Institute Studies in the Sci

ences of Complexity, Proc. Vol. XV, Addison-Wesley, Reading, Mass., 387-413.

Timmermann, A., J. Oberhuber, A. Bacher, M. Esch, M. Latif, E. Roeckner, 1998: ENSO response to greenhouse warming. submitted to *Nature*.

Timmermann, A., M. Latif, R. Voss, A. Grötzner, 1998a: Northern Hemispheric Interdecadal Variability: A coupled air-sea mode. *J. Clim.*, **11**, 1906-1931.

Timmermann, A. 1998: Detecting the Nonstationary Response of ENSO to Greenhouse Warming. *J. Atmosph. Sc.*, accepted.

Weisse R., U. Mikolajewicz, A. Sterl and S.S. Drijfhout, 1997: Stochastically forced variability in the Antarctic Circumpolar Current. *J. Geophys. Res.* submitted .

White, W.B., and R.G. Peterson, 1996: An Antarctic Circumpolar Wave in surface pressure, wind, temperature, and sea-ice extent. *Nature*, **380**, 699-702.